國立臺灣大學工學院材料科學暨工程研究所

碩士論文

Institute of Materials Science and Engineering

College of Engineering

National Taiwan University

Master Thesis

摻雜錳之矽酸鋅/氧化矽殼/核微球之合成與光閘晶體(PBG)光譜之分析

Synthesis of Mn-doped Zn_2SiO_4/SiO_2 core-shell structure and characterization of photonic band-gap crystal (PBG)

謝函育

Hsieh, Han-Yu

指導教授：韋文誠 博士

Advisor: Wei, Wen-Cheng, Ph.D.

中華民國 97 年 7 月

July, 2008

致謝

時光飛逝，碩士生涯即將結束。

在台大的這段時間，承蒙了許多人的教導、幫忙、以及支持。首先要感謝的韋老師，能孜孜不倦的教育學生無論是在課業、生活、或是待人處世各方面。在即將畢業的這段期間，更是要常常麻煩老師晚上或是假日加班改論文，真是辛苦了。同時要感謝擔任口試委員的黃啟原老師、劉如熹老師和林清富老師對於我論文中的疑問或是缺失給予寶貴的意見和指教。

在 Wei group 中，頌恩學長是最萬能最樂於幫忙的，感謝學長無論是在實驗、課業的幫忙(對了還有體育活動)；邦英學姐同樣是很樂意幫忙，感謝學姐在 TEM 和 XPS 實驗的協助，同時也祝福學姐在結婚之後要更幸福喔；浚傑學長與我相處的時間比較少，不過浚傑學長在做人處世的積極態度一向是讓我相當欣賞的；一中學長在實驗室的時間不長，但只要是學長能力範圍之內，向他開口沒有不答應的；右儒學長則是擔任我一年級時的小老師，以前遇到問題常常就先想到找右儒學長討論；銘璁和佳明學長也經常在做實驗或是功課上給我建議；家嘉和哲彥則是一齊打拼和互相加油的好夥伴；怡如和嬿雯兩個可愛的學妹給實驗室添加了許多的活力，同時也平衡了實驗室的陽剛之氣；士岳、勤文、敬閎還有智淵，以後也要在課業和實驗上繼續加油。

感謝系上辛苦的行政人員，林由莉小姐、張瑛梅小姐、周麗美小姐、李玉玲小姐、李苑慈小姐、陳學人先生、高崇源先生等等，有你們的幫忙使我能順利完成學業。感謝貴儀的蔡錫昌先生、凝態中心的張秀如學姐、鶯歌陶瓷中心的沈俊良先生、陳彥涵小姐、東元奈米應才的方金壽博士，有你們的幫忙讓我的論文更完整。

感謝平時幫我加油打氣還有分享心情的好朋友們，彥亨、宜蓉、小羽、黃小曼、奇勳，還有族繁不及備載的大同高中、成大材料的同學們；感謝台大材料系壘的學長同學學弟們，我會記住和你們一起在 2007 年拿下台大盃冠軍的榮耀。

最後感謝我的家人，爸爸媽媽，能夠一直支持我，謝謝。

摘要

摻雜錳之矽酸鋅(Mn-doped Zn$_2$SiO$_4$)是一種具有高亮度綠光放射(520 nm)的光致發光和陰極發光之螢光材料。在本篇研究中，我們嘗試了六種方法製備矽酸鋅螢光粉。其中ZSpII和ZSpVI具有最好的效果。以膠粒製程和強迫析出法製備氧化矽/矽酸鋅核殼組成之膠體溶液。鋅離子和錳離子會鍍膜於氧化矽顆粒。在乾燥和熱處理之後，在表面析出之鋅/錳離子會與氧化矽反應成為矽酸鋅結晶相。鋅/錳離子的析出行為以感應耦合電漿-原子放射光譜(ICP-AES)做分析;核殼之微結構則由電子顯微鏡做分析；結晶相由X光繞射儀鑑定；光致發光及陰極發光由光譜儀測量。實驗結果顯示隨著熱處理溫度上升，析出物首先形成氧化鋅，並與氧化矽反應形成矽酸鋅結晶。最後可得到由矽酸鋅鍍膜於具有光子晶體特性的氧化矽模版。此外，矽酸鋅粉末也製作成漿料塗佈於透明電極以作為陰極發光元件，同時對於此元件之光學表現做分析。

關鍵字：光子晶體、核殼/結構、螢光粉、摻雜錳之矽酸鋅、膠粒製程、光致發光、陰極發光

Abstract

Manganese doped zinc silicate (Zn_2SiO_4:Mn) is a kind of phosphor materials that has a photoluminescent (PL) (at 520 nm) and cathode-luminescent (CL) properties with relative high intensity green light emission. In this study, six methods were tried to synthesis Zn_2SiO_4 powder. Two (ZSpII and ZSpVI) methods have the best performance. The colloidal particle consisted of SiO_2 core-Zn_2SiO_4:Mn shell has been synthesized via colloidal process and forced precipitation. The reactants Zn/Mn ions were coated on the SiO_2 particles. After drying and calcination, the Zn/Mn precipitates reacted with SiO_2, then transformed to Zn_2SiO_4 phase. The behavior of Zn/Mn ions precipitation on silica spheres were studied by ICP-AES. The morphology of core-shell structure was investigated by electron microscopy. The phase identification was studied by X-ray diffraction. The PL and CL properties were determined by photon spectrometer. The results showed that with the increase of annealing temperature, the precipitates formed ZnO first, then reacted with SiO_2 and transformed to Zn_2SiO_4 phase. Finally, SiO_2 template with PBG structure coated by $ZnSiO_4$:Mn shell was obtained. Besides, Zn_2SiO_4 powders as a paste coated on transparent electrode for assembling a CL device. The performance of the device was characterized as well.

Keywords: PBG**,** core-shell, phosphor, Mn-doped Zn_2SiO_4, colloid, photoluminescence, cathode-luminescence

Content

List of Figures

List of Tables

Chapter 1 Introduction

Photonic band-gap crystals with a structure similar to opal which composes of materials arranged in periodic way has been discovered over 15 years. The characteristics of a PBG crystal (Fig. 1- 1) appear band gap that could fully reflect electromagnetive wave [1]. Opal that constructed by silica particles is a nature PBG crystal. Some materials, e.g. TiO_2, and CdSe have also been tried to assemble a PBG crystal. If silica particles are substituted by phosphoric materials, we may improve photoluminescence property of the assembled crystal.

Different kinds of phosphor materials are widely used for illumination and display. Televisions, fluorescent lamps, neon lamps, cathode ray tube (CRT) monitors field emission display are the most common products that use phosphors. Fluorescent lamp is a typical example that contains electrodes which supply electrons as applied with high voltage. These electrons strike mercury vapor and thus emit UV light. Phosphor coating on the lamp adsorbs the UV spectrum and emits visible light. The lamps, which are operated with phosphors and excited by UV light, perform at a higher efficiency and low heat. The phosphor materials used in the past 3 decades include tungstate (WO_3^{2-}), phosphate (PO_4^{3-}) or halide (X^-). Oxide and rare-earth based oxide with Tb, Sm, and Ce activators have been discovered.

Phosphors can be classified into several categories: organic phosphors, inorganic phosphors, and radioactive phosphors. Organic phosphors are synthesized by polymer and affected by different substitutional function groups, sites, and activators. Inorganic phosphors are activated by the electrons in the orbits, or by rare-earth or transition oxides which are excited and relaxed between band gaps. Radioactive phosphors are capable of emitting light spontaneously by the energy releasing from radioactive element so to activate phosphors.

Ceramic-based, organic or sulfate-based phosphors are compared, the oxide-based phosphors have good luminescent characteristics, high chemical stability and good resistance against moisture. Therefore, ceramic-based phosphors operate and last longer life time. So oxide-based phosphors become more popular in display industry. [3, 4]

The objectives of this study are to (1) synthesize spherical submicron sized particles with a SiO_2 core-Zn_2SiO_4 shell structure, (2) construct a PBG crystal with the core-shell particles and measure the optical (PL and EL) properties of the products, and (3) design a device that allows the phosphor performing luminescent property.

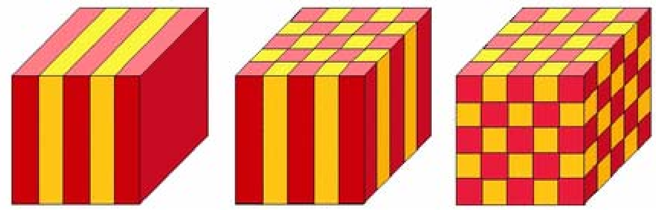

Fig. 1- 1 Schematic diagrams illustrating PBG crystals with 1-D, 2-D and 3-D dimensional structure. [2]

Chapter 2 Literature Review

2.1 Photonic Band-Gap Crystals

2.1.1 Basic Concepts of Photonic Band-Gap Crystals

As a general knowledge, a material with components or atomic elements arranged in a periodic way could be named as a crystal. Salt or so called NaCl is a typical example that represents a crystal with face centered cubic (FCC) structure, which Na^+ and Cl^- situated one by one and have a coordination number of 6. The same concept could be finely describing the photonic band-gap (PBG) crystals. The crystal structure such as FCC or else, is defined by how the elements packing in the system. However, the scale of PBG crystals in this topic is much larger than the traditional crystal structure. In other words, the size of the elements (particles or components) which are used to construct a PBG crystal ranged from submicron to micron size.

Opals and wings of some insects are the examples that have nature PBG structure [5]. Opals are the minerals full of spherical submicron silica particles. The colorful surface is resulting from the geometric structure of the silica particles which back-scatters the light of specific spectrum, instead of the original white color of the silica surface, as Fig. 2- 1. With the different band-gaps, the color would be varied. If the size of the components lies in the range of about half of wavelength of the incident electromagnet wave (generally we consider about the half of 300-700 nm visible light), the behavior of electromagnetic wave that goes though a highly ordered PBG crystal could be controlled by the packing structure, packing period, and also the dielectric constant. Fig. 2- 2 is a typical band diagram of a PBG crystal with diamond structure. The designation of those parameters could define the functions on the various applications, e.g. integrated optical circuits. [5, 6]

The term “photonic band-gap crystal” consisting of the medium with different dielectric constants in a periodic packing was first mentioned by John and Yablonovitch [7]. When the particle size approaches to the wavelength of an incident light and packed as a crystal, the band-gap will exist in this medium. Due to this special band-gap, the light that has the wavelength located in the band-gap is trapped, and not allowed to propagate through the medium. Base on this phenomenon, a component performed as a wave guide that could be used to transmit light signal with low energy loss will be a good application for PBG crystals.

In 1999, Russell *et al*. [8] tried to draw glass tubes into a specific array in a furnace (Fig. 2- 3). This technique provides a whole new process fabricating photonic crystal fiber (PCF) with different requirements (such as to maximize interaction between laser and low density media formed gas-based nonlinear optical devices) that we want and improves the performance of fibers.

Photo lithography is also a useful process to prepare PBG crystals. This method shows perfect accuracy making the PBG structures on a substrate with 2-dimensional designation. Further, photo lithography method offers designed defects. If there are designed defects in PBG structure, some light would not go through this material and thus become a “light capacitor”. In this situation, the energy of light is trapped in these crystals and become resonant, just like a laser generator [10]. Besides, the pattern may lead to the change of direction on light path (Fig. 2- 4), thus a wave guide is obtained.

2.1.2 Assembly of Photonic Band-Gap Crystals

Several materials including InGaAs, InAs, SiO_2, and etc., have been used to fabricate PBG crystals [11]. Among those, SiO_2 based PBG crystal is the most common one found whatever in nature or by man made.

There are several methods to establish PBG crystals, including nature sedimentation, electrophoresis method, template method, and so on [12]. Nature sedimentation is the most common and convenient method to fabricate PBG crystals. In order to set up a perfect PBG crystal, some points have to be paid attention to. Whatever a fabrication is applied, (1) slow sedimentation or assemble rate, (2) careful drying, (3) good dispersion, and (4) mono-size dispersibility of used particles are the most 4 important factors. If the speed of solvent evaporation too fast, particles will not be able to have enough time packing at proper sites, and thus various defects occur.

Small particles dispersed in water experienced energy turbidity in random direction which is called “Brownian motion”. It’s believed that van der waal force, electric potential force balanced with Brownian motion offer the driving energy for particles to move to the sites that have the lowest energy. Besides the Brownian motion, the solvent flow during sedimentation also should be concerned. In 2004, Norris [13] supposed that when particles depositing on an ordered packing layer, two kinds of the location were possible for sedimentation: clear and obstructed niches as pointed in Fig. 2- 5. Solvent flowed through the surface of particles. As the solvent evaporating from the system, more solvent traveled through the sites of clear niches than obstructed ones. In Fig. 2-5(b), the distance for particles moving form clear to obstructed niches is four times than from clear to obstructed ones. This phenomenon may be a reason to explain why a planar PBG crystal often packs as a face-centered-cubic (FCC) structure.

There is still one more important key point to create a perfect PBG crystal during sedimentation: the dispersion. Mono-sized ceramic particles dispersing in water will have some interesting chemical reactions occur on the surface, and thus lead to the charging effects. The possible reasons of creation of surface charge on colloidal particles are:

(1) Hydration and base-acid reactions: colloidal surface adsorbed H^+ or OH^-, and thus oxides compounds dispersed in solvent are affected by pH value, actually by electrical potential.

(2) Induced orientation of dipoles: colloid and solvent have different dielectric constant, so dipole-dipole moment may exist between these interfaces.

(3) Defects existing on colloidal surface: atoms or ions imperfectly packing may lead to the particle charged on the surface.

(4) Adsorption of foreign ions: foreign ions adsorbed by the colloid give rise to extra charge.

(5) Partial ionization in solvent: ions that dissolve in solution should satisfy its K_{sp}. therefore, the colloid and ion solubility are considered in balance.

So, if the particles have same sign of charging, such as strongly positively charged, then, these particles are kept in stable because the electrostatic repulsion force can keep colloids dispersed well in water without agglomeration. Otherwise, if the particles carry a low surface potential (usually less than 10 mV), they tend to coagulate together and become unstable compared with the previous one. Equations. 2.1 and 2.2 describe the Coulomb force and ven der Waals force, where F is force, k is a constant ($1/4\pi\varepsilon_0$), d is distance between particles, q is charge, A is Hamaker constant, R_s is radius of particles.

$$F_r = \frac{kq_1q_2}{d^2} \qquad (2.1)$$

$$F_a = -\frac{AR_s}{12d^2} \qquad (2.2)$$

The competition between particles, i.e. attracting and repulsing forces, is mainly dependent upon eq. 2.1 and 2.2. A colloid with poor dispersion gives rise to a poor packing density [14, 15], and of course a perfect PBG crystal will not be obtained.

Measuring zeta- (ζ-) potential of colloid could give us the information to predict the behavior of ceramic particles in water. Table 2- 1 shows the IEP of some oxide materials [16]. Sometimes, IEP may vary with several factors: impurities, phase (single or polycrystalline), and etc. Al_2O_3 in Table 2- 1 shows a range. The reason is that bauxite contains significant impurities, including SiO_2, Fe^{3+}, Ti^{4+}, Na^+, and so on. These impurities may cause the particle surface reacted with water, and make the IEP shift from the pure oxide.

If we take SiO_2 for an instance, the zeta potential of SiO_2 approaches to zero as acidity of the aqueous solution is at pH = 2. The potential (absolute value) will rise up when pH value away from IEP. So it is concluded that dispersion SiO_2 in a basic solution at pH = 10 leads to a stable suspension. As for the other cases [17], adding surfactant to modify the surface charge is also a good way to keep particles from agglomeration. Usually, surfactant that carries a specific function group can offer some mechanisms to achieve this goal, i.e. Coulombic repulsion and steric repulsion. As polymer attaches on colloidal surface by ven der Waals force in water, the function group (-COOH, $-NH_2$ or the others) can be ionized and become partial positive or negative. Therefore, the surface potential will be fully changed by polymer instead of the initial one carried by the particle surface. Base on this procedure, particles are dispersed well by the potential contributed from attached polymers. Another mechanism could be mentioned below. Some polymers attached on particles do not ionize. However, polymer branches will stretch or spread out in water, and this resulte in steric hindrance. This phenomenon makes polymer molecules repulsing on to each other, and then the colloids are well dispersed.

Guoy and Chapman [18] explained this phenomenon by a model considering electric double layer. Particles that carry strong zeta-potential have a thick double layer, which offers the repulsion force to maintain the stability. When the double layer is compressed, the effect contributed by ven der Waals (attractive) force becomes dominated. Fig. 2- 6 illustrates the distance between two particles vs. net attractive or repulsive force. The maximum of the net force provides an energy barrier that allows particles without contact permanently. In the other hand, primary and second minima are the sites that the net force will become attractive, therefore, gives rise to particle agglomeration.

Im *et al.* [19] and Park *et al.* [20] created PBG crystals with PS (polystyrene) spherical particles by nature sedimentation. The particles were closed packed as FCC ordered structure by self-assembly. Capillary force during solvent evaporation plays an important role because of causing the particles into a closed packing. Consolidation occurs at the interface of particles, solvent and air. The existence of meniscus between two particles drives them to stable position. After drying, these particles could be fixed on substrate. With the moving of liquid/air interface, consolidation occurs continuously until the whole suspension getting dried.

PBG crystals could also be assembled on template with patterns. Therefore, if there are periodic holes or grooves on a substrate, the particles will fill into the holes or grooves spontaneously. Base on this concept, a template with a designed pattern could be prepared for the assembly of particles. Xia *et al.* [20] prepared a Si substrate with coated photo resist, using lithography and RIE (reactive ion etching) to etch the required pattern. After that, 1 wt% silica colloidal suspension was spin-coated on the substrate. The advantage for this method is that the template could be prepared with any designed 2 dimensional pattern, such as holes, rectangular, groove, or the holes arranged in FCC, HCP, etc. [23]

Fig. 2- 1 Images showing the natural PBG structures. The top one is an opal and the bottom ones are a butterfly and enlarged structure. [6]

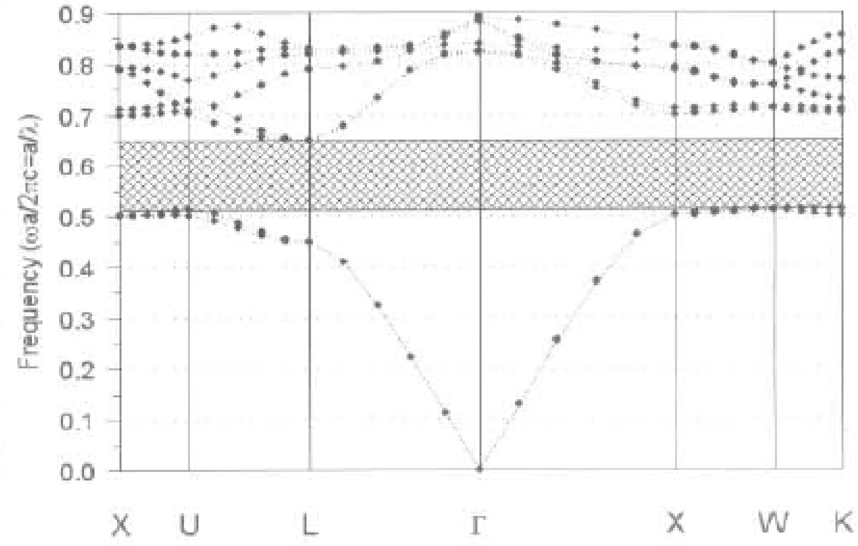

Fig. 2- 2 A typical band-gap diagram representing a PBG crystal with diamond structure. The components are in spherical shape and have a dielectric constant of 12. [11]

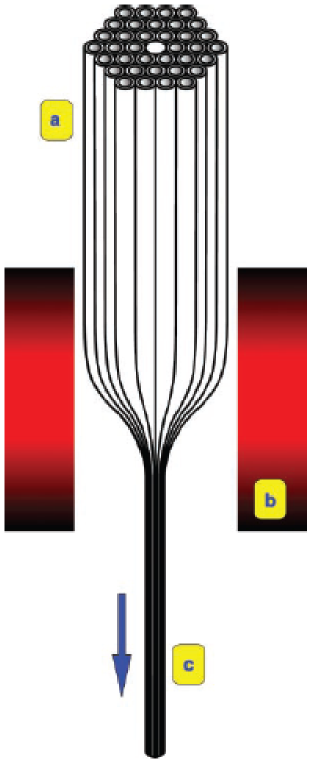

Fig. 2- 3 Schematic diagram that illustrates the silica glass tubes constructing a 2D-PBG crystal structure into fiber with the furnace operating at about 1800-2000°C. [8]

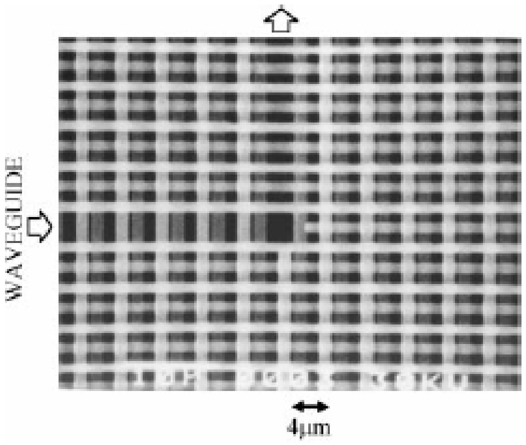

Fig. 2- 4 SEM image illustrating the microstructure of a success waveguide consist of 12 stacked layers with a period of 4 μm. The designed waveguide itself is sandwiched by the upper and lower complete PBG crystals. [9]

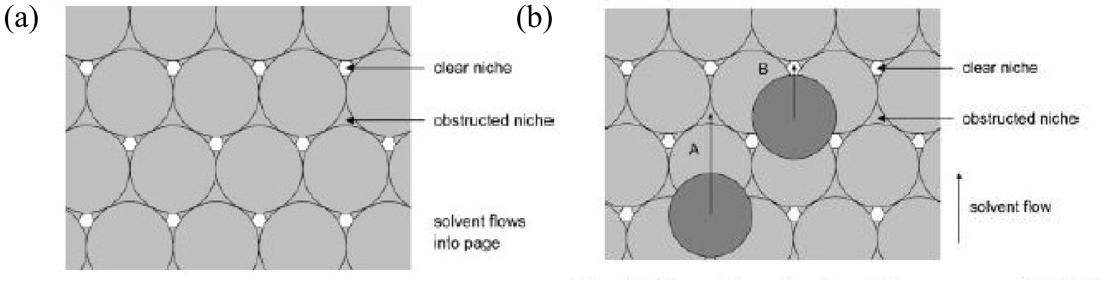

Fig. 2- 5 A schematic diagram illustrating the behavior of particles by solvent flow along upward direction. Both clear and obstructed niches are possible packing sites for the moving particles. [13]

Table 2- 1 A list showing the IEP point of some ceramic materials [16]

Materials	**IEP**
WO_3	0.43
SiO_2	1-3
Soda lime silica glass	2-3
Potassium feldspar	3-5
SnO_2	4-6
Zirconia	4-6
Apatite	4-6
TiO_2	4-6
Kaolin	5-7
Mullite	6-8
Cr_2O_3	6-7
Fe_2O_3	8-9
Al_2O_3	6-10
ZnO	9-10
$CaCO_3$	9-10
MgO	12

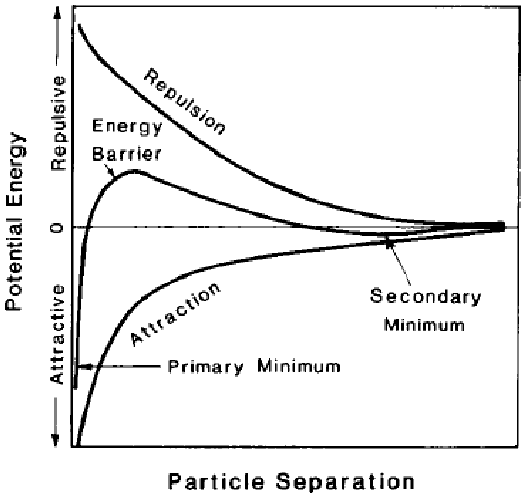

Fig. 2- 6 A potential diagram representing the net force resulting from summation of repulsive force (electric double layer) and attractive force (ven der Waals force). [16]

2.2 Luminescence Properties

The main application for phosphors is for image displays. TV is the most common one. A CRT (cathode ray tube), in which phosphor coating on the screen, could be excited by accelerated electron beam, and emit light in the different colors. Red, green, and blue (RGB) are three basic optical elements that can create various colors visible to eyes. Red color can be generated by Y_2O_3:Eu. For green one, Cd_2O_2S:Tb and Y_2SiO_5:Tb are reported in literature. As for blue one, ZnS:Ag is the best. Several potential phosphors with Tm^{3+}, Ce^{3+} and Eu^{2+} activators are still investigated [24]. Table 2- 2 lists several green phosphors and their properties. However, in the last 10 years of 20th century, CRTs displays become less common. In the contrary, flat panel displays (FPD) becomes popular with its advantages of low power consumption and light weight. FPD generally includes liquid crystal displays (LCD), plasma displays (PD), field emission displays (FED), and electroluminescent displays (ELD). Among those, the ELD shows the longest operation life time (more than 50,000h) with less luminescence decay [24].

Briefly speaking, luminescence properties could be divided into three categories: photoluminescence (PL), electroluminescence (EL), and cathode luminescence (CL). As ceramic oxide based phosphors are concerned, there are two materials that we are interested in, host material and activator [25]. The host materials are usually insulators or semiconductors (with the band gap of about 1.5-3.0 eV), and have to be optical inert.

Therefore, it could allow the inlet energy (e.g. UV light) exchanging by activators with limited energy loss. Aluminate ($MAlO_3$), silicate ($MSiO_4$), indiante ($MInO_3$), galliante (MGa_2O_4) and phosphate (MPO_4) are common ones that have been selected for host materials. As the activators, transition metals and rare earth elements are currently chosen due to their electron configuration with full or just half occupied orbital, e.g. Mn^{2+}, Tb^{3+}, and Eu^{3+}. Activators that doped in host materials induce substitutional defects if the ionic size and valence is not fully match. Thus a limitation of activators selection is concerned. The ion radius of substitutional ions and host cations should match one to each other. Otherwise, the lattice will suffer a residual stress. Table 2- 3 shows ionic radius of some cations with a coordination number (CN) of 4. All of the luminescence properties follow Stokes law or Stokes shifts, [26] which a higher energy (E_a) is adsorbed, and photons (hv) or heat (ΔH) are emitted or dissipated. Luminescence is described in more details as consisting of the following steps: (1) energy adsorption, (2) excitation of activators, as to form excited states, (3) relaxation of heat from excited states by lattice vibration, and/or (4) emission of lower energy photons, and relaxed to ground state.

The sources of activation energy able to create visible light emission include UV light (for PL), electric field or current (for EL), or accelerated electrons (for CL). For the case of PL, the electrons on their ground states adsorbed energy of. UV light, and being excited to excited states, which correspond to un-occupied orbital existing in transition metals or rare earth elements. The band-gap between the states defines the emission wavelength of PL spectra.

For the case of EL, a typical thin film electroluminescence (TFEL) device was fabricated to a sandwich structure (or so called “M-I-S-I-M structure”), which composed of electrode, dielectric layers, phosphor layer, dielectric layers, and another electrode, as shown in Fig. 2- 7. Of course, at least one electrode must be transparent that the generated light is capable of emitting from the device. ITO (In-Sn-O) glass is the most common material that is used for one electrode. The other electrode is usually established by metal, especially aluminum which is cheap and able to fully reflect emitted light. Then, the insulators are coated or deposited on the electrode whatever by spin coating, vapor deposition methods or else.

In order to satisfy the activation mechanism of EL device, several properties for selection of capacitor are necessary, high dielectric constant, high electric field strength, and uniform thickness [27]. In the original state (i.e. no energy is applied), the insulators and phosphor layer act as three capacitors in series as Eq. 2.1:

$$\begin{aligned} \frac{1}{C} &= \frac{1}{C_i}\times 2+\frac{1}{C_p}=\frac{2C_p+C_i}{C_iC_p} \\ \therefore C &= \frac{C_iC_p}{2C_p+C_i} \end{aligned} \qquad \text{(eq. 2.1)}$$

where C is the total capacity of the system, C_i and C_p are the capacitance of insulator and phosphor layer, respectively. As the electric field increases, phosphor will break-down when a threshold voltage of the material is achieved. Thus, the equivalent circuit of the M-I-S-I-M structure could be seen in this circumstance as two capacitors in series (phosphor layer could be treated as a simple resistor). Therefore, the total capacitance could be expressed as eq. 2.2.

$$\begin{aligned} \frac{1}{C} &= \frac{1}{C_i} \times 2 \\ \therefore C &= \frac{C_i}{2} \end{aligned} \qquad (2.2)$$

Generally, if there is a material which generates light with an applied current, this light emission is so called as electroluminescence. Usually, in a semiconductor, a doped material with p-n junction has separated electrons and holes (and also can be generated by impact of energetic electrons accelerated by electric field). Electroluminescence is a result due to the recombination of electrons and holes and thus releases the energy as visible light [29]. There are four steps that describes the mechanism of EL: [28]

1. electrons tunnel from the insulator/phosphor interface
2. electrons are accelerated to be energetic
3. the energetic electrons impact-ionize the luminescent center or create electron-hole pairs that lead to the activation of the luminescent center
4. the luminescent center relaxes toward the ground state and emits visible light.

The required electric filed for operating an EL device at a frequency that high enough to prevent from flicker for human eyes should be over than 60 Hz, and thus the applied field must be >2x10^8 V/m [27]. This correspondent electric field created a voltage drop (a basic threshold voltage) across a phosphor layer of 500 nm could be easily calculated by Eq. 2.3, where V is voltage drop; E is applied electric field; and s is the thickness of phosphor layer:

$$V = \int E \cdot ds \qquad (2.3)$$

For the case of CL [30], the mechanism for CL is quite different form the above two. First, we will have an equipment to generate electrons with high velocity and voltage, such as CRT or field emission gun. In order to lower the threshold voltage, a vacuum environment is required. As the accelerated electrons strike samples, the surface creates electron-hole pairs. The separated p-n pairs will recombine together due to the attraction form Coulomb force at the p-n junctions [32]. Therefore, the electrons and holes encounter one another and continuously recombine if a reverse bias does not exist. Energy releasing occurs and could be expressed as the following equation:

$$eletrons + holes \rightarrow energy \qquad (2.4)$$

When the released energy is in visible spectrum, then we call this as cathode luminescence (CL). The released visible light could be observed by naked eyes. The photons could be also collected by PMT (photomultiplier tube) and transformed into electron signal.

Table 2- 2 Green phosphors that have been used for optical instruments and their performance. [24]

Materials	Brightness	Color purity	Temp. stability	Operation lifetime	Chemical stability
Zn_2SiO_4:Mn	Normal	Good	Good	Normal	Good
Cd_2O_2S:Tb	Good	Normal	Bad	Good	Good
Y_2O_3S:Tb	Good	Normal	Bad	Good	Good
Y_3AlO_{12}:Tb	Normal	Bad	Good	Good	Good
Y_2SiO_5:Tb	Normal	Good	Good	Good	Good
LaOBr:Tb	Good	Bad	Good	Good	Bad
$InBO_3$:Tb	Normal	Good	Good	Good	Good
$SrGa_2S_4$:Eu	Good	Good	Bad	Good	Bad
CaS:Ce	Good	Good	Good	Good	Bad

Table 2- 3 Radii of some ionic species existed in crystals with CN = 4 [55]

Ion	Radii (nm)	Ion	Radii (nm)
Ag^{+}	0.100	Hg^{2+}	0.096
Al^{3+}	0.039	In^{3+}	0.062
As^{5+}	0.034	Li^{+}	0.059
B^{3+}	0.011	Mg^{2+}	0.057
Be^{2+}	0.027	Mn^{2+}	0.083
C^{4+}	0.015	Mn^{4+}	0.039
Cd^{2+}	0.078	Na^{+}	0.099
Co^{2+}	0.058	Nb^{5+}	0.048
Cr^{4+}	0.041	Ni^{2+}	0.055
Cu^{+}	0.060	P^{5+}	0.017
Cu^{2+}	0.057	Pb^{2+}	0.098
Fe^{2+}	0.063	Sn^{4+}	0.055
Fe^{3+}	0.049	Ti^{4+}	0.042
Ga^{3+}	0.047	Zn^{2+}	0.074
Ge^{4+}	0.039		

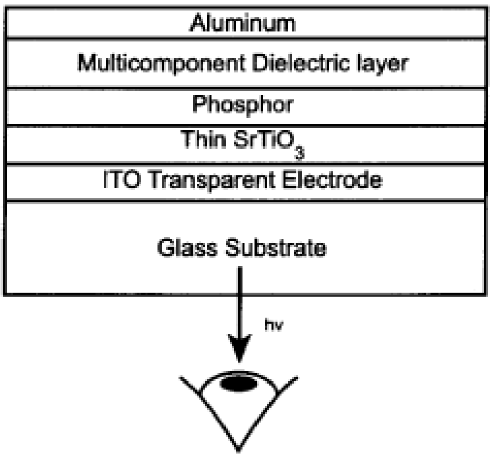

Fig. 2- 7 Structure of an EL device. The thickness of the phosphor layer in this case is about 700 nm. [31]

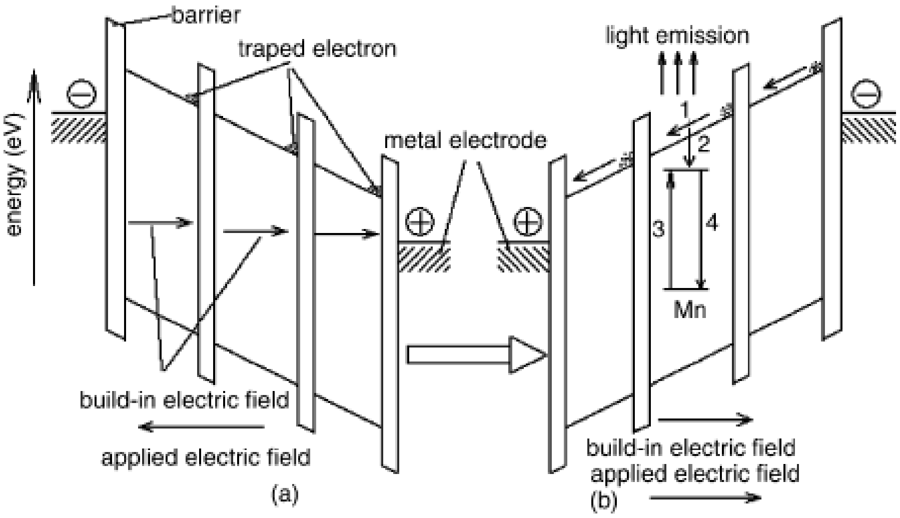

Fig. 2- 8 A schematic diagram showing EL mechanism in an EL device. [28]

2.3 Synthesis of Core-Shell Structures

Coating of colloidal particles with a layer of different material is used as a convenient way to modify the surface chemistry, reactivity, catalytic, optical, or magnetic properties of the particles. Such CS (core-shell) particles can be prepared either by controlled precipitation of inorganic precursors onto core particles or by other methods [33].

Colloidal particles with a low-index core and high-index shell, such as titania, are the suitable precursor for photonic crystals. The articles provided that the CS particles can be made monodispersive with a smooth coating [34]. Particles coated with titania are generally exceptionally difficult to synthesize because most of the titania precursors are highly reactive, making the steps difficult to control as precipitation [35]. Used titanium alkoxide in non-aqueous solvents as the precursors, only a monolayer of titania was deposited on copper, zinc oxide, silica, and gold nanoparticles by the hydrolysis of the alkoxide. The concentration of the reactants needed to be well controlled because high concentrations easily leaded to particle aggregation or formation of second titania particles.

Generally speaking, there are several ways to synthesis core-shell structure. For example, hydrothermal method, layer-by-layer method, osmotic swelling method, sol-gel method, and water/oil/water emulsion method are the most common techniques reported in literature. These techniques are applicable to synthesize polymer core of polystyrene particles coated with titania, iron, silica-core alumina-shell, etc. [36-39].

2.3.1 Hydrothermal Method

The synthesis of submicron powders and thin films by hydrothermal method has been reported by Walton *et al.* [40], who indicated that there were two extremely models controlling the formation mechanism of t-$BaTiO_3$. One was a homogenous solution phase reaction between titanium and barium hydroxyl anions by the dissolution- precipitation mechanism. The other is the reaction between solid titania and soluble barium salts (the in-situ heterogeneous transformation mechanism). The advantage of this method is appreciated to create the products at lower temperature. The products with good crystallization and uniform chemical composition can be obtained due to the homogeneous solution during the whole reaction.

2.3.2 Layer-by-layer Method

Layer-by-layer method is a kind of processing mechanism, by which the core and shell materials would be able to be attracted by each other. When these two materials dispersed in solvent, the surface of the coating materials (normally in smaller scale) will react with the solvent (for example, water) and become partial positively or partial negatively charging [41]. Therefore, base on the opposite charges, the coating material could coat on the core electro-statically. In addition, if the core is consisting of polymeric materials, then the core can be removed by calcination, or by dissolved in selected organic solvent to obtain a hollow sphere.

In Zhang's study [42], they used PS, silica, and tetrabutyl titanate (TBT) to synthesize well-defined spherical silica-core PS-shell nanoparticles (SiO_2-PS-CSNs). The TBT was added into the sulfonated SiO_2-PS-CSNs with ethanol and then hydrolyzed to allow TiO_2 nano-particles coating on the surface, as the schematic diagram shown in Fig. 2- 9. The original size of SiO_2-PS-CSNs is about 330 nm. After coating and calcination, the products experienced 29% shrinkage, and the TiO_2 shell is 28 nm in thickness, as TEM micrographs shown in Fig. 2- 10. Besides, there is a silica layer which could be observed by TEM. Therefore, this method offered the possibility to construct double functional hollow spheres.

2.3.3 Osmotic Swelling

Osmotic swelling is starting from a nucleus on which coated with carboxylic function group. First, there is a hydrophobic monomer attached on the nucleus, when the base is added into the system, the core becomes a carbonate ($R\text{-}COO^-$), then the part with carbonate group will be pulled to the surface of the shell due to the solubility of the carbonate group in the water is much greater than a carboxylic acid (R-COOH) [43]. The hydrophobic shell will be pushed to the core. Finally, the core-shell structure becomes denser.

2.3.4 Sol-gel Method

In general, alkoxide is used as a precursor, which reacts with water, undergoing hydrolysis and condensation reaction. The Fig. 2- 11 illustrates a basic concept of sol-gel reaction that started from a metal alkoxide solution. If silica is synthesized as an instance, the mechanism could be described as follow: [44]

Hydrolysis: $\equiv SiOC_2H_5 + H_2O \Leftrightarrow \equiv SiOH + C_2H_5OH$

Condensation: $\equiv SiOH + \equiv SiOH \Leftrightarrow \equiv SiOSi \equiv + H_2O$

$\equiv SiOC_2H_5 + \equiv SiOH \Leftrightarrow \equiv SiOSi \equiv + C_2H_5OH$

Oxide materials made by sol-gel process have good performance on homogeneity, optical transparency, wearing resistance, and widely applied on various technical products.

In Wang's study [38], they used α-alumina slurry and TEOS as starting materials. The alumina slurry was diluted with ethanol to a suspension with 1~5% solid loading. Then, the tetraethyl orthosilicate (TEOS) was dissolved in ethanol. Ammonia was used as reactor by adjusting the pH value to 11 at 50~75℃. Core-shell particles were collected after centrifuged and washed. In this case, the thickness of uniform silica layer coating on alumina particles was about 20 nm observed by TEM. No individual sol particles were found. The coating was a heterogeneous nucleation process. The SiO_2 was surely bonded with the Al_2O_3 particles.

2.3.5 Water/oil/water (W/O/W) Emulsion

There are two phases in the beginning, water phase and oil phase. One surfactant was used to make latex. Then, another latex was added to obtain a w/o/w solution. After drying, the water phase in the center will disappear and a hollow particle presented, as shown in Fig. 2- 12.

In Kim's study [45], the latex A consisted of SLS (sodium lauryl sulfate), $Na(PO_3)_6$, APG (Glucopen), water. The latex B contained MMA (methacrylate), EGDMA (ethylene glycol dimethacrylate), UA (urethane acrylate), Span 80 (sorbitan monooleate) and water. All ingredients of mixture A were dissolved in a container with a stirrer. The water-in-oil emulsion, which was prepared by sonification of mixture B, was dropped into the mixture A. Thus the w/o/w emulsion was prepared. Then, emulsion polymerization was carried out at 60 °C for 4 h. The precipitate was washed and dried. In this study, it was concluded that PMMA hollow particles can be prepared by w/o/w emulsion polymerization. The increase in the viscosity and the hydrophilic of the monomer mixture caused by UA prevented the droplets coalescence during polymerization, and helped to form a multi-hollow particle.

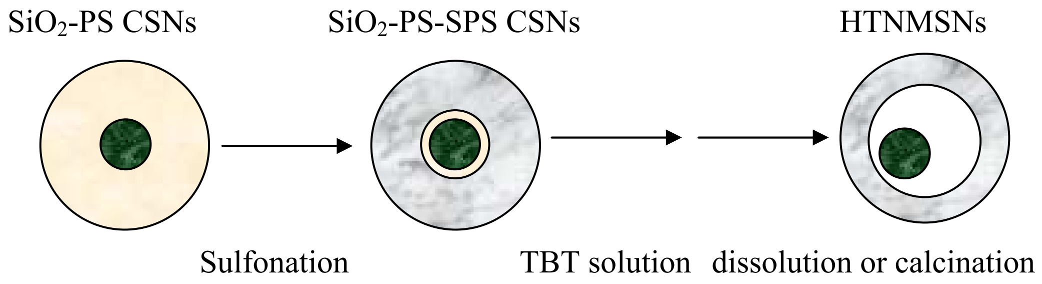

Fig. 2- 9 Schematic diagram indicating the processing steps to prepare hollow core-shell particles with layer-by-layer method. [42]

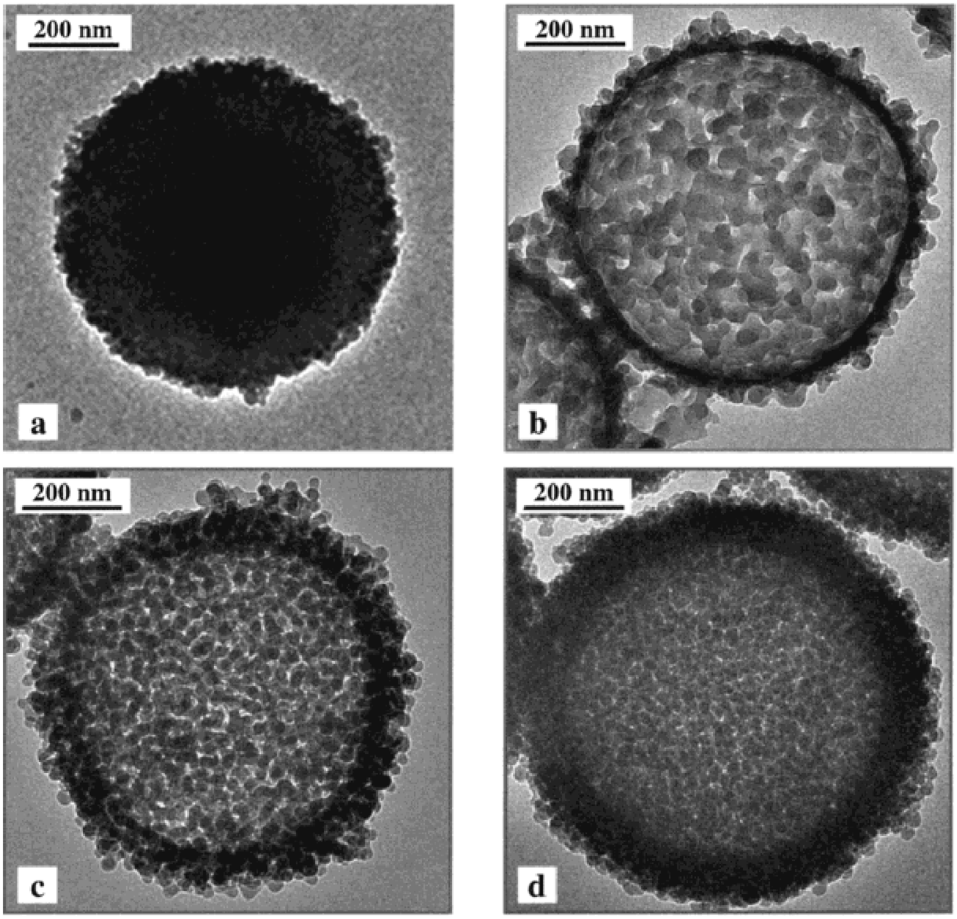

Fig. 2- 10 TEM micrographs showing the (a) $(SiO_2/PDADMAC)_2$-coated PS latex particles and hollow silica spheres after calcination with (b) one, (c) two and (d) three layers coating. [42]

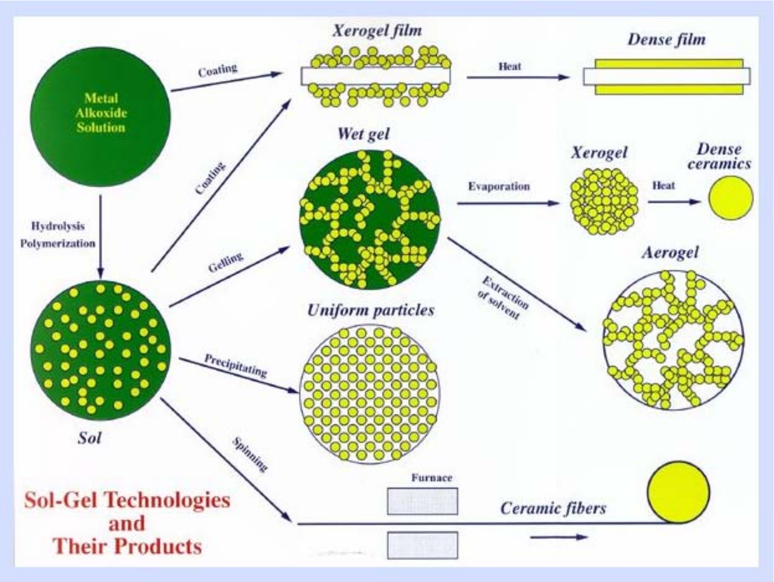

Fig. 2- 11 Schematic diagram illustrating a sol-gel reaction resulting in the products of different morphologies. [46]

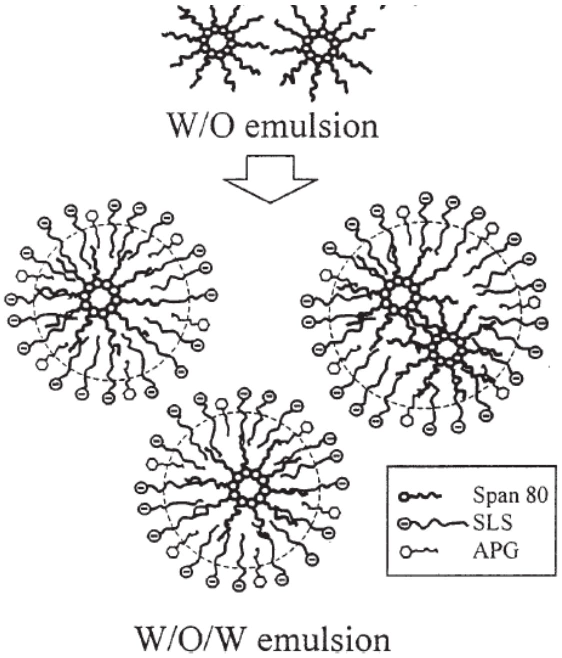

Fig. 2- 12 Schematic diagram representing the reaction steps of W/O/W emulsion. [45]

2.4 Synthesis of Zn_2SiO_4:Mn Material

Oxide phosphors have been practically used for fluorescent lamps, field emission displays, and plasma display panels. With the better chemical stability which leads to a longer operation life time and also the low toxicity compared to sulfate-based or polymer based phosphor materials (such as ZnS and organic-based LED), ceramic oxide phosphors materials are being more and more popular. The manganese doped zinc silicate is one of these materials that are going to be discussed.

Zinc silicate, or the so called willemite, is a phosphor belonging to the rhombohedra structure with the density=4.221 g/cm^3 [46], having the cell parameters of a=b=c=0.86280 nm and $\alpha=\beta=\gamma=107.87^o$ and coordination number of 4 [47]. The crystalline structure of willemite was shown in Fig. 2- 13. It's easy to see that each of Zn and Si ion bonding with 4 O^{2-} ions and thus a tetrahedron is formed. Since the Mn and Zn ions have similar ionic radius (Mn^{2+}=0.083 nm and Zn^{2+}=0.074 nm) [55] and also the same coordination number of 4, Mn^{2+} ions are easily to diffuse into Zn_2SiO_4 system during heat treatment to substitute Zn^{2+} ion and then becomes a solid solution which could be marked as $Zn_{1-X}Mn_XSiO_4$ or Zn_2SiO_4:Mn. The Mn-doped zinc silicate has photoluminescence with the applied energy, for example, UV light, the $3d^5$ electron in Mn will be exited.

In the case of photoluminescence, an applied UV source is required. As everyone knows, the Mn-doped zinc silicate has a 520-530 nm green light emission and could be observed by our naked eyes. Also, the electroluminescence property presents if there is an applied electric field as Fig. 2- 14.

There are several processes to synthesis Zn_2SiO_4:Mn. Solid state reaction, sol-gel, and hydrothermal method are the well known processes that were be applied commonly. Most of them prepared Zn_2SiO_4:Mn in a thin film on various substrates, e.g. glass, silicon wafer, ITO (indium-tin oxide).

2.4.1 Zn_2SiO_4 Powders

In 2000, Ahmadi et al. synthesis Zn_2SiO_4:Mn by hydrothermal method at low temperature (<250^{o}C) without heat treatment to prevent formation of agglomeration and changing of valence state at elevated temperature [50]. $(CH_3O)_4Si$, water and ammonia were mixed and having a hydrolysis reaction for an hour in a container. And then, a designed ratio of manganese and zinc chloride were added into the container and placed into an autoclave with nitrogen has been bubbled in (to maintain the system in an inert atmosphere). The autoclave was heated to 250^{o}C for 4 hours. The solution after the reaction was centrifuged and the supernatant was discarded. Finally the product was dried in an oven at 120^{o}C and then being analyzed. The Zn_2SiO_4:Mn products were observed in this study. Fig. 2- 15 is the TEM micrograph that shows the morphology of

Zn_2SiO_4:Mn made by this method. Two structures were found: the spherical one had an average diameter of 150 nm; the acicular particles had widths from 20-50 nm with the length range form 200-600 nm. The reason to the different particle shape may be resulted from the molar ratio of ammonia to zinc: if the ratio is lower than 1.7 then the spherical particles were formed; if the ratio is more than 4.9, then the acicular particles were presented.

Since the willemite is non-dissolvable in water, thus the Zn_2SiO_4:Mn powders could be dispersed in water with ultra sonic bath and with limited agglomerations. The suspension has a great polydispersity up to over than 25%, this phenomena was resulted form the two different morphologies (spherical and acicular shape) as which has been mentioned in the previous paragraph. The contribution of this research is the low temperature synthesis process. Crystallization formed as the reactants mixed in the autoclave at about 250^{o}C instead of high temperature annealing and provided Zn_2SiO_4:Mn particles with green light emission under applied UV light.

A similar process was applied to synthesis the Zn_2SiO_4:Mn phosphor by sol-gel method. Thomas and his coworkers demonstrated their process in a basic solution, too [51], which included TEOS, $Mn(CH_3COO)_2$ and $Zn(CH_3COO)_2$ as precursors. The "seeding" process was applied which completed by mixing those precursors to form a gel with ammonium polyacrylate (APA) and polyoxyethylene sornitan monooleate

($C_{12}H_{10}ClNO_3$). This seeding process leaded to a greater crystalline phase and a larger mean particle size (30=>180 nm).

A typical method for preparing Zn_2SiO_4:Mn is mixing both ZnO and SiO_2 powders together and firing at elevated temperature with about 2% Mn-doping. The precursors for solid state reaction perhaps are: oxidized wafer or SiO_2 powder for Si; ZnO, $Zn(NO_3)_2$ or $Zn(CH_3COO)_2$ for Zn^{2+}; and $Mn(NO_3)_2$, $Mn(CH_3COO)_2$, $Mn(CO_3)_2$, or MnO for Mn^{2+} [49, 50, 56, 57]. Base on the phase diagram in Fig. 2- 16, it's obvious to see that the pure zinc silicate phase formed at the molar ratio of Zn/Si=2:1. In fact, the homogeneity of powder mixing limits the purity of product. In other words, there should be either ZnO or SiO_2 phases left after reaction unless the annealing temperature is high enough or even the whole system becomes in liquid state. Higher heat treatment temperature costs a lot.

Adding flux into this system may be a good way to solve this problem. In Kitai's study [31], ZnO, SiO_2 and MnO were mixed with the addition of lithium fluoride (LiF). The mixture was annealed at 800-850^{o}C in argon atmosphere and then Zn_2SiO_4 was obtained. The reaction progress was examined by the differential thermal analysis (DTA). Fig. 2- 17 showed the results of two exothermic peaks: the first one may be the transition state, which indicated that an intermediate compound was formed at 630^{o}C (the exactly phase was not mentioned in this literature, however), and the other one was the reaction of ZnO reacted with SiO_2 and become Zn_2SiO_4 phase occurred at 650°C. Compared to the sample without LiF, the result shows a stronger exothermic behavior, and the reaction occurred at the temperature approaching to 1000°C. So, the difference of flux adding or not was apparent.

Besides, adding flux into this system not only decreased the reaction temperature but also improved the brightness and efficiency on electroluminescence property. In Fig. 2- 18, the LiF was concerned. It’s easily to find that with the more flux doping, the brightness and efficiency raised up 33-50% at the 300 V applied voltage with frequency at 60 Hz. There are still some other flux that have been tried, including NaCl and K_2SO_4, which were also successfully reduced the reaction temperature on forming Zn_2SiO_4:Mn. However, these materials did not be mentioned too much in Kitai’s study.

2.4.2 Zn_2SiO_4 Thin Film

Silicon-based opto-electric materials were also studied. The thin film zinc silicate was wildly used in optical application. Yun *et al*. [59] created phosphor thin film via chemical (precursors) solution depositing on ITO plates, and also, some other substrates were tried: Kitai [31] and Minami [60] constructed oxide phosphors EL devices like a sandwich structure (i.e. electrode/dielectric layer/phosphor layer/dielectric layer/electrode) with the dielectric layers composed of $BaTiO_3$, $SrTiO_3$ or else. The thickness of the phosphor layer and dielectric layers ranged of 0.2-1 and several μm, respectively. Wafer is a common substrate that has been used in lots of researches. Taghavinia [57] synthesized Zn_2SiO_4 on porous silicon layers. The solution that contains Zn and Mn salts was deposited on the silicon and then followed bt heat treatments. Ji [52] fabricated the zinc silicate thin film coated on oxidized silicon wafer by spin coating. Silicon wafer was set to be the substrate and being annealed at 1100°C to be oxidized into SiO_2. This SiO_2 layer was controlled to be less than 130 nm. The liquid solution contained $Mn(CH_3COO)_2$ and $Zn(CH_3COO)_2$ which dissolved in 2-methoxyethanol and a little bit of monoethanolamine ($NH_2CH_2CH_2OH$). The reaction was completed at 60°C for 1 hr with stirring. Then, the solution was spin-coated on the surface of the substrate with the rotation speed of 5000 rpm. The film was dried and then annealed between 800-920°C for 4 hr in air. In this case, ZnO phase appeared first after 800°C annealing. With the increasing annealing temperature, the ZnO would react with silica substrate and thus transformed into zinc silicate (willemite) phase as Fig. 2-19. For the samples processed at the temperature higher than 920°C, the willemite phase was presented instead of ZnO with the rhombohedral structure which could be identified by X-ray diffraction. The surface morphology was also observed by SFM (scanning force microscopy). The surface was covered with the densely coated Zn_2SiO_4:Mn with the grain size about 100 nm. The surface roughness was measured:

only 30.88 nm in the area of 2*2 μm^2.

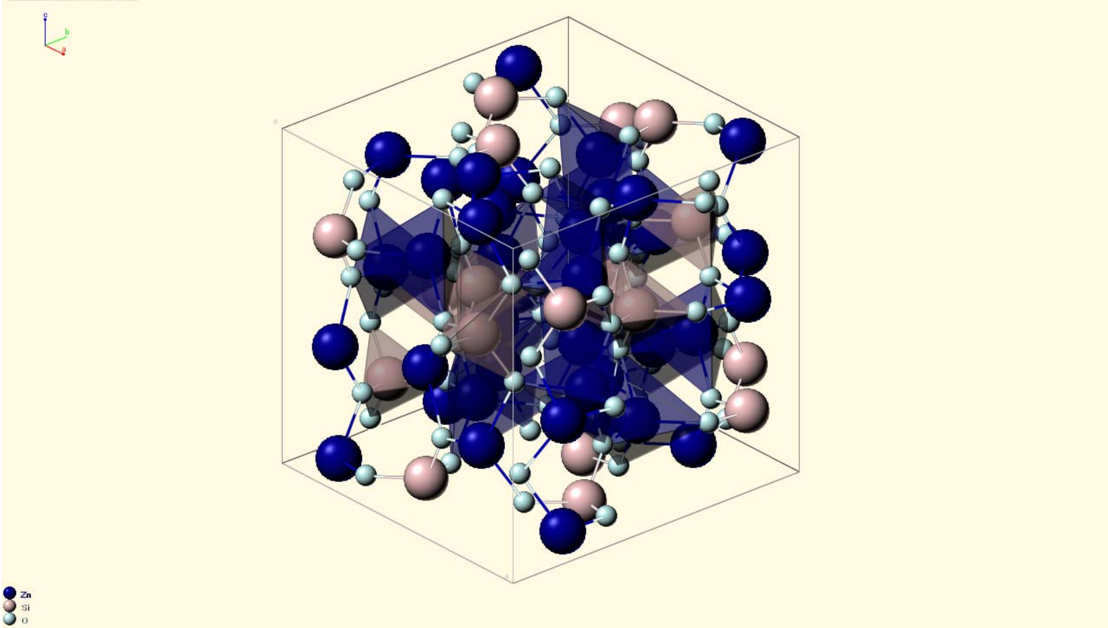

Fig. 2- 13 Crystal structure of willemite unit cell in this diagram represents the positions of Zn (dark balls), Si (light balls), and O (small balls) ions in this system. [53]

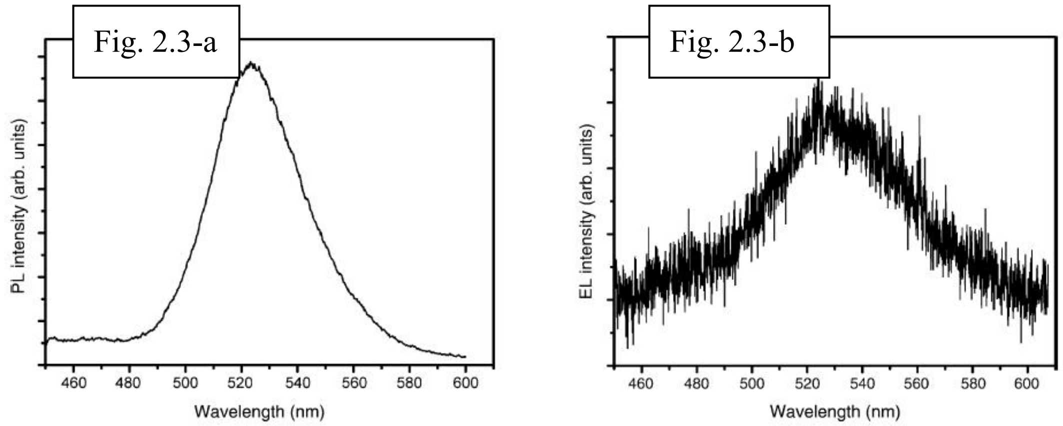

Fig. 2- 14 Two figures showing the PL and EL spectra, respectively. The PL and EL spectra of Zn_2SiO_4:Mn was coated as a thin film on wafer. [49]

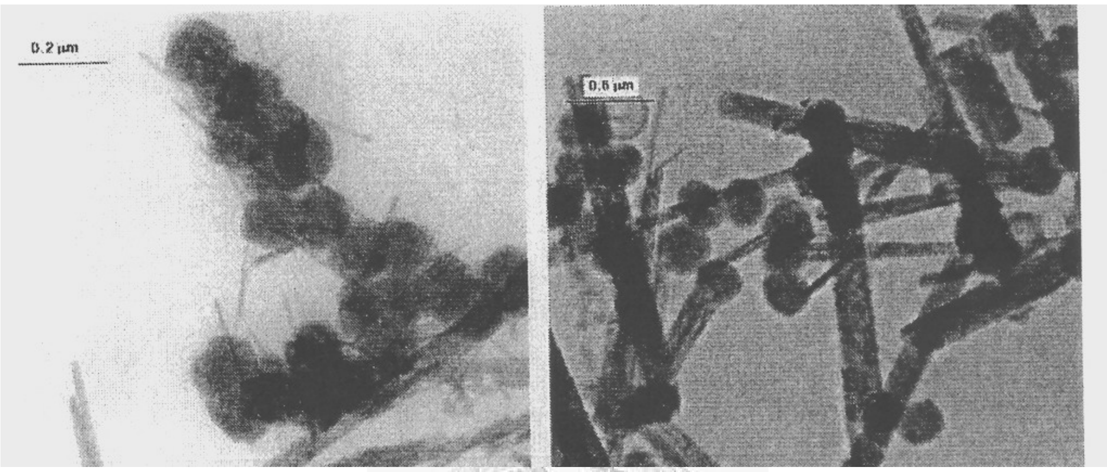

Fig. 2- 15 TEM images showing the Zn_2SiO_4:Mn made by Ahmadi's method contains both the spherical and acicular shape. [50]

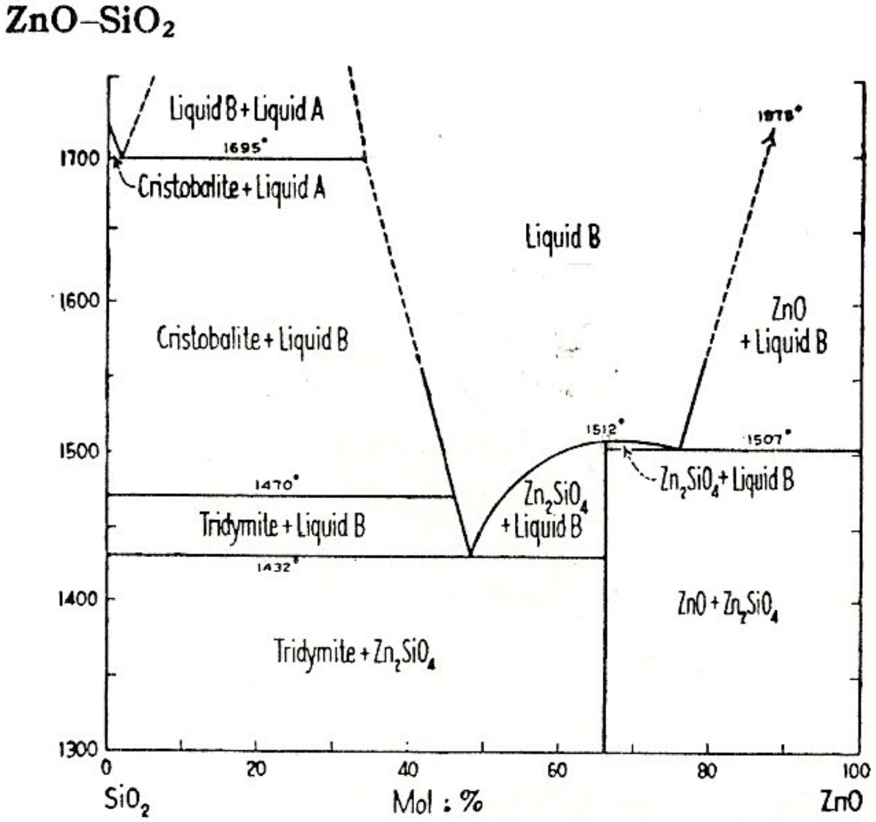

Fig. 2- 16 Phase diagram of ZnO-SiO$_2$ system. [56]

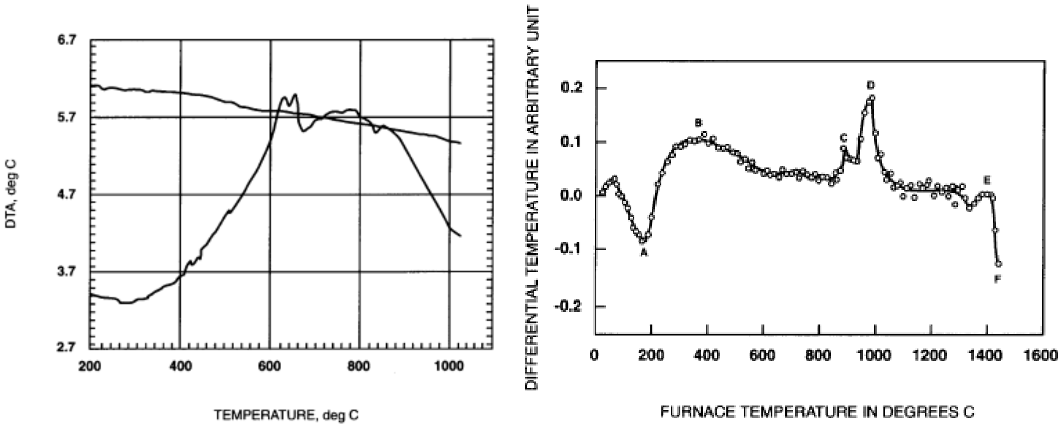

Fig. 2- 17 DTA results of the ZnO-SiO_2 mixture with LiF (left) and without LiF (right). The reaction temperature was reduced by adding flux (LiF in this case) into the system. [31]

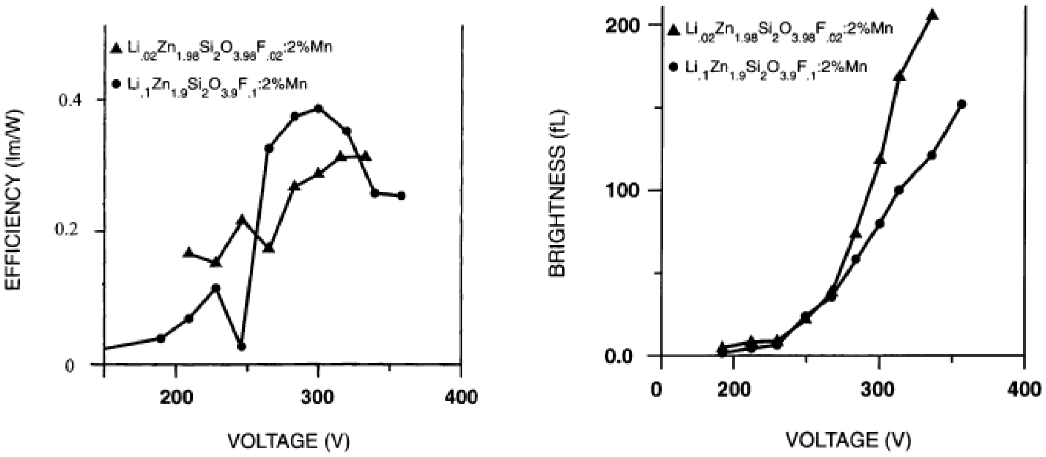

Fig. 2- 18 Two EL spectra showing the emitting brightness and efficiency versus applied voltage of Zn_2SiO_4:Mn with adding LiF as a flux. [31]

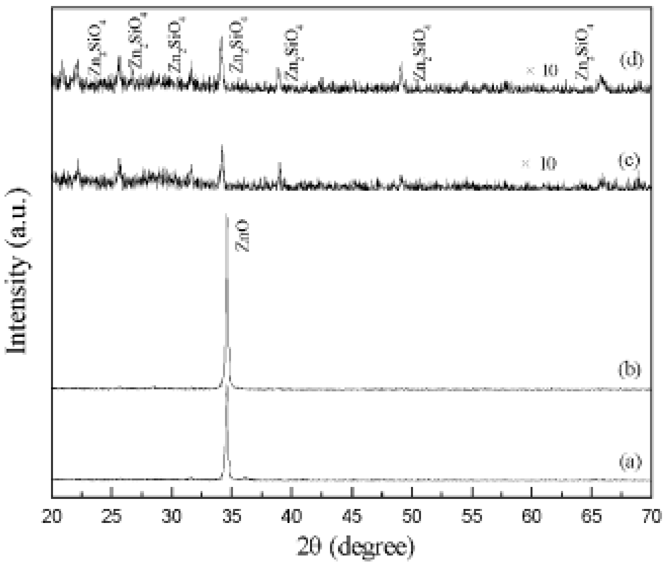

Fig. 2- 19 X-ray diffraction analysis of the samples illustrating phase transformation temperature. The annealing temperatures varied with (a) 800°C, (b) 840°C, (c) 920°C and (d) 980°C [52].

Chapter 3 Experimental Procedure

3.1 Materials

The starting materials used in this study included TEOS (tetraethyl orthosilicate, 98 wt%, ACROS, USA), NH_4OH (ammonium hydroxide, 28-30 wt%, ACROS, USA), C_2H_5OH (ethanol, 99.5% pure, SHIMAKYU, Japan), $Zn(NO_3)_2$ (zinc nitrate, which was prepared by dissolving ZnO powder in HNO_3 solution; ZnO powder (億研堂, Lot: 0213012306, Taiwan); HNO_3 solution (65 wt%, SHOWA, Japan), $Mn(NO_3)_2$ (98% pure, SHOWA, Japan).

3.2 Experimental Design

Fig. 3- 1 shows the flowchart of this study. The first part is to synthesize spherical silica particles in uniform size. These particles were used to react with Zn^{2+} and Mn^{2+} ion in order to form Zn_2SiO_4 shell on SiO_2 particles. The products are fabricated in different morphologies, e.g. powders or photonic-bandgap (PBG) crystalline templates, which were assembled to form optical-electronic device. Therefore, various properties, photo-luminescence (PL), cathode-luminescence (CL), and microstructure were investigated to correlate the properties of loose particles and PBG with their core-shell

microstructure.

3.3 Sample Preparations

First of all, submicron spherical silica particles were prepared by Stöber method, which included the following steps: First, dissolved TEOS in C_2H_5OH, then titrated the mixture with diluted NH_4OH solution until the formulation reached a volume ratio of TEOS: NH_4OH:C_2H_5OH = 24:25:450. This colloidal suspension was aged for 24 hr at room temperature. Then the precipitates were washed by de-ionized water and centrifuged for at least three times. The supernatant was discarded and the sediment (submicron spherical silica particles) was dried for next processing steps. Table 3- 1 lists the trial batches in this study. The processing methods include colloidal process, glass forming, hydrothermal method, SSR (solid state reaction), and PBG forming.

ZSpII case: The dired silica particles were re-dispersed in de-ionized water in a solid content of 1.0 wt% in ultrasonic bath to prevent from agglomeration, while the preparation steps of ZSpI were similar with that of ZSpII except re-dispersing in de-ionized water. 0.1M $Zn(NO_3)_2$ and 0.01M $Mn(NO_3)_2$ were added into the suspension in designed molar ratio. Then, the pH value of the mixture was titrated drop-by-drop by NH_4OH solution [61] to the pH range of 8.6-8.8. The mixture kept stirring during titration, so Zn and Mn ions could form nano-precipitation coating on the surface of the suspended silica particles. After the reaction, the suspension was either dried in an oven at 80°C for at least one day, or centrifuged to separate the coated silica from the suspension. Then the dried powders were annealed in furnace at various temperatures (800°C to 1200°C). Submicron spherical Zn_2SiO_4:Mn particles in some degree of agglomeration were obtained.

ZSpIII case: this process was suggested by Y. J. Chen [62], which started from ZnO-B_2O_3-SiO_2 ternary system. The powder mixture was turbo-mixed and then heated to 1300°C to form Zn-B-Si glass. Boron oxide (B_2O_3) in this system acted as a flux and used to lower down the glass forming temperature. The formula of the glass in this case was set as ZnO-B_2O_3-SiO_2 = 60:10:30. After quenching, the glassy frit was ground into powder and annealed at 800°C for several (0-10) hours. This idea is to grow Zn_2SiO_4 crystals from this frit at lower temperature. As the Zn_2SiO_4 is formed, acid-etching would be used to purify the annealed batch.

ZSpIV case: This method followed a hydro-thermal procedure, which started from the solution consisted of $ZnCl_2$ (ZnO pre-dissolved in diluted HCl solution) and $Na_2SiO_{3(aq)}$. Two reactants were mixed in Teflon tubes and heated by a micro-wave sample preparation system (Multiwave 3000, Anton Paar, Germany) with pressure = 60 bar, temperature = 240°C, and power = 1200 W for 4 hr.

ZSpV case: Fused silica and ZnO powders were mixed in a molar ratio of 2:1, i.e. 8.10 g of ZnO and 3.00 g of fused silica powder. The powder mixture was dispersed in alcohol as a suspension with 28 vol% of solid loading, then turbo-mixed for 24 h with a dopant of 5 mol% $Mn(NO_3)_2$ (based on ZnO). The dried mixture was annealed at specific temperatures.

ZSpVI case: the silica particles were naturally sedimented as an ordered PBG structure (a template), then the template was immersed in the solution consisted of $Zn(NO_3)_{2(aq)}$ and $Mn(NO_3)_{2(aq)}$ (Mn doping in this case was set as 5 mol%). This precursor was diluted with ethanol to several times so the diluted solution can wet the surface of template. After reaction, the coated PBG was annealed at specific temperature (600-1200^{o}C).

Preparation of disk samples: Some of SiO_2:Zn/Mn powder before annealing was die-pressed into a disk of 0.6 mm by a die-pressure of 40 kg/cm^2 (about 3.9 MPa) holding for 1 min. The sample mass was 0.05 g.

Preparation of an CL device: Zn_2SiO_4:Mn particles were send to 東元奈米應材 (TECO Nanotech Co., Ltd., Taiwan). The particles were first prepared as a paste, then the paste was screen printed on an ITO substrate with area = 0.25π cm^2 to be anode. This anode was heated to de-binder and then install in a vacuum chamber (under 3.0×10^{-5} torr) with cathode constructed by CNT (carbon nano tube). Fig. 3- 2 is a schematic diagram of this design. A DC current was applied to the whole device and thus we can observe the CL behavior and also the electrical property could be measured.

3.4 Characterization

3.4.1 Phase Identification by XRD

Crystalline phase identification was determined by X-ray Diffractometry (XRD, PW1710, Philips, Co., Eindhoven, Netherlands) with Cu K_α radiation. The analyzing parameters were set at 30 kV, 20 mA and 4^o/min. Samples which have been prepared as disks were fixed on sample holder by clay. The diffraction patterns were compared with JCPDS files (PCPDFWIN, v2.4, June, 2003, JCPDS-ICDD), and therefore the crystal structure could be identified.

3.4.2 Thermal Analysis by DTA

Thermal property of sample after coating was examined by Differential Thermal Analysis (1600 DTA, DuPond, USA) to determine the characteristic temperature of any phase transformation during heat-up of ZnO:Mn coated SiO_2 particles. About 10 mg of the powder was filled into Pt crucible and heated in open air atmosphere. The difference of the temperature between sample and Al_2O_3 standard was detected.

3.4.3 Zeta Potential Measurement

The calcined Zn_2SiO_4:Mn particles were dispersed in de-ionized water at a concentration about 100 ppm and aged for at least one day which lets the chemical equilibrium established between particles and water. Then we adjust the pH value of the suspension with 1M NaOH or HCl solution. The pH meter (SP-7, Digital pH Meter, SUNTEX) was used after calibration with standard buffer solutions of pH = 4.0 and 7.0, respectively.

Several pH values of the suspensions were selected. Zeta potential was measured by Zeta Meter 3+ (Lazer Zee Meter, Model 501, Bedford Hill, NY. USA.). The applied DC voltage was 100 V. The moving velocity of particles was measured to calculate zeta potential (ζ) according to the equation (3.1) [16], where V_e/E is electrophoresis mobility; ε_r is dielectric constant and f_H is Henry constant:

$$\zeta = \frac{f_H \eta V_e}{\varepsilon_r \varepsilon_0 E} \qquad (3.1)$$

3.4.4 Microstructural Analysis by SEM/EDS and TEM

Particles morphology was observed by Scanning Electron Microscopy (field emission SEM, model 1530, LEO Instrument, England) and Transmission Electron Microscopy (TEM, 100CX II, JEOL Co., Japan).

Calcined particles were dispersed in de-ionized water with ultrasonic bath. One drop of the suspension was placed on an Al stage and being dried in air. After that, the whole stage was coated with ultra thin Pt or C layer to improve electrical conductivity for SEM.

PBG crystals were polished by sandpaper and washed by alcohol with ultra sonic bath to remove contaminations on the sample surface. Then, the crystal was fixed on an Al stage by carbon tape and coated with thin Pt layer for SEM. The samples for TEM observation need a thin cross-section of < 200 nm. A small piece of assembled crystal was polished and adhered on a Cu grid as Fig. 3- 3. After ion milling (Precision Ion Polishing System, GATAN, model 691), the specimen was coated by C film for TEM.

The chemical composition was characterized by X-ray Energy Dispersive Spectroscopy (EDS), which is the accessory part of the Scanning Electron Microscope (field emission SEM, model 1530, LEO Instrument, England), operated with an accelerated voltage of 15 kV. The data was compiled and analyzed by t-student distribution [63].

3.4.5 Chemical Composition Analysis by ICP-AES and XPS

The absolute amount of each element in the Mn-doped Zn_2SiO_4 particles was examined by ICP-AES (Induced Coupled Plasma with Atomic Emission Spectroscopy, ULTIMA 2000, Jobin Ybo, France). Powder samples were dissolved in HF solution (hydro fluoric acid, 48 wt%, Merk, Germany) by a Microwave Sample Preparation Platform System (Multiwave 3000, Anton Paar, Germany) with an acid-digestion at 240^{o}C for 2 h. No solid residues were allowed in the solution after digestion. Then the solution was diluted to the range of STD calibrated solutions with 0, 5, 10, 20, and 100 ppm of Zn and Mn. The diluted solution was drawn and excited by high energetic plasma. The emission spectra resulting from ions releasing the adsorbed energy and thus the quantitative analysis could be obtained.

The valence state of doped Mn ions was determined by XPS (X-ray Photon Electron Spectroscopy, VG Scientific ESCALAB 250, England). The powder was die-pressed into disks. The surface was milled by ion gun to remove surface layer which may contain impurities. The X-ray was generated by XR5 monochromatic X-ray gun with Al target [64], and then ionized the electrons on sample surface. The binding energy of ions in the material could be measured so that the chemical composition and also the valence state of the elements can be determined.

3.4.6 Luminescence Property Analysis

The photoluminescence (PL) property was measured by Fluorescent Spectrometer System (USB2000, OOII rad, beta, Ocean Optics, USA) with 254 nm ultra violet light sources (MINERALLIGHT LAMP, UVGL-25, Upland, CA91786, USA). Samples were either die-pressed or assembled as a crystalline form and then placed in a cavity. The device is shown in Fig. 3- 4 and Fig. 3- 5. Data collection was set for 500 ms and ranged from 450-650 nm.

The visible cathode luminescence (CL) property was measured by TECO Nanotech. The light emission was collected by the detector, Luminescence color meter, Bm-7, TOPCON, Japan, and electrical property could be obtained by parallel connected with voltmeter or serial connected with current meter.

Table 3- 1 List of methods tried in this study.

	methods overview	***annealing temp.***
ZSpI (colloidal)	SiO_2 suspension reacted with Zn and Mn directly	1000^{o}C
ZSpII (colloidal)	dried SiO_2 reacted with Zn and Mn	800-1200^{o}C
ZSpIII (glass forming)	annealing of Si-Zn-B glass to obtain Zn_2SiO_4	1300^{o}C melting, Then 800^{o}C annealing
ZSpIV (hydrothermal)	$ZnCl_2$ and Na_2SiO_3 reacted in autoclave	240^{o}C
ZSpV (SSR)	co-fired of ZnO:Mn and SiO_2 powder mixture	900-1200^{o}C
ZSpVI (PBG)	assembled PBG reacted with Zn and Mn	600-1200^{o}C

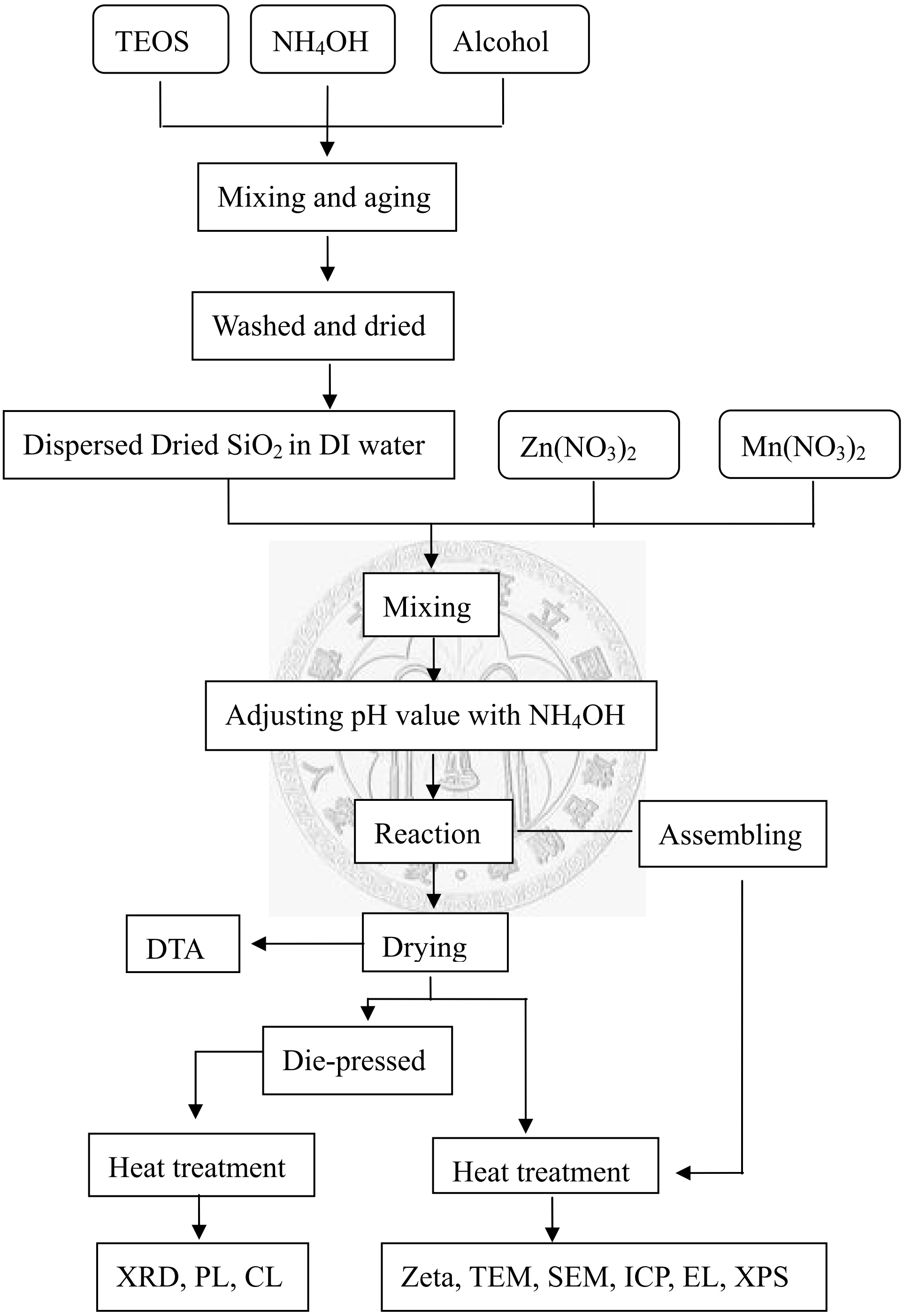

Fig. 3- 1 Experimental flowchart of this study.

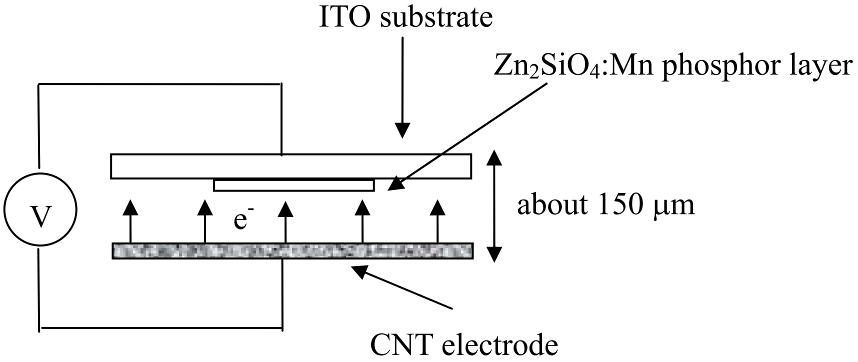

Fig. 3- 2 A schematic diagram of a CL device. CNT electrode acted as a field emission electron source. The electrons accelerated by applied DC power source then stroke on phosphor layer and thus generated light.

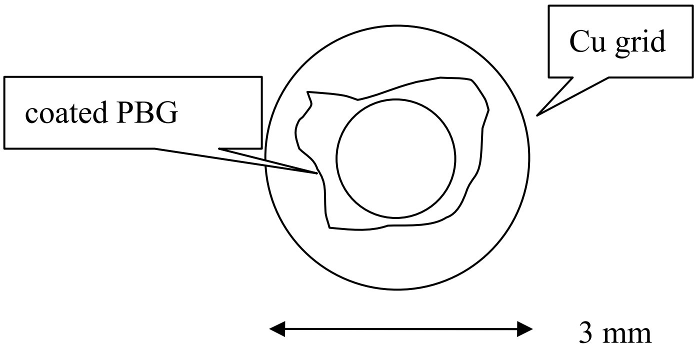

Fig. 3- 3 Schematic diagram of particles in G1 glue on a Cu grid.

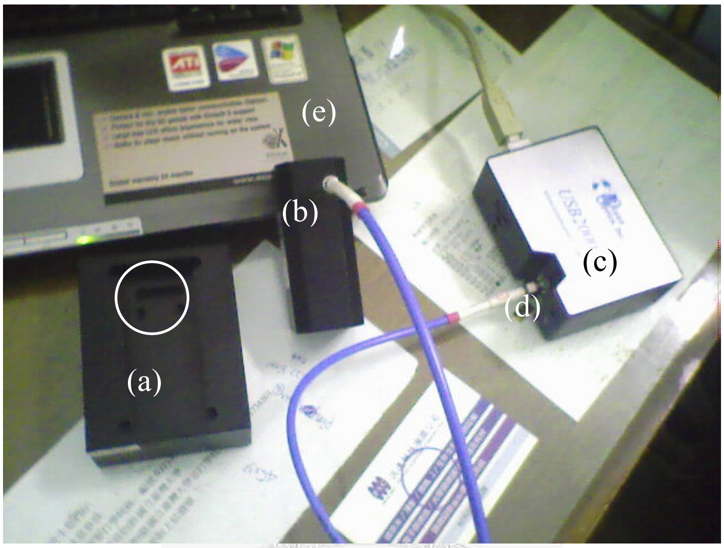

Fig. 3- 4 Image showing the fluorescent spectroscopy system with (a) sample cell, (b) detector (with optical fiber), (c) fluorescent spectrometer, (d) optical fiber connected to UV source, and (e) computer. The white circle is a cavity where samples could be placed in.

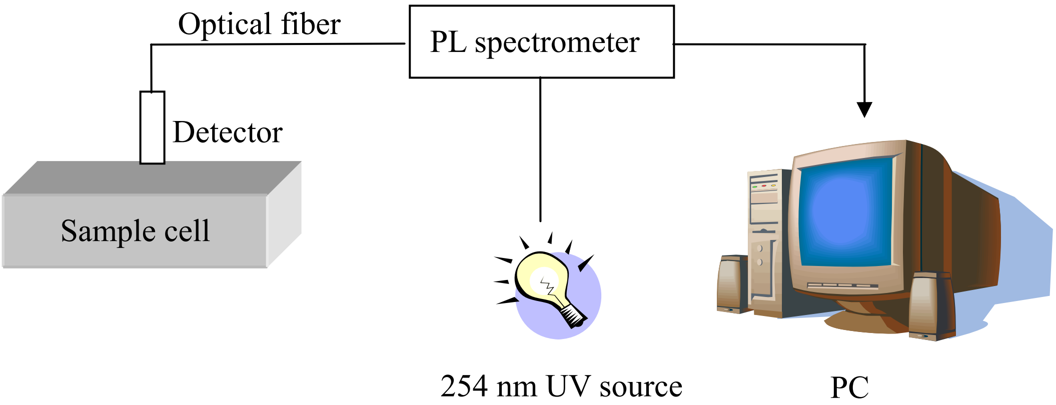

Fig. 3- 5 Block diagram representing the setting of PL measuring.

Chapter 4 Results

4.1 Synthesis of Zn:Mn Coating on SiO_2 Particles

Mn ions are the activators in Zn_2SiO_4 that is capable of generating green visible light under an applied UV source which has been mentioned in chapter 2. The optimal amount of Mn doping, that makes Zn_2SiO_4:Mn performing at a strongest light emission, have been mentioned by Kang and Park [65] as well as Cho and Chang [66]. However, Mn is a really active ion as a common sense; therefore it's easy to be associated that during heat treatments, Mn^{2+} is possible to evaporate from sample during heat treatment. Therefore, the Mn^{2+} content is possibly different from the designed amount of Mn-doping. In this study, several manganese nitrate ($Mn(NO_3)_2$) standard solutions were prepared in order to measure the concentration of calcined Zn_2SiO_4:Mn by comparing the emission spectra from standard one which has an emission peak at 259 nm. The result is shown in Fig. 4- 1. The measured concentration of Mn was always a little lower than the designed one, the reason to this result could be compared with Fig. 4- 2 and will be discussed in the next paragraph.

The behavior of titration during the coating process is also important. Fig. 4- 2 is the titration curve of the solution containing $Zn(NO_3)_2$, $Mn(NO_3)_2$, and SiO_2 particles, titrated with NH_4OH solution. It's obvious that the concentration of Zn ion have a sharp drop starting at pH = 7 and almost becomes to zero as pH value approaching to 9. The results revealed that zinc ions nearly precipitated as pH approaching to 9. In the other hand, the concentration of Mn ion became minimal at pH approaching to 11. If we consider the K_{sp} of $Zn(OH)_2$ and $Mn(OH)_2$, the K_{sp} are $3x10^{-17}$ and $2x10^{-13}$ at 298K, 1 atm, respectively [67, 68], then the equilibrium solubility of Zn^{2+} and Mn^{2+} could be calculated as following equations:

$$Zn(OH)_2 \Leftrightarrow Zn^{2+} + 2OH^-$$

$$K_{sp1} = [Zn^{+2}][OH^-]^2 = 3\times10^{-17} \qquad (4.1)$$

$$Mn(OH)_2 \Leftrightarrow Mn^{2+} + 2OH^-$$

$$K_{sp2} = [Mn^{2+}][OH^-]^2 = 2\times10^{-13} \qquad (4.2)$$

The initial concentration of $[Zn^{2+}]$ is 380 ppm in Fig. 4- 2. Therefore, we calculate the molar concentration if takes the atomic weight of Zn = 65.4:

$$[Zn^{2+}] = \frac{380\times10^{-6}}{65.4} = 5.810\times10^{-6}M \qquad (4.3)$$

And the equilibrium solubility of $[Zn^{2+}]$ under different pH values is:

pH = 7,

$$[Zn^{2+}] = \frac{3\times10^{-17}}{(10^{-7})^2} = 3\times10^{-3}(M) \qquad (4.4)$$

pH = 8,

$$[Zn^{2+}] = \frac{3\times10^{-17}}{(10^{-6})^2} = 3\times10^{-5}(M) \qquad (4.5)$$

pH = 9,

$$[Zn^{2+}] = \frac{3\times10^{-17}}{(10^{-5})^2} = 3\times10^{-7}(M) \qquad (4.6)$$

As the pH of solution approaches 9.0, the concentration of Zn^{2+} ion is over its solubility, and resulted in precipitation, as shown in Fig. 4- 2. Similarly, the initial concentration of [Mn^{2+}] is 17 ppm. The molar concentration of [Mn^{2+}] is calculated as below.

$$[Mn^{2+}] = \frac{17\times10^{-6}}{54.9} = 3.09\times10^{-7}(M) \qquad (4.7)$$

And the solubility of [Mn^{2+}] under different pH values is:

pH = 9,

$$[Mn^{2+}] = \frac{2\times10^{-13}}{(10^{-5})^2} = 2\times10^{-3}(M) \quad (4.8)$$

pH = 10,

$$[Mn^{2+}] = \frac{2\times10^{-13}}{(10^{-4})^2} = 2\times10^{-5}(M) \quad (4.9)$$

pH = 11,

$$[Mn^{2+}] = \frac{2\times10^{-13}}{(10^{-3})^2} = 2\times10^{-7}(M) \quad (4.10)$$

The similar results as the previous case is noted that the Mn^{2+} ions in solution should precipitate nearly complete and the concentration reduced to zero as the pH rises to 11. According to this result, the measured [Mn^{2+}] is always a little lower than the prepared value (in Fig. 4- 1).

Another titration experiment had been tried, and the titration curve is shown in Fig. 4- 3. 0.5 ml 0.1M $Zn(NO_3)_2$ dissolved in 20 g de-ionized water, then titrated with NaOH solution. $Zn(NO_3)_2$ could be treated as a binary acid, e.g. sulfuric acid (H_2SO_4), which is able to accept two OH^- per molecule in acid-base reaction. Therefore, there are two plateaus existing in Fig. 4- 3 due to the balances of eq. 4.11 and 4.12:

$$Zn^{2+} + OH^{-} \Leftrightarrow Zn(OH)^{-} \qquad (4.11)$$

$$Zn(OH)^{-} + OH^{-} \Leftrightarrow Zn(OH)_2 \qquad (4.12)$$

where the inversion points of the reactions are at pH = 4.8 and pH = 11.5, respectively. Comparing with the Fig. 4- 2 and Fig. 4- 3, it is concluded that the pH value we designed is suitable for Zn^{2+} coating or precipitated.

In order to investigate the behavior of Zn_2SiO_4:Mn particles dispersed in aqueous solution, a zeta-potential measurement was conducted. The result is shown in Fig. 4- 4. There is an iso-electric point (IEP) at pH = 2.7 measured from the curve in Fig. 4- 4. However, there's a potential abnormal in strong base condition, i.e. pH > 10. The possible reasons may be:

(1) dissolution of $Zn(OH)_2$, and resulting in a complex ion [67],

$$\begin{aligned} &Zn(OH)_{2(s)} + 2OH^{-} \Leftrightarrow [Zn(OH)_4]^{2-}{}_{(aq)} \\ &K_d = 5\times10^{-21} \end{aligned} \qquad (4.13)$$

(2) chemical reactions occurring on the particle surface [69],

$$Si(OH)_4 + OH^{-} \Leftrightarrow SiO_4H_3{}^{-} + H_2O \qquad (4.14)$$

(3) the reverse reaction of Zn^{2+} precipitation,

$$Zn(OH)_2 \Leftrightarrow Zn^{2+} + 2OH^{-} \qquad (4.15)$$

In order to realize what is happening with the zeta-potential curve, another experiment was conducted and described in the next section.

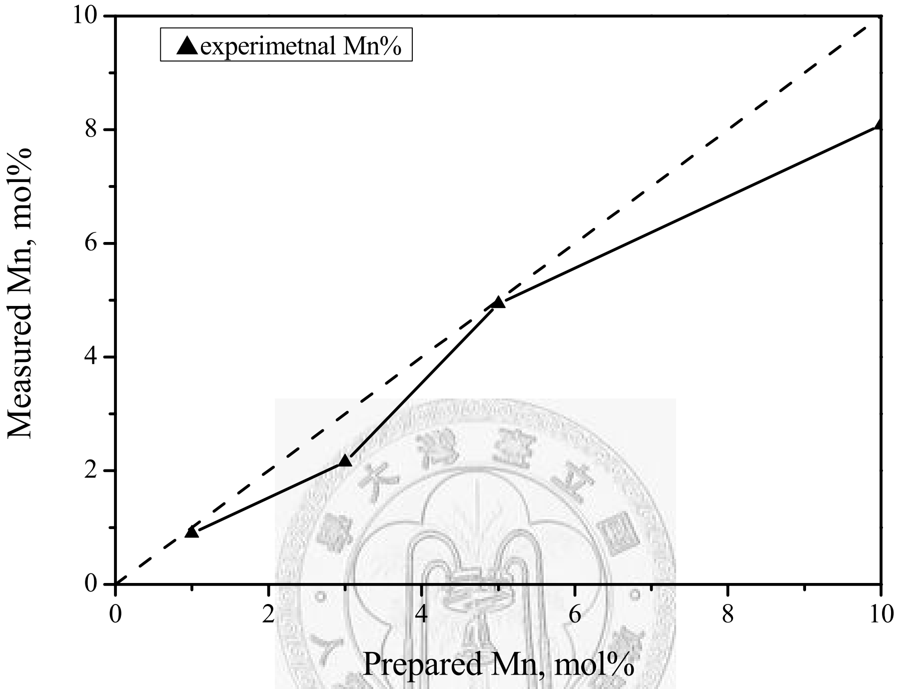

Fig. 4- 1 The measured contents of Mn^{2+} doping from calcined Zn_2SiO_4:Mn particles analyzed by ICP-AES. The unit is defined as molar percent of Mn/Zn.

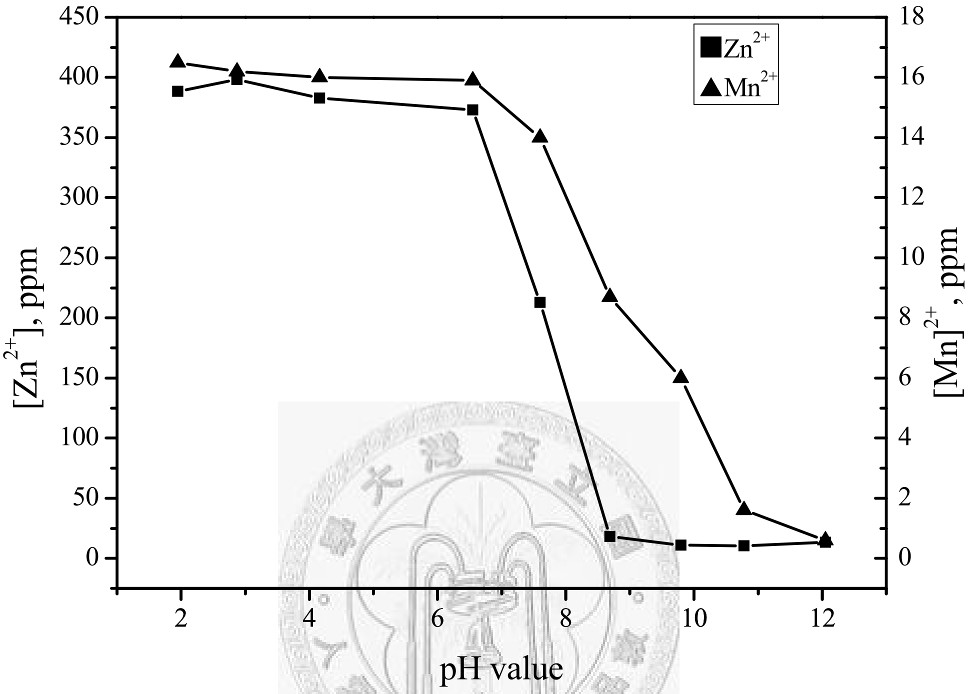

Fig. 4- 2 Titration curves of [Zn^{2+}] and [Mn^{2+}] versus pH of solutions, respectively.

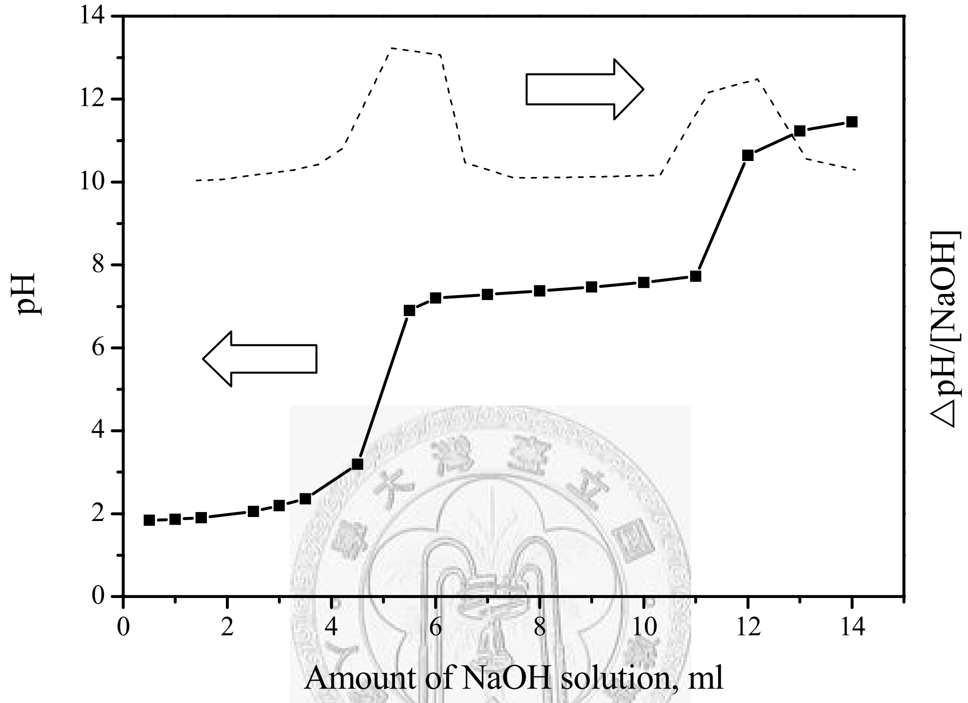

Fig. 4- 3 Titration curve of 0.5 ml 0.1M $Zn(NO_3)_2$ dissolved in 20 g de-ionized water titrated by $NaOH_{(aq)}$. The dash line is the first order derivative curve of the titration curve.

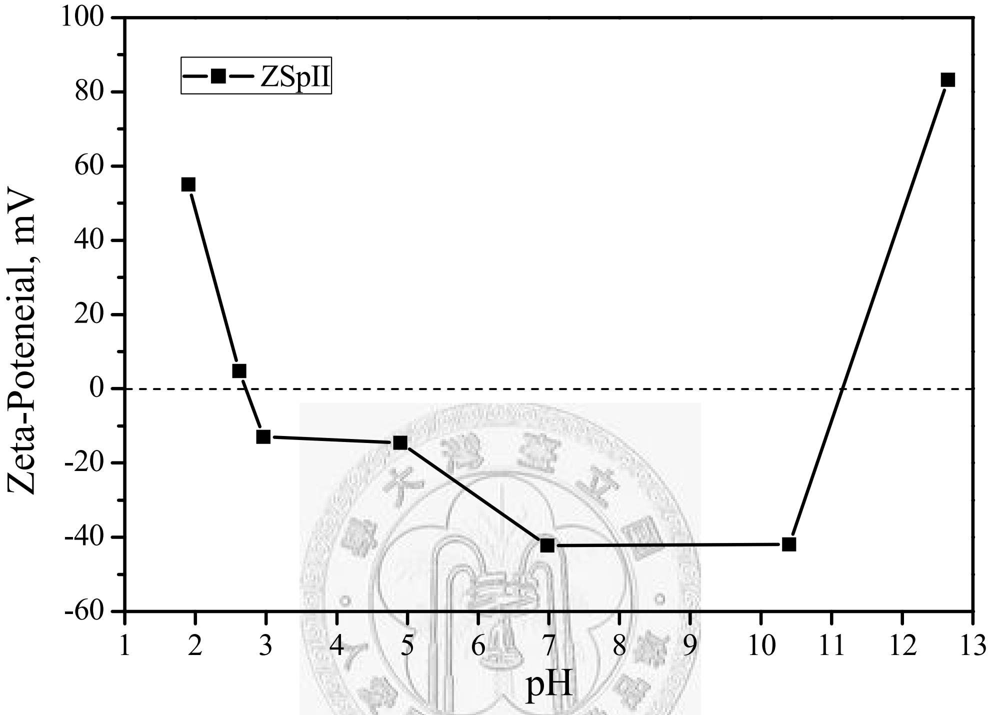

Fig. 4- 4 Zeta-potential of calcined Zn_2SiO_4:Mn particles as a function of pH value.

4.2 Formation of Zn_2SiO_4:Mn

Fig. 4- 5 shows the crystalline phases of ZSpII samples identified by X-ray diffraction. According to the JCPD standards, both willemite and cristobalite phases exist in the synthesized samples. At lower temperature, however, the ZnO oxide phase existed at 500°C with the peaks located at 31.73° and 34.37° which belong to the planes (100) and (002) of ZnO (#89-1397). It's believed that the ZnO phase reacted with silica core and thus formed Zn_2SiO_4 phase at higher temperature. In fact, PL (photoluminescence) property was observed (in chapter 4.4) as the heating temperature reached up to 800°C which indicated that Zn_2SiO_4:Mn did exist. The strong peaks located at $2\theta = 31.53^{\circ}$ and 34.00° belong to the planes (113) and (410) of willemite (#37-1485), respectively. Mn-doping in this case was 5.0 mol% which did not cause apparent lattice shift compared with the standard. Because the radius of Mn^{2+} (0.083 nm) is really close to that (0.074 nm) of the Zn^{2+} in coordination site (which has been listed in Table 2- 2, with CN = 4). Therefore, Mn^{2+} diffuses into the Zn_2SiO_4 lattice, and then substitutes Zn^{2+} without lattice distortion.

Fig. 4- 6 shows that two exothermic peaks started at about 850 and 1050°C. The first one represents the reaction of ZnO reacted with SiO_2 core to form Zn_2SiO_4, this result was corresponding to the PL effect which didn't appear until annealing temperature higher than 800°C (which will be described in section 4.4). Another one is

believed as the growth of cristobalite phase. The existence of this peak also explains the change of morphology for the particles under SEM images.

Peak intensity of Zn_2SiO_4 increases greatly with increasing annealing temperature, as shown in Fig. 4- 5. However, as the temperature reaches to 1200°C, the peak intensity of cristobalite at $2\theta = 22.04^{o}$ become apparent, that indicates that the growth of cristobalite takes place. Two disadvantages may take place if the heat treatment is conducted at 1200°C:

(1) The sintering behavior between particles is apparent at 1200°C , which is nearly 2/3 the melting point (1730°C) of SiO_2. The images of partially sintered are shown in Fig. 4- 7. The difference between those two images is easily recognized, i.e. the surface of samples is the particles which could be distinguished clearly after polished. The top layer (including impurities and contaminations) of the 1100°C calcined sample (Fig. 4- 7(a)) was easily to be removed. Therefore, the morphology of individual particles inside the bulk is visible, revealing slightly sintering at contact point between particles. The other one (Fig. 4- 7(b)) is nearly sintered to full dense. The surface becomes homogeneous and flat. So, 1200°C treatment is too high to keep PBG crystalline characteristics and does not satisfy the target we designed.

(2) The presence of cristobalite phase reduces the PL emission intensity due to the amount of Zn_2SiO_4 coated on the different surface area, for the un-sintered one having

larger surface area than the sintered one and which will be discussed in chapter 4.4.

According to these two reasons, it could be concluded that 1100^{o}C is the better heat treatment temperature for the synthesizing of ZSpII particles.

It has been mentioned in chapter 4.1 that the Zn_2SiO_4:Mn particles dispersed in strong basic solution presented a zeta curve of “U shape”, instead of “reversed S shape”. In order to understand the zeta-potential abnormal, we dispersed these particles into $NaOH_{(aq)}$ (sodium hydroxide solution) with pH = 12 and aged for 24 hr. The mixture was then dried in an oven, and the powder was examined by XRD. The parameter settings of XRD test were the same as the previous one. Fig. 4- 8 is the XRD result. The extra peaks locate at about 26^{o} and 50^{o} can be indexed as sodium silicate (#48-0867) or hydrate silicate (#42-1350) when Zn_2SiO_4:Mn particles immersed in basic solution. The sodium ion may react with silicate and form a 2-D laminar or 3-D tetrahedron structure. The un-expected phases in the strong basic system are responsible for a positive surface potential of pH = 12, and modify the chemical composition on the particle surface.

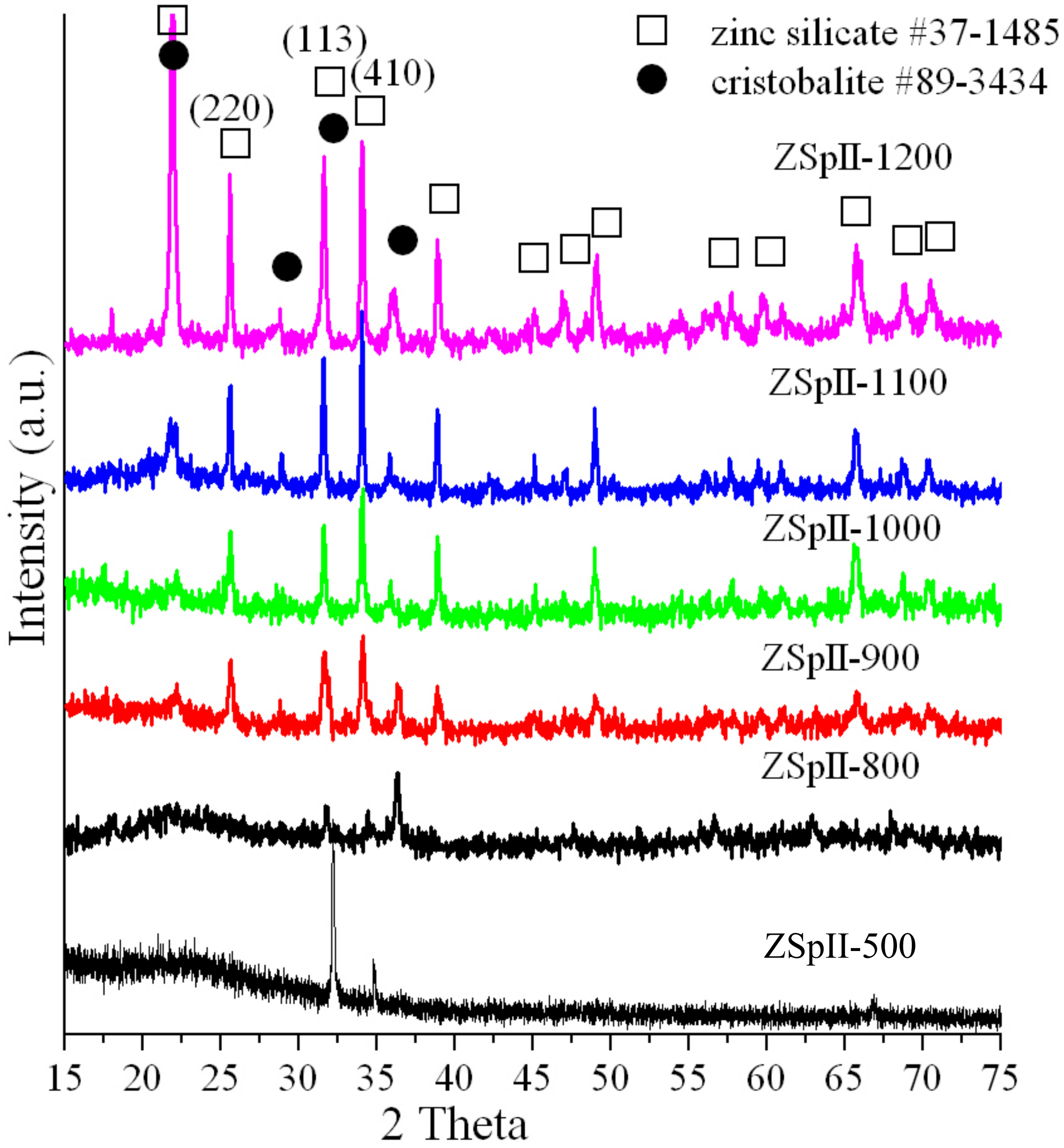

Fig. 4- 5 XRD patterns of Zn_2SiO_4:Mn (5 mol% doping) particles varies with different heat treatments of 1200-500°C from top to bottom, respectively.

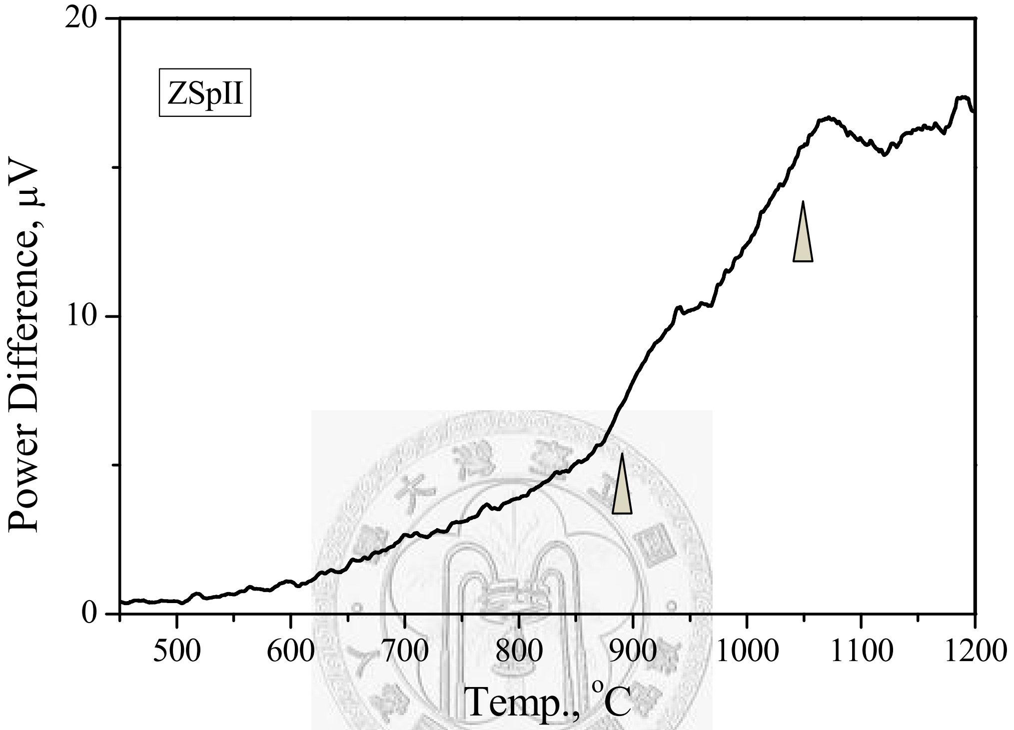

Fig. 4- 6 DTA curve representing the ZSpII samples annealing at 500°C for 2 hr.

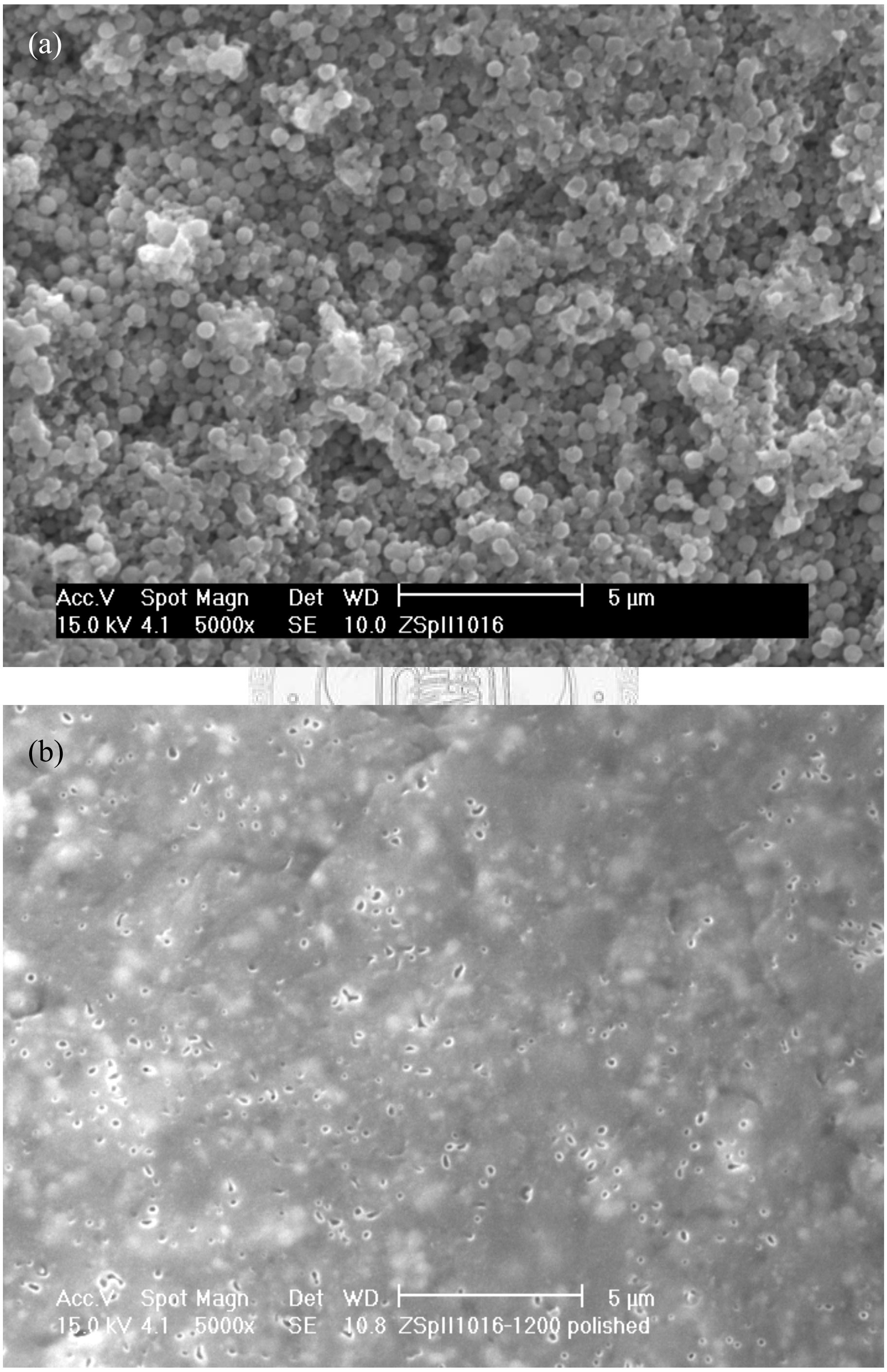

Fig. 4- 7 SEM images of ZSpII bulky samples after heat the treatment at (a) 1100^{o}C and (b) 1200^{o}C for 2 hr.

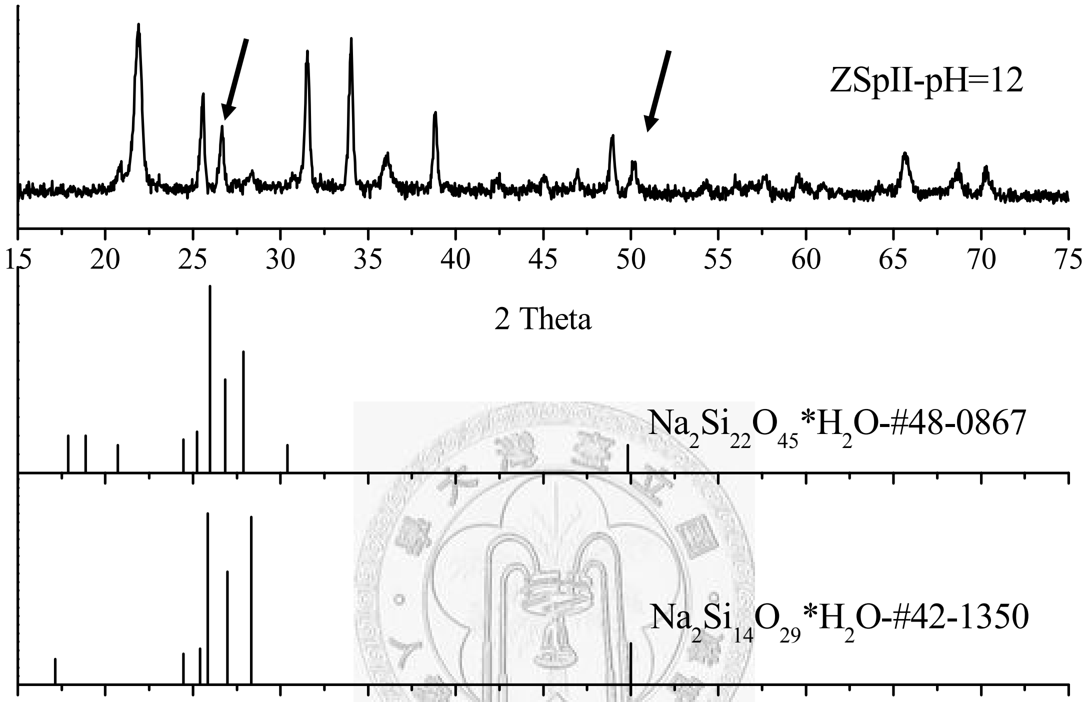

Fig. 4- 8 XRD pattern of Zn_2SiO_4:Mn powders dispersed in basic solution showing the possible phases. The arrows pointed out the extra peaks other than those belonging to Zn_2SiO_4 phase.

4.3 Microstructure Observations and EDS Measurements

Fig. 4- 9 (a) to Fig. 4- 9 (c) are the SEM images of three types coated SiO_2 particles. The initial silica particles in Fig. 4- 9 (a) had an average particle size of about 325 nm which was synthesized by the precursors in a ratio of TEOS: NH_4OH:C_2H_5OH = 24:25:450 aging for 24 hr. After the coating process, the particle size became 375 nm as shown in Fig. 4- 9 (b), which tells us that the thickness of the coating layer is about 25 nm. The Si/Zn ratio in this case was measured. 7 points were chosen in Fig. 4- 9 (c) randomly and calculated by t-distribution method. The average value of Si/Zn ratio is 6.088 with standard deviation of 0.612. The samples would have a 95% confidence ranged from 5.522 to 6.654.

The silica particle were assembled to photonic band-gap (PBG) structure, as shown in Fig. 4- 10 which started with TEOS:NH_4OH:C_2H_5OH = 10:20:200 aging for 2 hr. In order to provide strength, the assembled SiO_2 PBG was annealed at 1000^oC for 1 hr first. The average particle size in this case is 240 nm with a polydispersity of 5.5%. Then immersed the template in the designed molar ratio (as the previous case with 5 mol% of Mn doping) of Zn and Mn solution for 2 hr. Fig. 4- 11(a) represents non-uniform coating of precipitates. The reason to the non-uniform coating resulted from a strong surface tension that make the Zn and Mn solution did not “penetrate into” the pores of the silica template. In order to solve this problem, ethyl alcohol (σ = 22.6 N/m^2), a useful chemical, was added to reduce the surface tension of the solution coating and improve the wettability of the solution. In Fig. 4- 11(c), the Zn and Mn solution was diluted by alcohol to 3 times in volume. The improvement was obvious in the image, and so were the cases in Fig. 4- 11 (d) to Fig. 4- 11 (f), which were diluted to 5, 10 and 20 times, respectively. The segregation of non-uniform Zn/Mn coverage on the SiO_2 PBG surface was no longer existed. Therefore, reducing the surface tension of the precursors by adding ethyl alcohol was a good step to offer a better coating condition.

The morphologies of coated SiO_2 PBG crystal with different annealing temperature are shown in Fig. 4- 12. Different annealing temperatures seemed not to change the morphology, except the case by 1200^oC (Fig. 4- 12 (d)). Zn_2SiO_4:Mn coated silica particles remained its original spherical shape below 1100^oC. The particles could still be distinguished clearly at 1000^oC. While the PBG structure disappeared and densified after sintering at 1200^oC for 2 hr which was similar to the trend in Fig. 4- 7. The SiO_2 template experienced an extensive sintering behavior. Therefore, proper conditions for fabricating Zn_2SiO_4:Mn coated SiO_2 PBG crystals is sintering at $<1200^oC$ 2 hr in air.

The EDS measurement of ZSpVI series was shown in Fig. 4- 13. The sample in this case was diluted to 5 times. The results from top site to bottom were 1.05, 0.32, 0.33, and 1.24 (At% base on Si), respectively. The reason is that during the drying process, the un-coated (or excess) ions were discard instead of forming precipitates, and also, the solution diffusions and evaporates from sample to the surface and thus resulting in a higher concentration at the surface and that of a lower one inside the sample.

Fig. 4- 14 was the microstructure of pure silica particles assembled as PBG crystal. The particles were arranged in nearly ordered closed-pack structure with mono- and two-layer stacking in (a) and (b), respectively. The cross-sectional view of the coated particles was shown in Fig. 4- 15. The coated particle with original concentration shows a phosphor layer in a thickness of about 50 nm. In the other hand, particles coated a phosphor layer became extremely thin if the $Zn(NO_3)_2$ and $Mn(NO_3)_2$ precursors were diluted to 5 times by alcohol as shown in Fig. 4- 15. The thickness of the coating layer for diluted sample is about 20 nm. Some black spots in image are copper contamination after ion-milling. The diffraction pattern in this case is too weak to identify the Zn_2SiO_4 crystalline phase because of the G1 glue covering on observation area. However, in section 4.2 and 4.4, the XRD pattern and PL spectra can be evidence to prove that the Zn_2SiO_4 phase does exist on the surface of silica particles as annealed at temperature higher than 800°C. The thickness of the coating layers determine the PL intensity, i.e. the thinner the phosphor layer, the weaker the PL intensity (which will be shown in chapter 4.4).

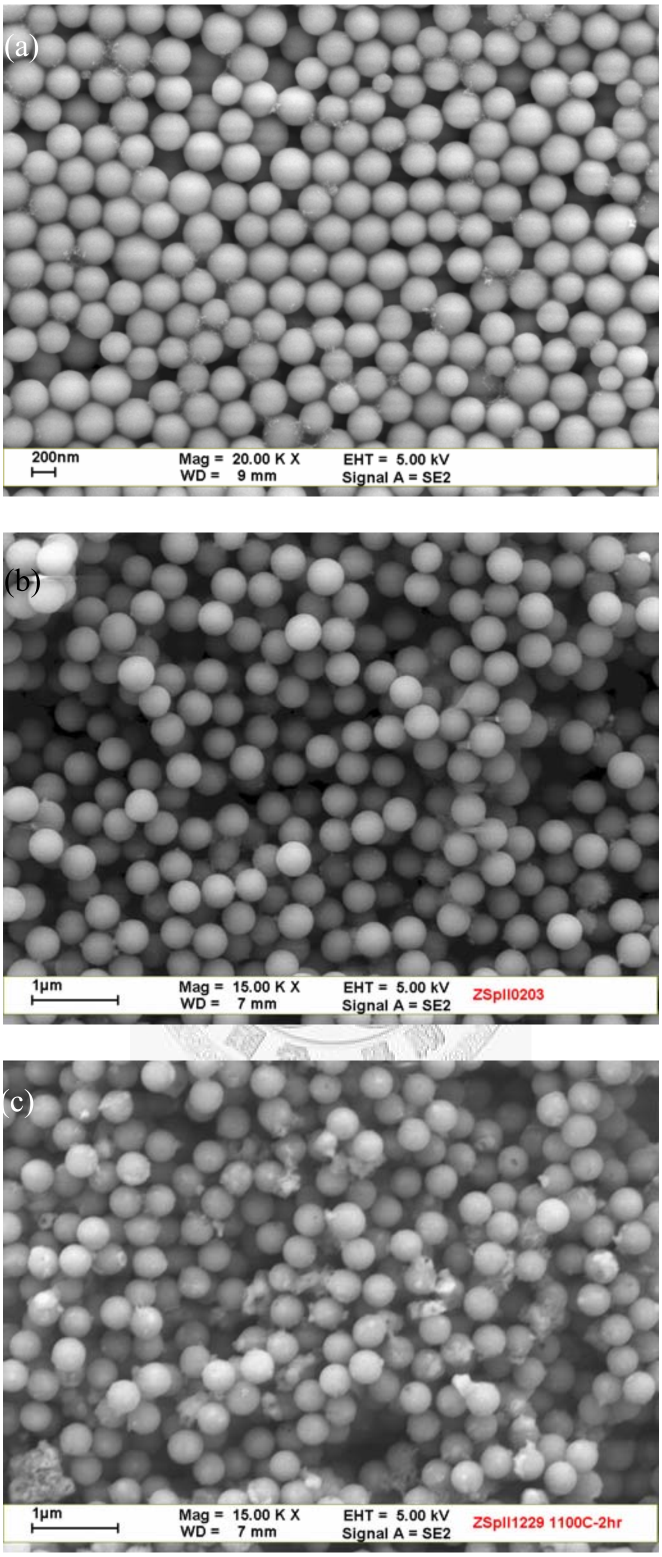

Fig. 4- 9 SEM images showing the morphologies of (a) silica particles prepared by Stöber method, (b) silica particles coated with Zn^{2+} and Mn^{2+} before calcinations, and (c) dried and after 1100^{o}C calcination for 2hr.

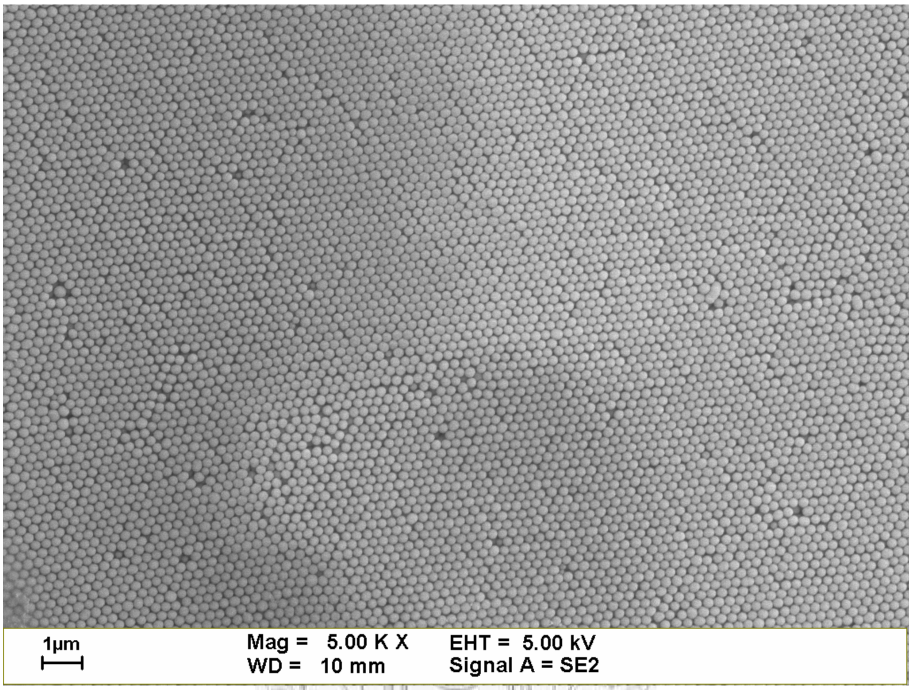

Fig. 4- 10 SEM image showing silica particles with PBG structure at 1000°C heat treatment for 2 hr. The precursors consists of TEOS:NH_4OH:C_2H_5OH = 10:20:200.

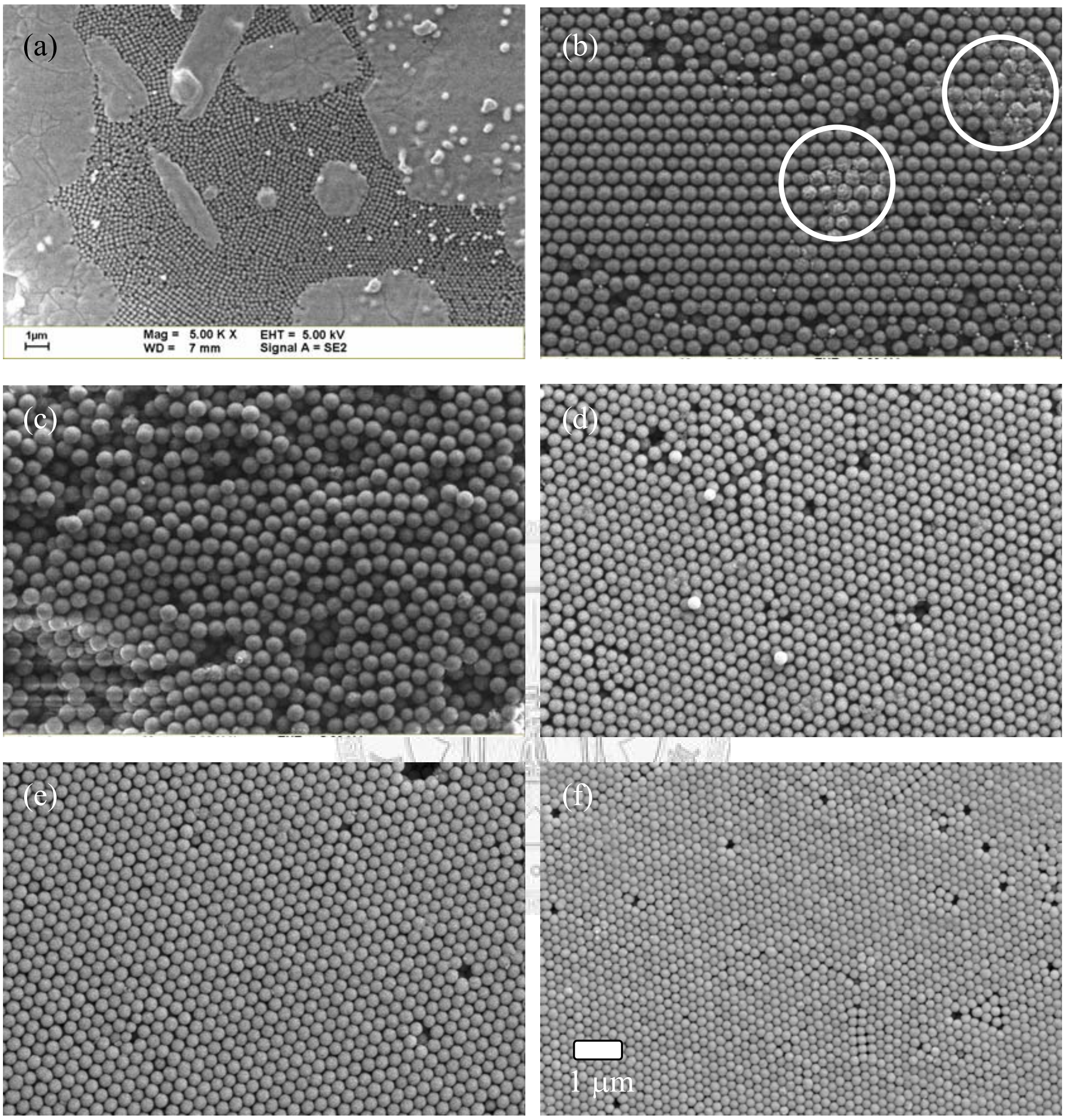

Fig. 4- 11 SEM images of SiO_2-template coated with Zn and Mn solution (a) original concentration, or diluted by ethanol in volume to (b) 2, (c) 3, (d) 5, (e) 10 and (f) 20 times, then dried and annealed at 1000^{o}C for 2 hr. The white circles illustrate that there are still a little amount of non-uniform coating, however, this non-uniform coating did not exist at all as the precursors were diluted to 3 times.

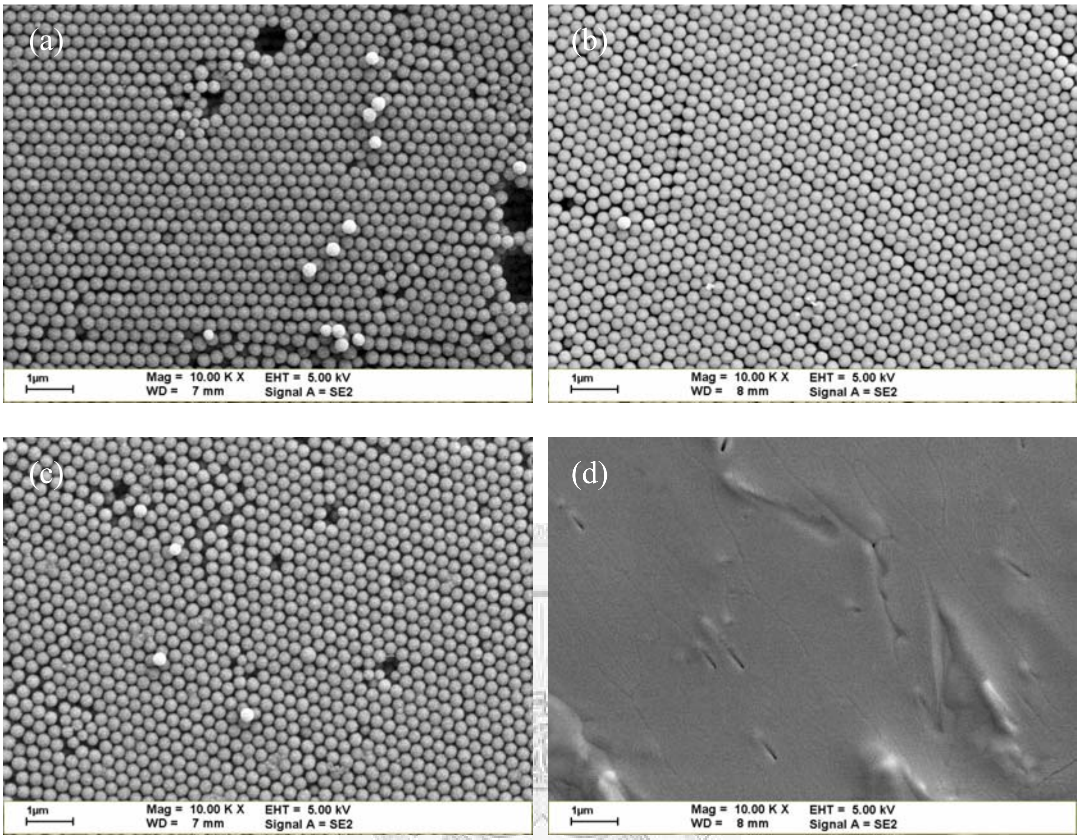

Fig. 4- 12 SEM images of coated SiO_2-template by the Zn/Mn solution diluted with alcohol to 5 times. The samples were dried and annealed at (a) 600^{o}C, (b) 800 ^{o}C, (c) 1000 ^{o}C, and (d) 1200 ^{o}C, respectively.

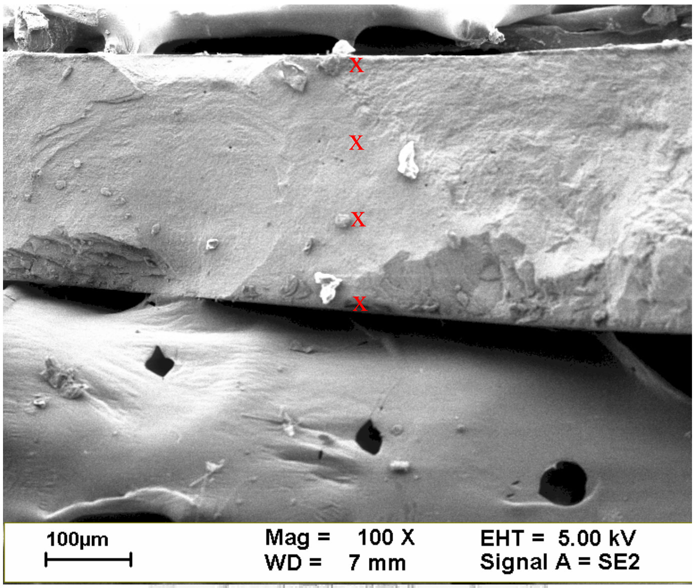

Fig. 4- 13 SEM image showing the positions of EDS measurement on ZSpVI sample.

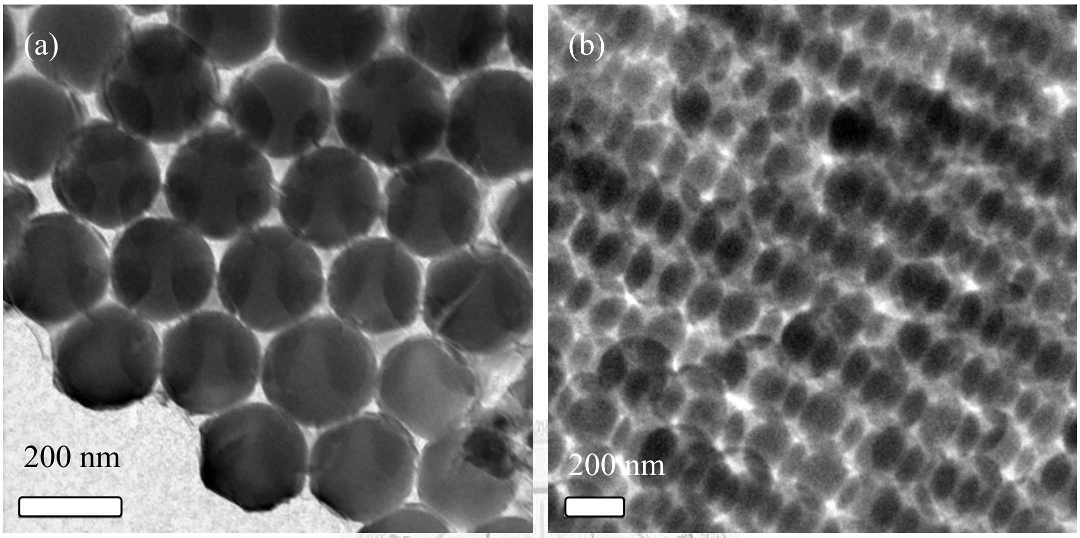

Fig. 4- 14 TEM images showing the detail morphologies of assembled SiO_2-template with (a) one layer and (b) two layers packing, respectively.

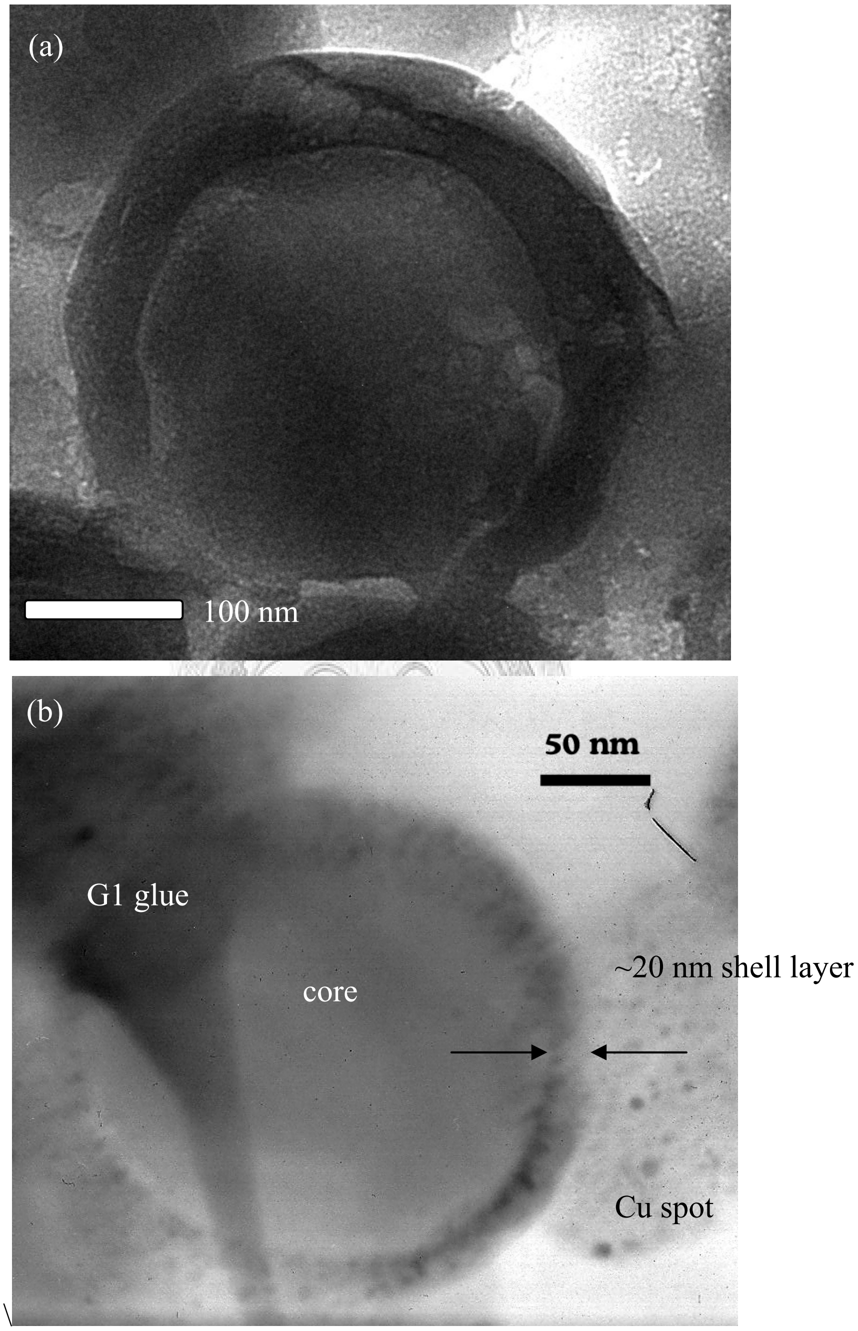

Fig. 4- 15 TEM cross-sectional view of SiO_2 particles coated with precursors (a) directly and (b) diluted by alcohol to 5 times, respectively.

4.4 Luminescence Property

Luminescence properties with different factors were studied, such as annealing temperatures, Mn concentrations, applied voltages and so on.

For the PL measurements, we use an UV lamp as a light source with a wave length of 254 nm. The spectrum is shown in Fig. 4- 16. Although there were noise existing in the spectrum, it did not make sense to our experiments due to the maximum emission peak for Zn_2SiO_4:Mn locate at about 520-530 nm as a visible green light. Fig. 4- 17 shows the images of coated samples after heat treatment and exposed under visible and UV light.

The doping amount of Mn in this study was concerned. Fig. 4- 18 shows the PL intensity varies with Mn doping. The PL property increased slightly with amount of Mn which performed a best PL intensity at 5 mol% doping. According to the concentration quenching effect [70], it is believed that there's a critical doping amount existing in phosphor, i.e. if the doping amount of activator is over than a specific value, the distance between activators inside the system decreased and thus the energy transferred from excited state to ground state became in heat loss in the matrix phase (silicate) instead of visible light and the PL intensity decreased. Therefore, when Mn doping in this case reach up to 10 mol%, then the PL intensity low down due to the concentration quenching effect.

In section 4.2, it has been mentioned that the higher annealing temperature led to the growth of cristobalite phase. When the temperature reached up to 1200°C, the silica particles sintered and became a nearly homogeneous surface in Fig. 4- 7 (case of ZSpII). This phenomenon resulted in the decreasing of PL (photoluminescence) intensity as Fig. 4- 19. In the figure, the PL intensity increased with temperature, and the 1000°C and 1100°C heat treatment (for 2 hr) performed a better PL property. However, the sample annealed at 1200°C showed a lower emission intensity which was believed that (1) the existing of the overaged cristobalite phase induced a strong lattice distortion and also the different reflection index (or even adsorption index) from the original amorphous SiO_2 matrix phase and (2) the great change of surface area, i.e. the amount of phosphor coating on the silica was different between un-sintered (more phosphor located at the surface) and sintered (less phosphor) one in a unit surface area. These reasons resulted to the lower PL intensity. This outcome is agreeable to the case in ZSpVI which shown in Fig. 4- 12 (d) and Fig. 4- 20 which represented that PL intensity increased with annealing temperature and performed a best PL property at 1000°C but the intensity low down as the temperature rose up to 1200°C.

In section 4.3, adding alcohol into Zn/Mn precursors (for the case in ZSpVI) did improve the uniformity to the coating process. Intuitively, the precursor without modifying contains the most precipitates on silica template and thus gave rise to the highest PL intensity shown in Fig. 4- 21, and then decreased with diluted ratio. The samples diluted to 1/2, 1/3, 1/5, 1/10 and 1/20 represented a lower intensity. However, samples those with diluted precursors did not show a great change. The possible reason is that adding of alcohol resulting to a uniform distribution of Zn and Mn during coating process, and the retained ions were discarded instead of precipitated as segregations. Therefore, the coated ions remain saturated and just slightly affected by alcohol.

ZSpII sample was used as phosphor layer in a CL device composed of CNT cathode and ITO anode, which installed in a chamber as shown in Fig. 4- 22. ZSpII sample performed a green-blue light under accelerated voltage as the applied voltage rose up. The I-V curve (Fig. 4- 23) illustrates the electrical behavior of ZSpII sample that contained three regions:

(1) sub-threshold region, which represented that the whole system acted as an open circuit without any current passing through.

(2) Linear region (175-310 V), which shows that the measured current increased with applied voltage.

(3) Cut of region (over 310 V), the current maintained as constant which was set to protect the testing machine against current flow over than a specific value.

The CIE analysis for ZSpII sample consisted of x = 0.2899 and y = 0.5048 where located at the position of green, blue and white region as shown in Fig. 4- 24.

Considering of the application for this material, a low threshold voltage is a beneficial advantage for a flat panel display because of a higher threshold voltage consumes more power (more energy was wasted), and also releases heat in device. Therefore, this material is potential used for displays.

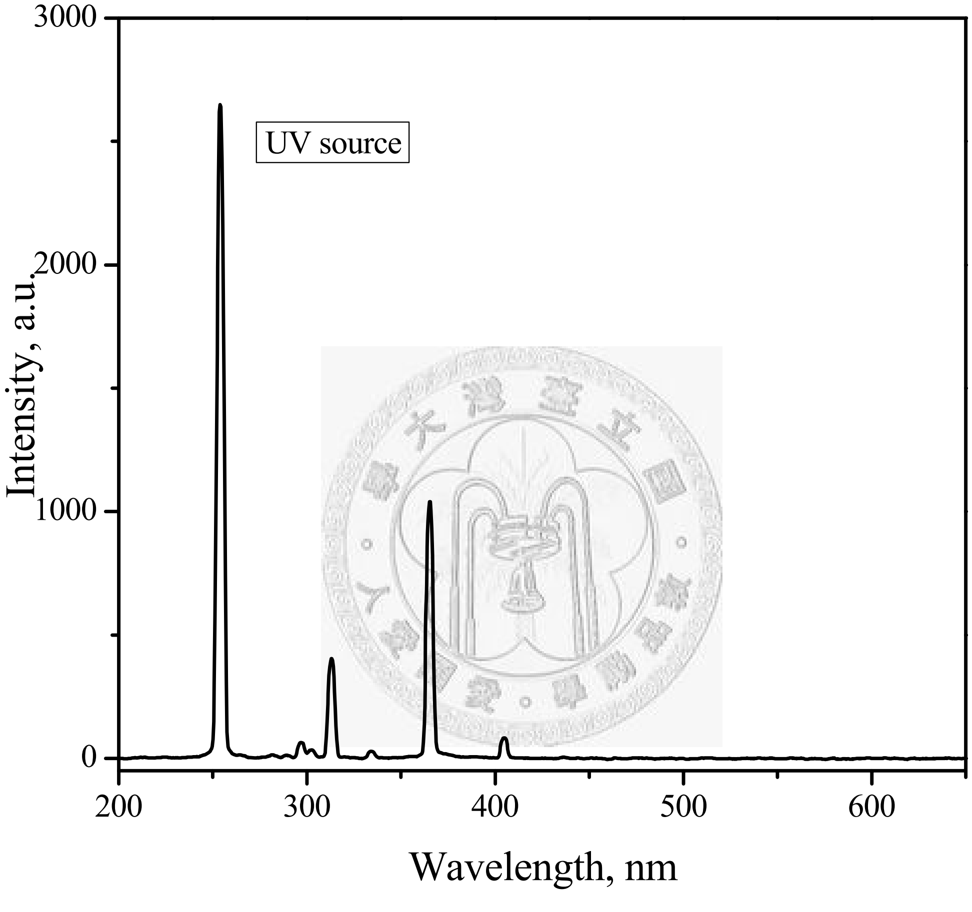

Fig. 4- 16 Optical spectrum of the UV source which was used in this study.

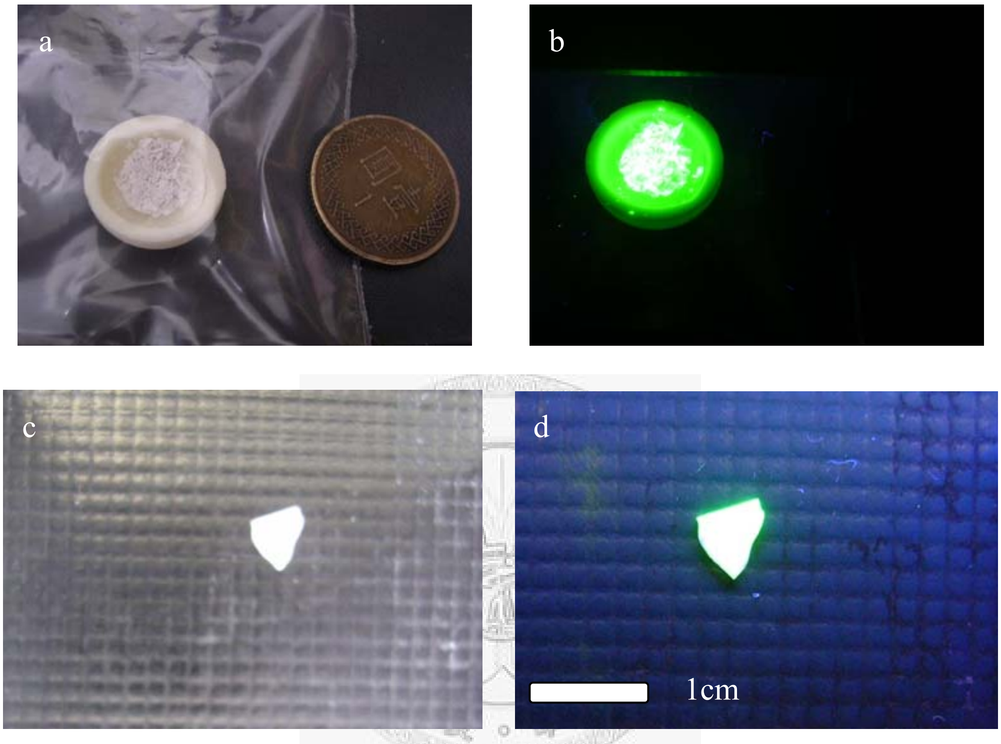

Fig. 4- 17 Photos of samples (a) and (b) prepared via ZSpII, and (c) and (d) via ZSpVI processes. (a) and (c) were exposed under visible light while (b) and (d) were exposed under 254 nm UV light.

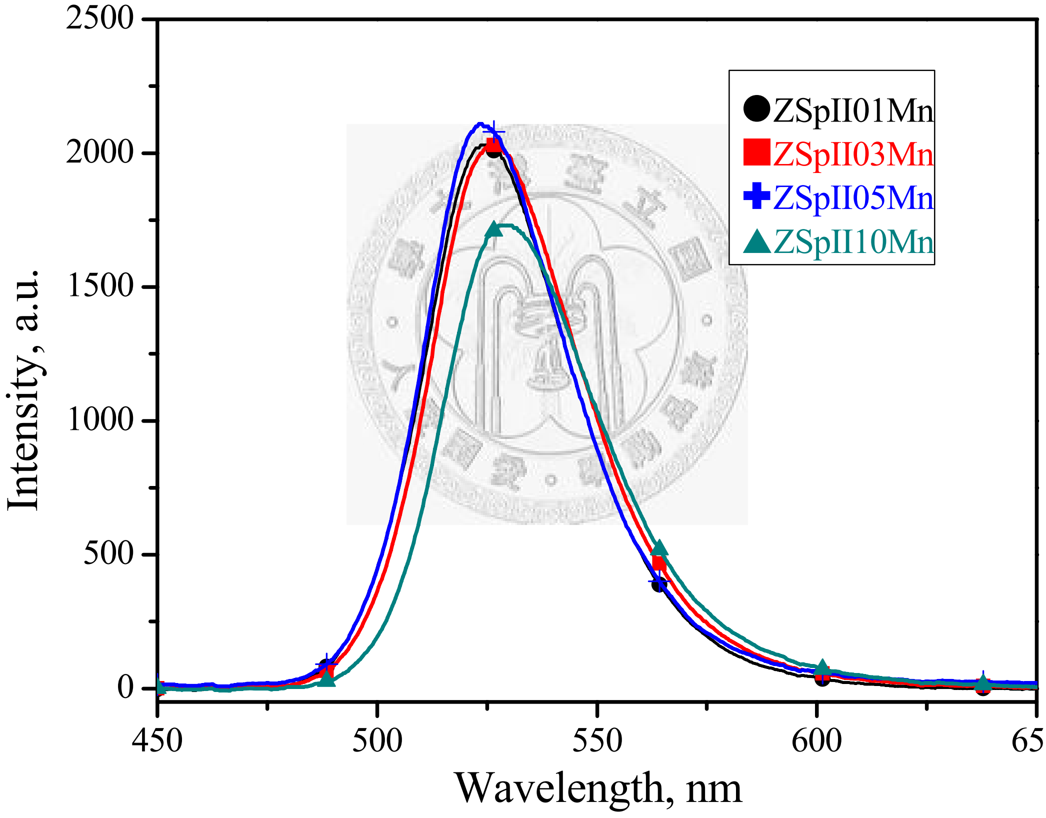

Fig. 4- 18 PL spectra of ZSpII intensity with different amounts of Mn ion doping. The doping ratio of Mn was defined as Mn/Zn.

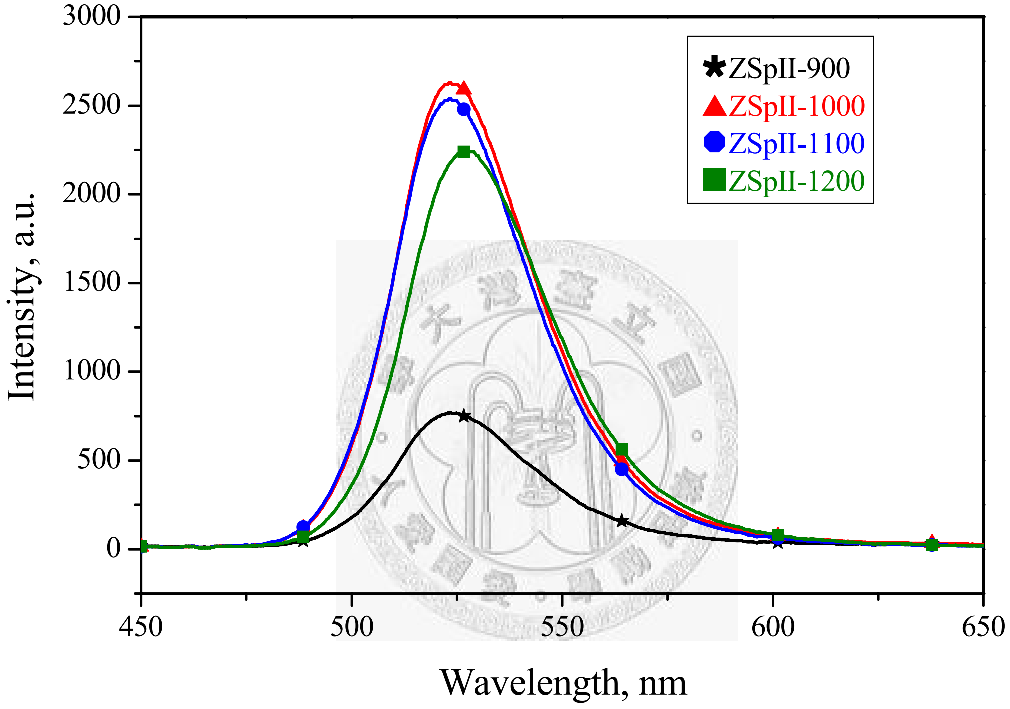

Fig. 4- 19 Spectra illustrating the PL intensity of ZSpII sample annealed at different annealing temperatures. The samples of 1000°C and 1100°C perform a better emission property, while the intensity decreased if the temperature rose up to 1200°C.

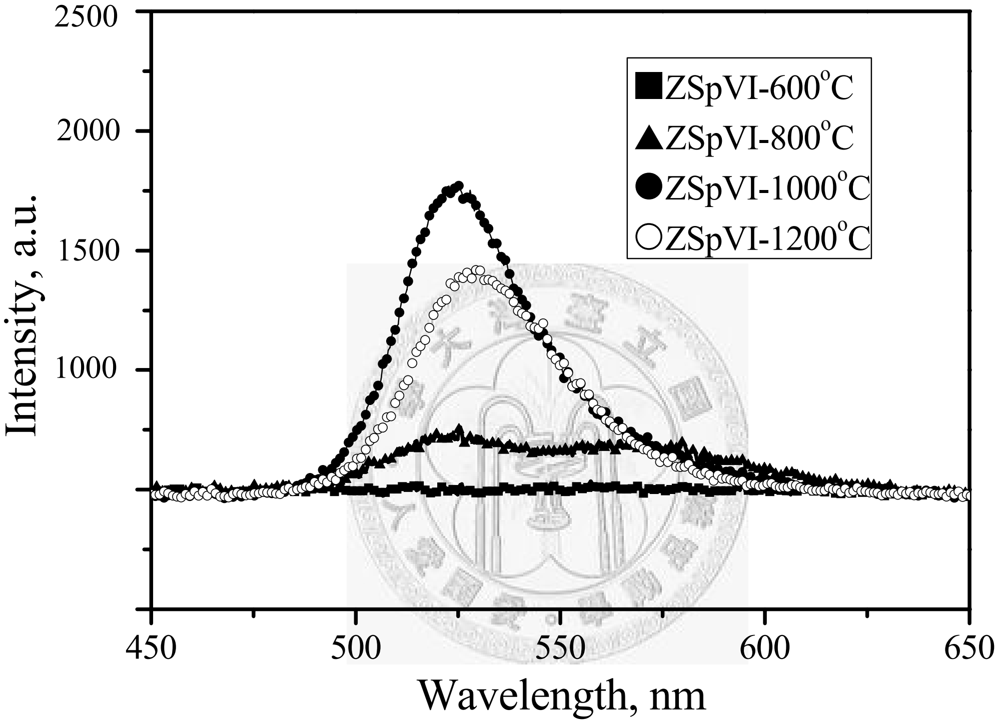

Fig. 4- 20 PL spectra of ZSpVI samples annealed at different annealing temperatures. The one annealed at 1000°C performed a better PL property.

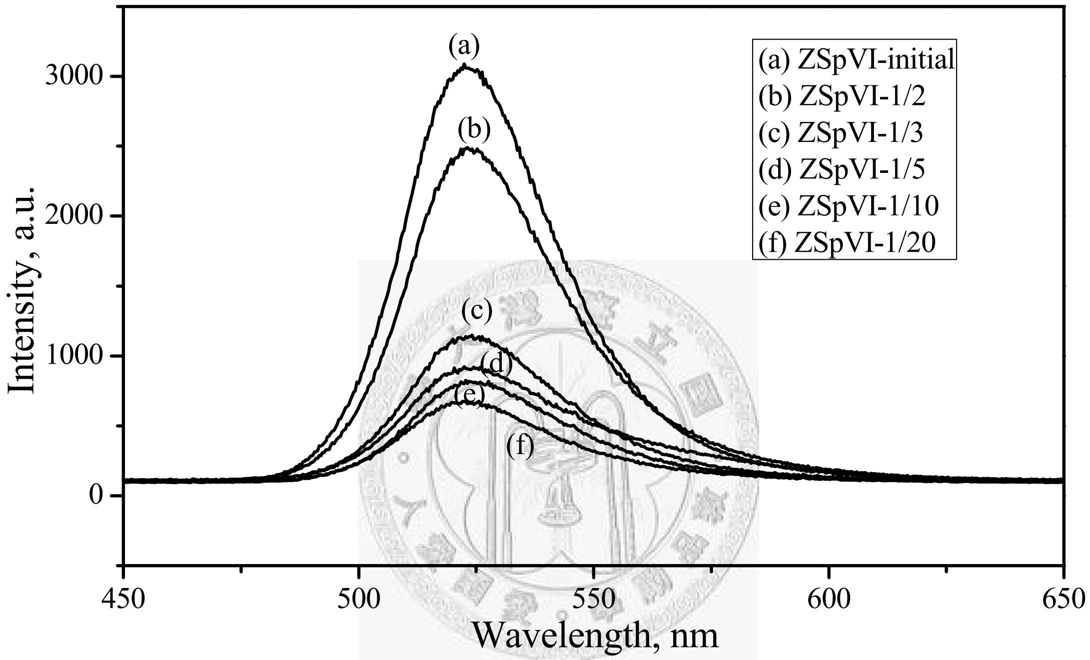

Fig. 4- 21 PL spectra of ZSpVI samples diluted by ethyl alcohol to specific concentration, then annealed at 1000^{o}C for 2 hr.

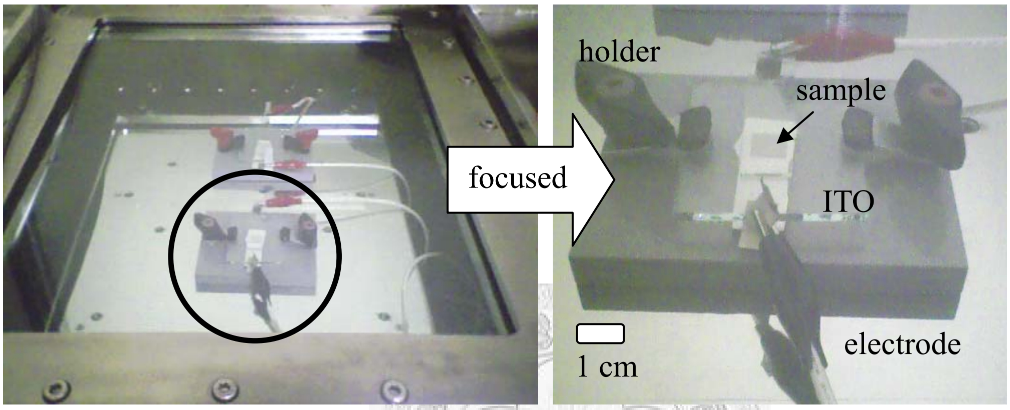

Fig. 4- 22 Photos showing CL device in a vacuum chamber.

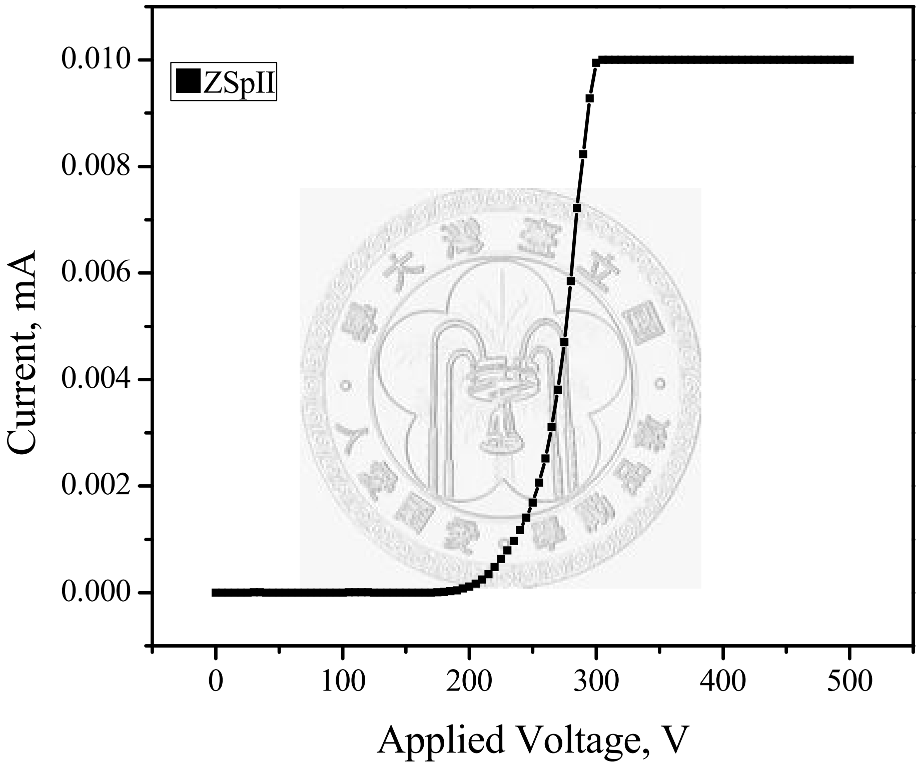

Fig. 4- 23 I-V curve illustrating the electrical property of ZSpII sample assembled in TECO/CL device existed by a threshold voltage at 175 V and saturated at 310V.

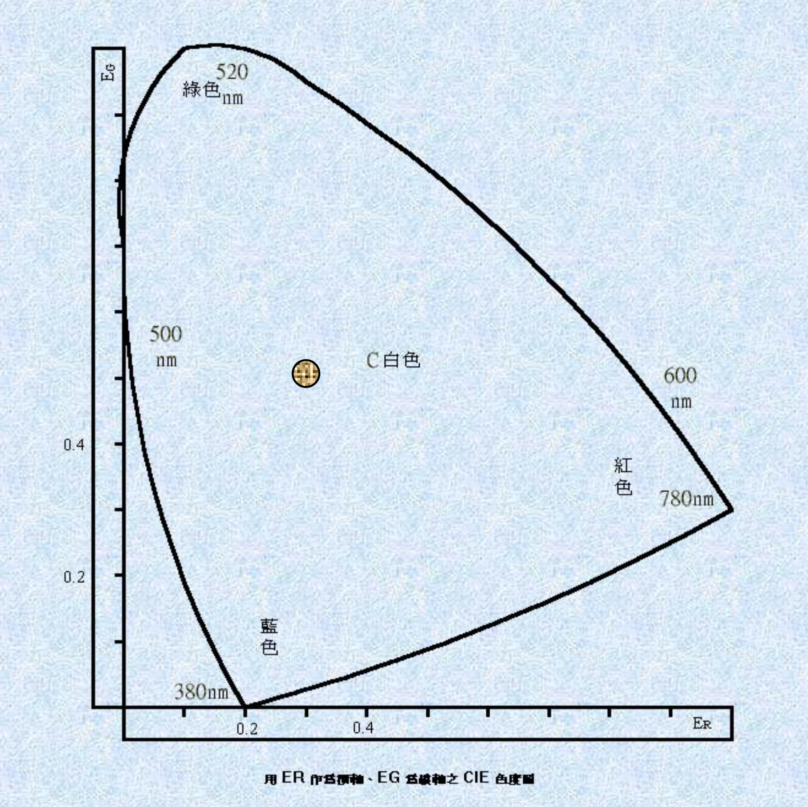

Fig. 4- 24 CIE analysis result of ZSpII sample in TECO CL device. The sample of studied is located at x = 0.2899 and y = 0.5048, which corresponds to the circle in this diagram [71].

Chapter 5 Discussions

5.1 Methods Comparison

Samples which developed by solid state reaction were denoted as ZSpV series, the other trials denoted as ZSpI, ZSpIII and ZSpIV will be described. Comparing with the solid state reaction, which is a very common, easy, and cheap process, and the results of the other three methods, the Zn_2SiO_4:Mn (ZSpII) by colloidal method shows an extremely good PL property.

The XRD results of ZSpV (Zn_2SiO_4:Mn made of **solid state reaction)** included not only cristobalite and Zn_2SiO_4 phases, but also ZnO phase. Three diffraction peaks of ZnO located at $2\theta = 31.7^o$, 34.4^o, and 36.2^o with the corresponding (hkl) = (100), (002), and (101), respectively, as shown in Fig. 5- 1. The Zn_2SiO_4 phase has appeared by calcined at 1000^oC, but not much changes in the intensity if calcined to higher temperatures. The effect of re-grinding/re-calcination (the treatment cycle) of ZSpV is shown in Fig. 5- 2, which shows slight decrease of ZnO as the treatment cycle increases from 1 to 3 times. The reaction of crystalline ZnO with amorphous SiO_2 is sluggish.

The difference between ZSpII and ZSpV could be easily distinguished in Fig. 5- 3. If ZSpV is ground and re-annealed for 1 to 3 cycles, the Zn_2SiO_4 phase is apparent, but the ZnO phase still exists (Fig. 5- 2). The un-desirable phase (residue ZnO) existing in

ZSpV series does reduce the light emission property, as shown in Fig. 5- 3 in much poor contrast to that of ZSpII. Also, the PL spectra of those samples are shown in Fig. 5- 4. Increasing the homogeneity by grinding/annealing for three cycles does enhance the emission intensity, but slightly. In fact, the emission intensity for ZSpII is much stronger than that of ZSpV-3. It can be speculated that the second phase existing in PL material may reduce the emission intensity due to:

(1) Lattice deformation or distortion that affected Mn^{2+} ions diffused or substituted the Zn^{2+} sites. The occurrence of this may reduce the efficiency of Mn^{2+} activation.

(2) The second phase provides another media with different reflection index that can adsorb or scatter the emission light. The reflection index of the matrix silica is 1.39.

In addition, the purpose of this study is to construct a PBG crystal based on Zn_2SiO_4:Mn particles that required PL particles in a uniform size (and also shape) arranged in a periodic way. Solid state reaction synthesizes a powder normally in irregular shape (as shown in Fig. 5- 5), and does not satisfy this requirement.

Besides, the methods of ZSpI, ZSpIII, and ZSpIV were also tried in this study. ZSpI also started from mono-dispersed SiO_2 suspension in basic solution (the pH value is about 11 in order to provide a repulsive force between SiO_2 particles). Unfortunately, the $Zn(NO_3)_2$ and $Mn(NO_3)_2$ solution that added into the suspension precipitated out in nanosized, and became suspended instead of coating on the SiO_2 surface (Fig. 5- 6). The precipitation behavior of Zn and Mn species has been mentioned in section 4.1. This result did not satisfy our requirement. Therefore, a modified method (ZSpII) was proposed, using a dried SiO_2 suspension as indicated in section 3.2.

ZSpIII was an idea from Y. J. Chen [62]. The method started from ZnO-B_2O_3-SiO_2 ternary system. This idea was to grow Zn_2SiO_4 crystals from melted Zn-B-Si oxide liquid at elevated temperature. The powder reactants were turbo mixed and then heated to 1300°C to get Zn-B-Si glass. Boron oxide (B_2O_3) in this system acted as a flux which was used to lower the glass forming temperature. The higher the concentration of B_2O_3, the lower the glass forming temperature of the system. The sample did totally transform to glass (amorphous) phase, as shown in Fig. 5- 7. Annealing was required to get Zn_2SiO_4 crystalline phase. Therefore, the ground glass powder was annealed at 800°C for several hr. However, there was an additional un-expected phase appearing in the system, zinc borate ($Zn_4O(BO_2)_6$). The morphology of the thermally treated ZSpIII is shown in Fig. 5- 8. Three different contrasts were seen in the BSE (back-scattering-electronic) images, brightest, gray, and dark features. Compared with the XRD patterns, the brightest features (marked as X) should be the Zn_2SiO_4; the gray one (marked as Y) should be the $Zn_4O(BO_2)_6$ due to the boron element, which shows a smaller atomic number and be darker under BSE mode; the dark feature is porosity. The porosity could be resulted from the crystallization of $Zn_4O(BO_2)_6$ phase competing with sintering [72]. If crystallization occurs before sintering is finished, the viscosity of glass matrix increases sharply and the sintering stops. Therefore, a porous glass-ceramic was produced, resulting in a higher porosity in Fig. 5- 8(b) than in (a). The Zn_2SiO_4 grains prepared by ZSpIII method were fixed in the Zn-B-Si matrix, and were hardly purified by acid etching. Therefore, this process was given up.

ZSpIV, a hydro-thermal method, started with the dissolution of $ZnCl_2$ (ZnO dissolved in HCl) and $Na_2SiO_{3(aq)}$ in aqueous solution. Two chemicals were mixed in Teflon tubes and heated by a micro-wave sample preparation system with a pressure of 60 bar, a temperature of 240°C by an input power of 1200 W holding for 4 hr. Generally, samples prepared by hydrothermal method should be crystallized after reaction, but ZSpIV sample is still amorphous. Therefore, the product was dried and annealed at about 400°C for 1 hr to see if there's anything occurred. The annealed sample did crystallize. However, a wrong product (see Fig. 5- 9) was made, to be sodium zinc chloride hydrate ($Na_2ZnCl_4(H_2O)_3$, #731757). Na^+ and Cl^- ions reacted in this system instead of SiO_3^{2-}. Therefore, this process did not synthesized Zn_2SiO_4 successfully and was given up.

Base on those experimental results, we conclude that the ZSpII colloidal process is a proper method to synthesize Zn_2SiO_4:Mn particles.

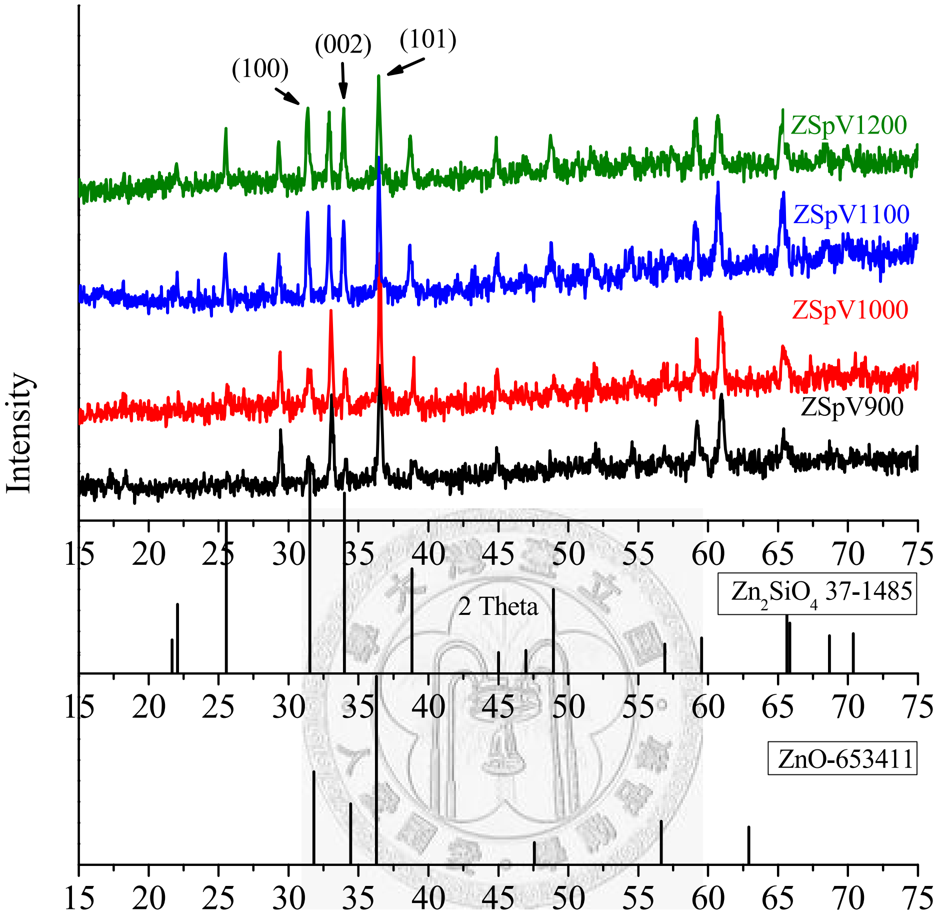

Fig. 5- 1 XRD patterns illustrating the Zn_2SiO_4:Mn particles prepared by solid state reaction. The patterns were arranged by different annealing temperatures from 900-1200°C for 2 hr (bottom to top).

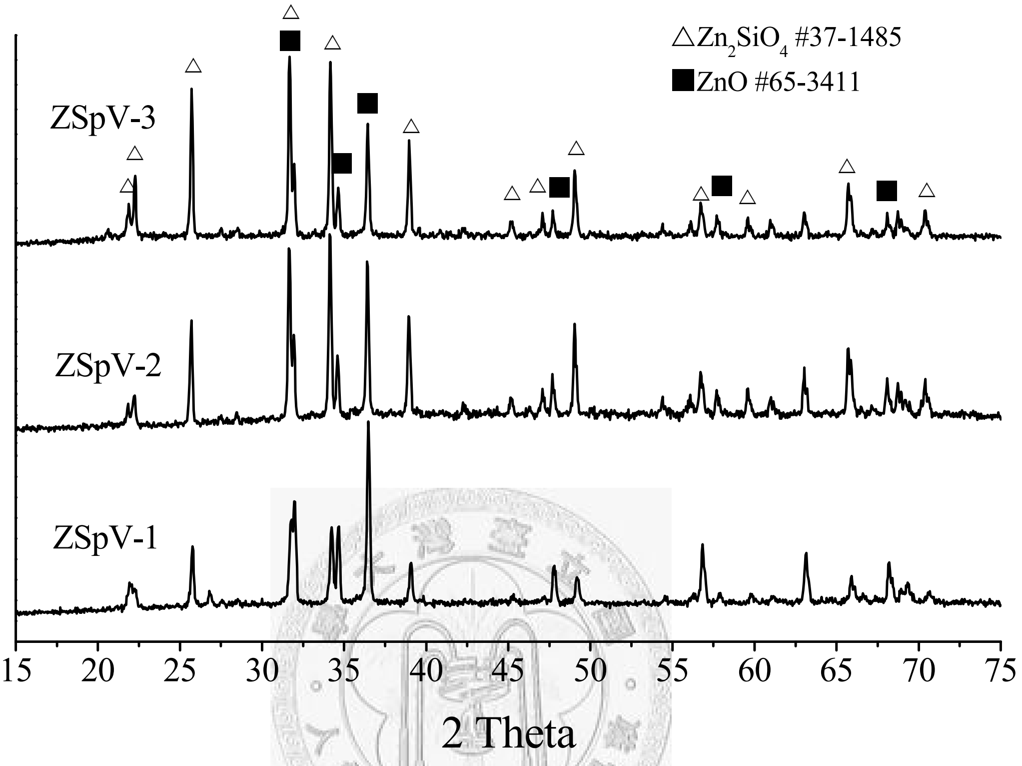

Fig. 5- 2 XRD patterns illustrating the Zn_2SiO_4:Mn particles prepared by solid state reaction, which samples were ground and re-annealed for one to three times at 1100°C for 2 hr.

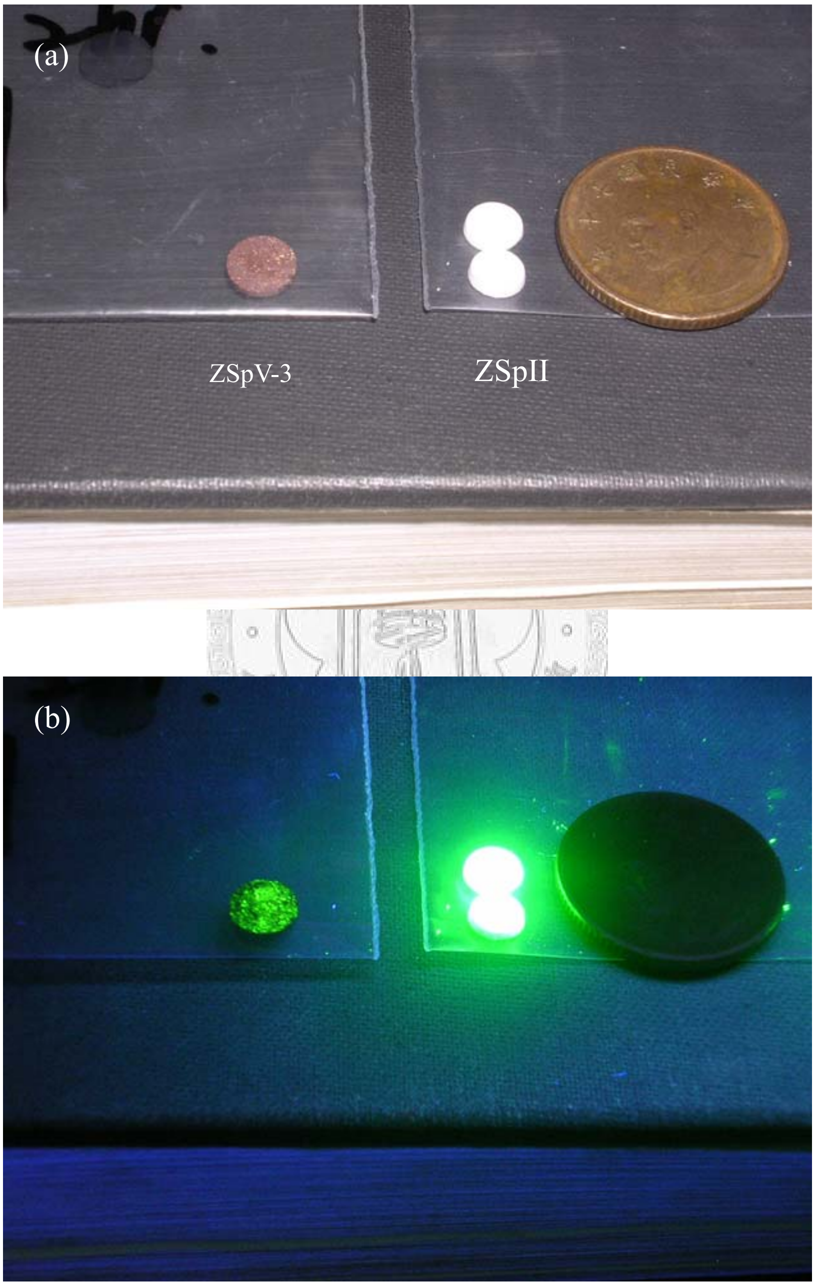

Fig. 5- 3 Photos showing the Zn_2SiO_4:Mn disks (1100^{o}C for 2 hr) exposed (a) without, and (b) with applied 254 nm UV light, where the left piece and right ones were synthesized via solid state reaction and colloidal process, respectively.

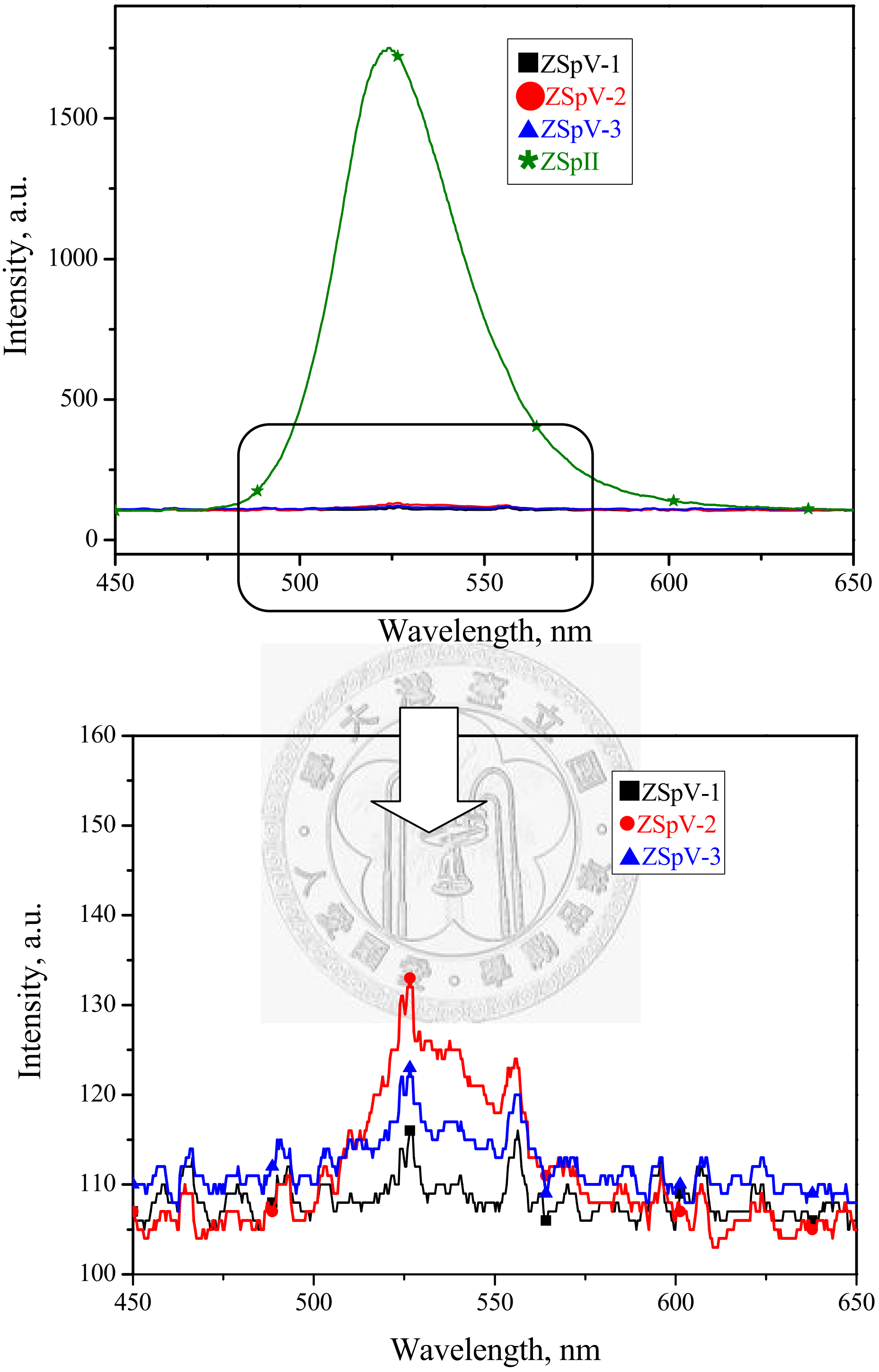

Fig. 5- 4 PL spectrum of the emission intensity of Zn_2SiO_4:Mn disks prepared by solid state reaction (ZSpV series) and solution process (ZSpII). All of these samples were annealed at 1100°C for 2 hr. The number following the sample notation (ZSpV) is the cycles of grinding and re-annealing for one (square), two (circle) and three (triangle) times.

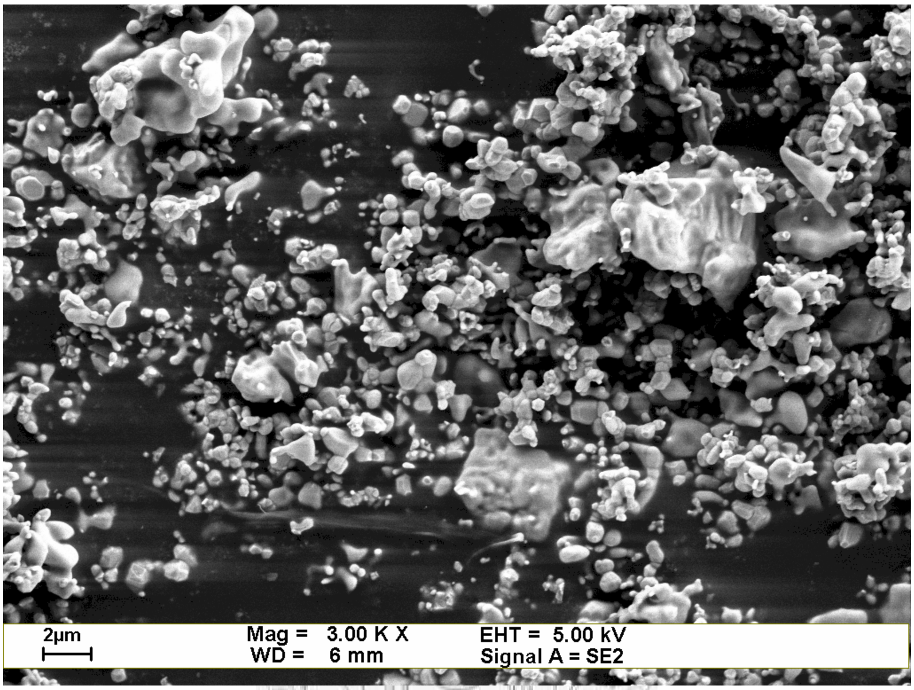

Fig. 5- 5 SEM image showing irregular shape of Zn_2SiO_4:Mn powder (ZSpV) synthesized via solid state reaction at 1000^oC for 2 h.

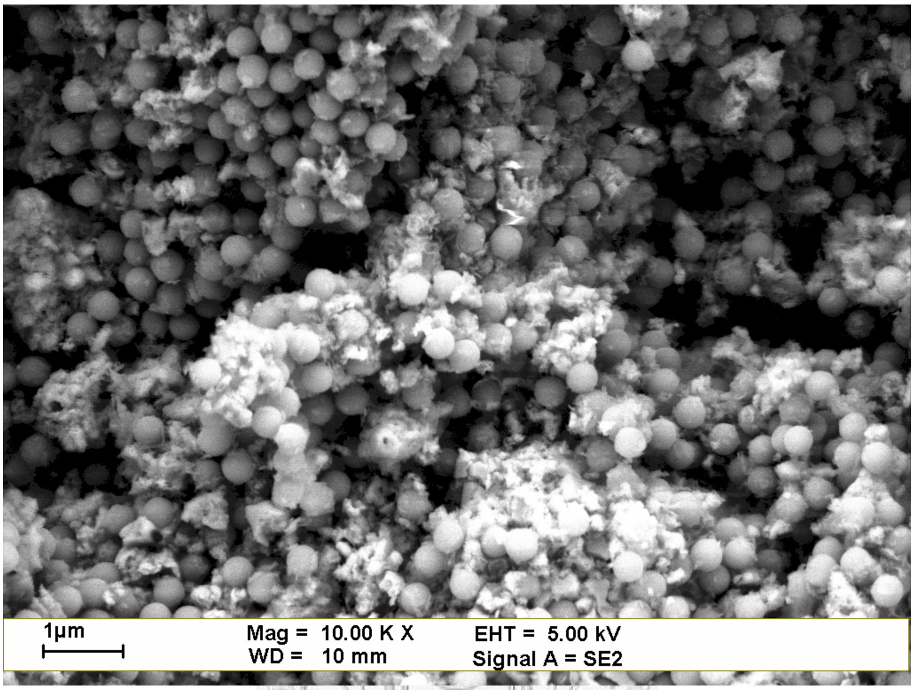

Fig. 5- 6 SEM image showing ZSpI samples annealed at 1000°C for 2 hr. The Zn and Mn ions precipitated randomly, instead of uniformly coating on SiO_2 particles surface.

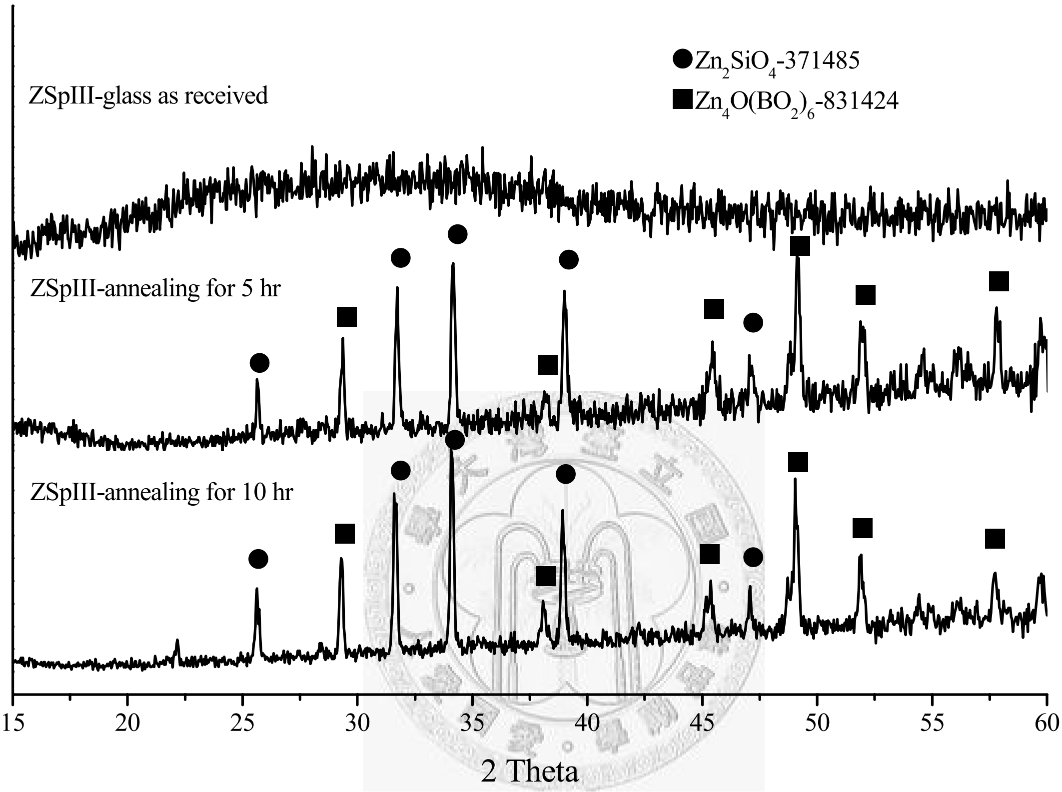

Fig. 5- 7 XRD patterns showing crystalline phase of ZSpIII powder series after quenching (top) and 800°C annealing (the other two patterns). The product contained not only Zn_2SiO_4, but also a $Zn_4O(BO_2)_6$ phase.

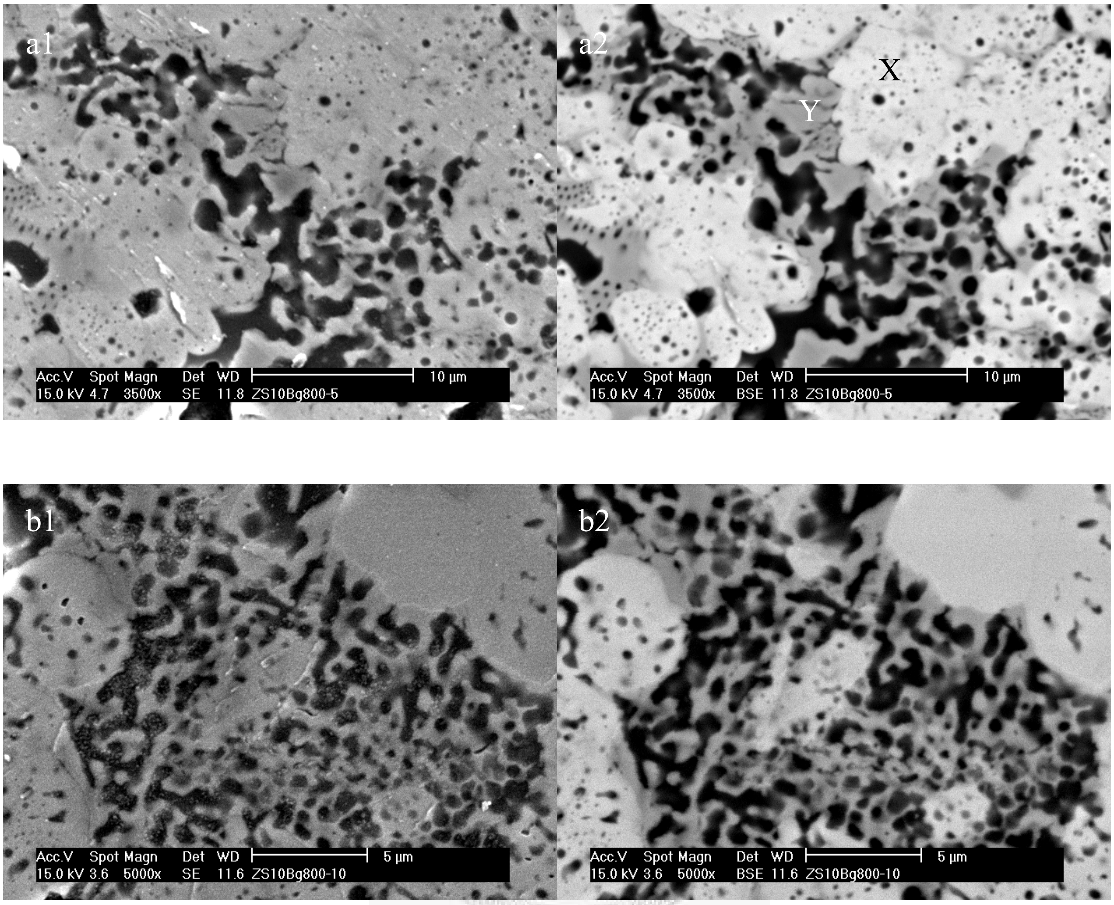

Fig. 5- 8 SEM images showing the morphology of ZSpIII series after calcination at 800^{o}C for (a) 5 hr and (b) 10 hr, where (a2) and (b2) were imaged under BSE mode. X area is Zn rich region; while Y area is B rich region. The black area is pores that are resulted from crystallization in the glass.

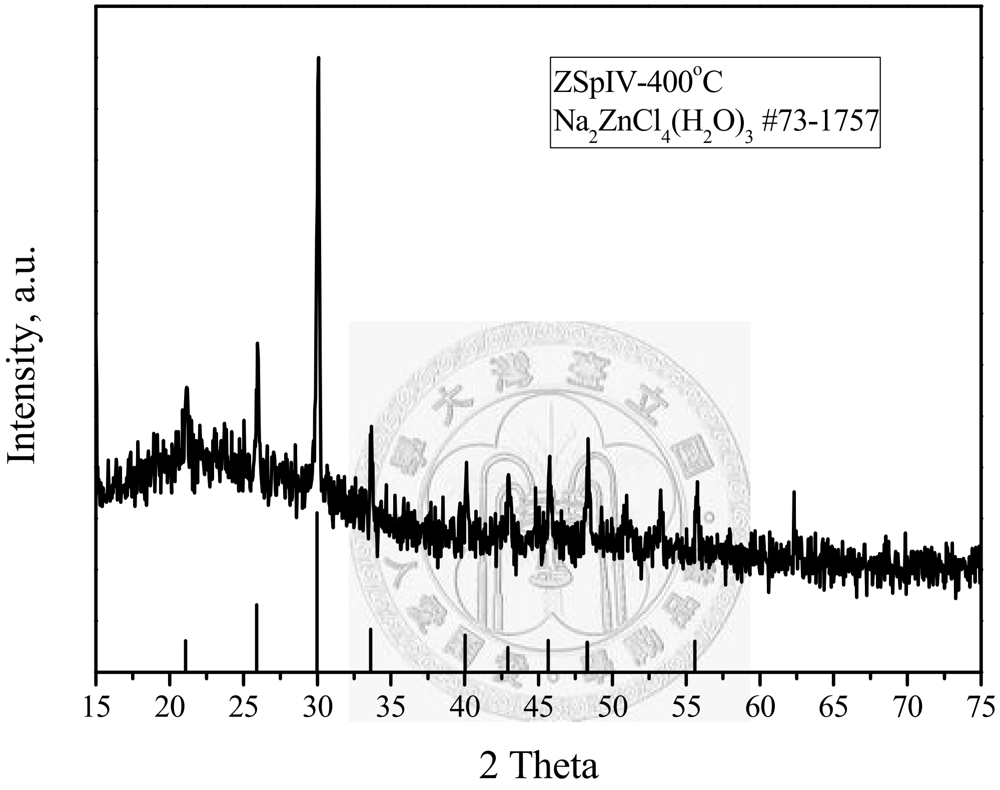

Fig. 5- 9 XRD patterns showing the crystalline phase of ZSpIV annealed at 400^{o}C for 2 hr. The crystalline phase is indexed as $Na_2ZnCl_4(H_2O)_3$.

5.2 *Effects of Mn^{2+} to PL Property*

The luminescence property contributed by Mn^{2+} has been mentioned briefly in chapter 2. In this section, the mechanism will be discussed in details.

First, Zn_2SiO_4:Mn is a willemite structure belongs to rhombohedral space group that Zn and Si ions bonded in a tetrahedron with coordination number = 4 [73]. The $3d^5$ electron configurations for Mn^{2+} ion follow the Zeeman Effect [74,75], i.e. when an atom is affect by a magnetic field induced by the circulating electrons constituting a current loop, the orbital magnetic moments would split into several quantum states. The excited state exists or not could be determined by eq. (5.1).

$$\int_{-\infty}^{\infty} X\psi_n\psi_m^* dx \qquad (5.1)$$

where X is position of electrons; and ψ is the wave function. Since the energy density of an electromagnetic field is proportional to the square of electric field, the energy density could be expressed as $1/2\varepsilon_o|E|^2 = 1/2\varepsilon_o E^* E$ (with the asterisk is “complex conjugate”). The mass is a kind of energy form and ψ is the wave function of the particle of mass m, and therefore $\psi^*\psi$ could be seen as energy density associated with mass. The transitions states of which the integral is finite are called allowed transitions, while those for which is zero are forbidden transitions.

A normal Zeeman effect could be explained by the following example (dividing into three parts, see Fig. 5- 10). A state of given orbital quantum number l splits into (2l

＋1) substates that differs in energy by $\mu_B B$ (where the potential energy of an magnetic dipole in a magnetic field B is expressed as $U = -\mu_B B$) when the atom is influenced by a magnetic field. Because $\Delta m_l = 0$ and ±1 (which obeys selection rule in Fig. 5- 11), a spectral line from a transition between two states of different l orbital is expected to split into only three components.

In this case, however, the tetrahedral structure for Mn^{2+} and the energy state could be expressed in the right–hand side in Fig. 5- 11 [76] with weak crystal field. The $3d^5$ electrons occupy five orbitals that can be donated as $(e)^2(t_2)^3$ instead of $(t_2)^5$ which is due to its high spin structure and thus gives rise to a lower energy state [77]. Then, we have the following term and symbols to describe the different configurations of energy state such as eq. 5.2 [27].

$$^{2S+1}L_J \quad \text{and} \quad J=L+S \qquad (5.2)$$

where 2S+1 is the multiplicity, J is the total angular momentum, L is the total orbital angular momentum. The term 2S+1 is determined by adding the total spin angular momentum (S) and could be easily completed by counting the number of un-paired spin electrons and multiplied by 1/2.

The schematic energy level is shown in Fig. 5- 12 [78]. Initially, the valence electrons ($3d^5$) occupy the ground state. These electrons adsorbed energy (e.g. light) and become to several existing state which determined by the location or states of orbits.

They first located at the ground state that denoted as $(e)^2(t_2)^3$ or $^6A_1$ and excited to the following excited states $^4A_1$, ^4E, $^4T_1$, and $^4T_2$ [77] while exposed under an external energy (254 nm UV light in this case). The relationship is easily to be described by eq. (5.3).

$$Mn^{2+} + h\upsilon \Leftrightarrow Mn^{3+} + e^{-} \qquad (5.3)$$

The excited electrons then release energy by light emission. Fig. 5- 12 illustrates that the 520 nm green light emission is corresponded to the energy state $^4T_1 \rightarrow {}^6A_1$. If we follow the formula that is used to calculate the energy carried by light:

$$E = h\upsilon = h\frac{C}{\lambda} \qquad (5\text{-}4)$$

where *E* is energy, *h* is Plank constant, λ is the wavelength (520 nm), and *C* is speed of light. Then, the value of E is about 2.38 eV which is also agreed with that reported by Chang *et al.* [79] They investigated the electronic structure of Zn_2SiO_4:Mn by using theoretical calculation (first principles) and did experiments to discover the variation of energy states. Although there was a little disparity between the calculated value (2.61 eV) and observed one (2.34 eV), the result was considered still reliable.

This outcome give us another important message that the green light emission was resulting from divalent Mn^{2+} ions instead of trivalent one, or others due to the trivalent Mn^{3+} ion having its own electron configuration ($^5T_{2(g)}$ for $3d^4$ ground state of Mn^{3+}, where the subscript g means gerade which is appropriate for octahedral stereochemistry only [77]). That is different from Mn^{2+}. In this study, the valence state of Mn was examined by XPS (X-ray photoelectron spectroscopy) and the result is showed in Fig. 5- 13. Samples were prepared with two levels of Mn doping (5 mol% and 50 mol% based on Zn). In fact, it could be seen that doping with a lower concentration did not led to result shifting, except a higher concentration gave a better S/N (signal/noise) ratio. However, the binding energy of valence states of Mn ions was too close to be distinguished from one to each other. Table 5- 1 lists binding energy of Mn under divalent, trivalent and also tetravalent states. ZSpII samples had the maximum signal located at about 641 eV, but this information could not be differentiated. Therefore, XPS maybe is not an appropriate technique to examine the valence states of Mn in this case. Another rational method to examine the valence state is to heat up the whole sample at elevated temperature, the weight change due to the oxygen varying with Mn valence states could be detected. Eq. 5.5 is an example that represents the weight change if the Mn ions vary from divalent to trivalent state:

$$2MnO + \frac{1}{2}O_2 \Leftrightarrow Mn_2O_3 \qquad (5.5)$$

there should be an excess of 11.27% weight change for oxidation of MnO per mole (8/70.93). In this study, however, Mn doping is 5 mol% (base on Zn) which is difficult to be detected by TGA (thermogravimetric analysis), i.e. if the sample prepared for TGA test was 10 mg, than the weight change in this system was expected as:

$$W_{Mn} = 10mg \times \frac{1}{5} \times 5\% = 0.1mg \qquad (5.6)$$

$$\therefore \Delta W = 0.1mg \times 11.27\% = 0.01127mg \cong 1.1 \times 10^{-5}\,g \qquad (5.7)$$

while 1/5 is the setting of Zn/Si ratio, 5% is the amount of Mn doping, and the calculated weight change is 10^{-5} g. This value could be a great challenge for the resolution of TGA.

To summarize those evidences, the 520 nm visible green light emission produced by Zn_2SiO_4:Mn results from divalent Mn^{2+} ions of the transition energy state (base on Chang's report [79]). The electrons experience a $^4T_1 \rightarrow {}^6A_1$ transition which is excited by UV light from Mn^{2+}.

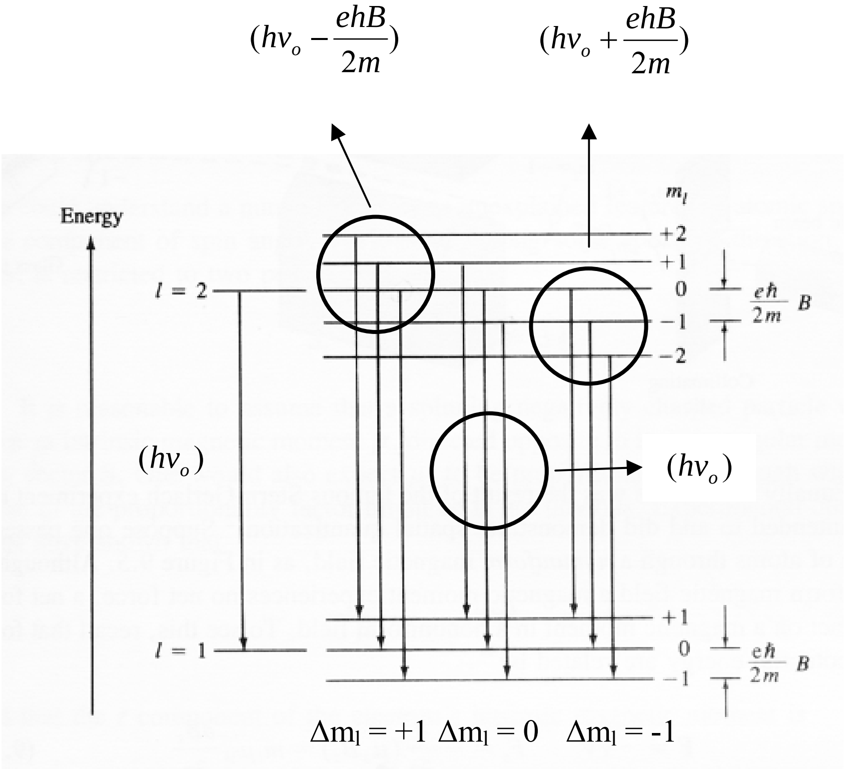

Fig. 5- 10 Schematic diagram explaining Zeeman effect, where υ is frequency, e is electron charge, m is mass, and B is the magnetic field. The transition states exists only when $\Delta m_l = 0$ and ±1, and the phenomenon had been proven by the Stern-Gerlach experiment [74, 75].

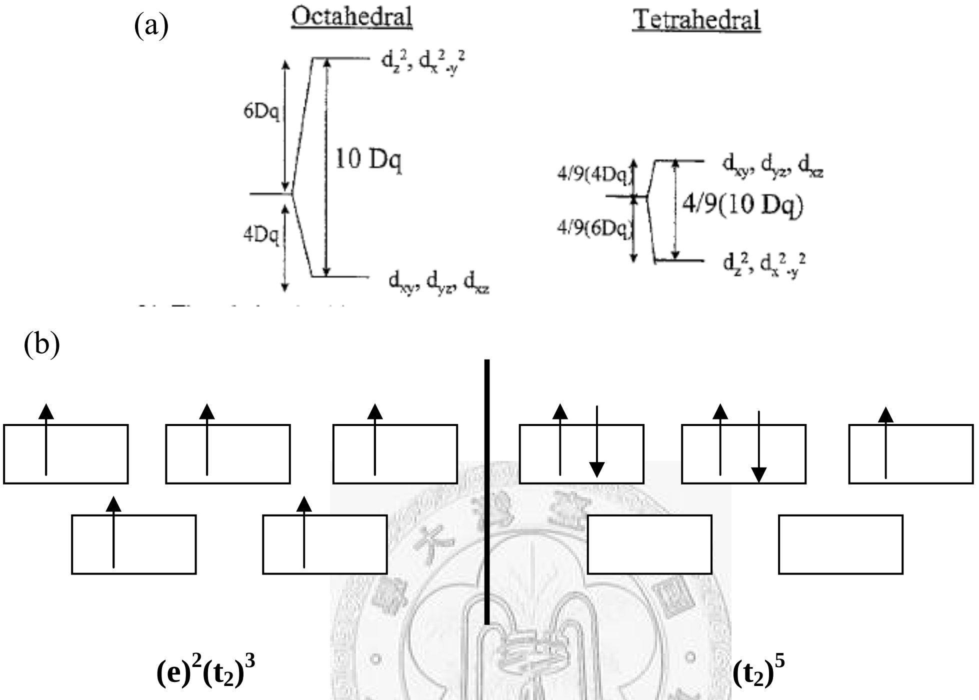

Fig. 5- 11 Energy of *d* orbital of transition metal ions with (a) ion in octahedral site or tetrahedral site with weak crystal field [76], where (b) represented the case of electron configuration of $(e)^2(t_2)^3$ and $(t_2)^5$, respectively.

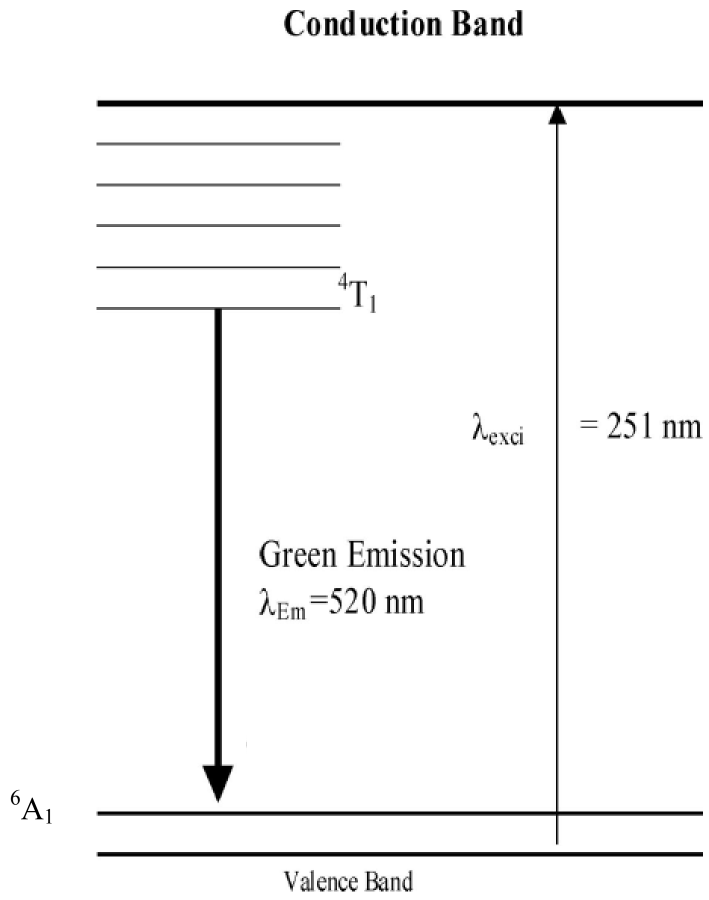

Fig. 5- 12 Schematic diagram showing the variation of energy level while Mn^{2+} is adsorbing or releasing energy by light [78].

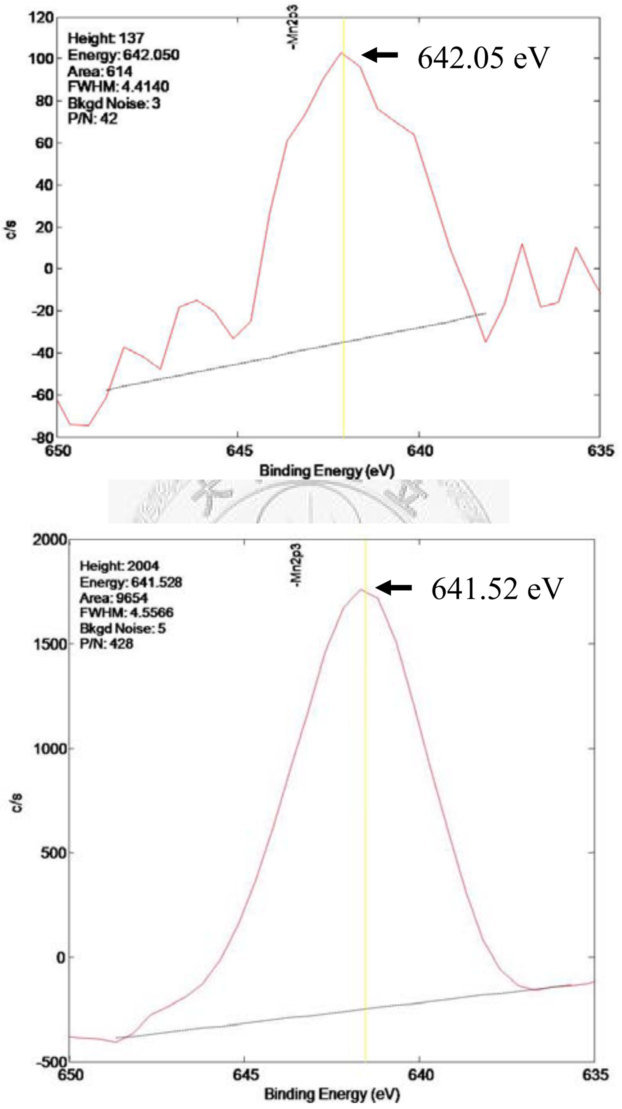

Fig. 5- 13 XPS spectra illustrating the binding energy of Mn ions. The samples calcined at 1100°C for 2 hr were doped with 5 mol% (top) and 50 mol% (bottom) Mn (based on Zn). Both of the maximum peaks located at 641 eV.

Table 5- 1 List of binding energy belonging to different valence states of Mn [80]. The unit in this table is eV and the spectrum considered in this case is 2p3/2.

MnO (2+)	**Mn_2O_3 (3+)**	**MnO_4 (4+)**
640.4[a]	641.2[f]	641.6[k]
640.8[b]	641.5[g]	642.0[l]
641.3[c]	641.6[h]	642.6[m]
641.7[d]	641.7[i]	642.7[n]
642.5[e]	642.8[j]	642.8[o]

a http://srdata.nist.gov/xps/XPSDetailPage.aspx?AllDataNo=26852

b http://srdata.nist.gov/xps/XPSDetailPage.aspx?AllDataNo=26859

c http://srdata.nist.gov/xps/XPSDetailPage.aspx?AllDataNo=26851

d http://srdata.nist.gov/xps/XPSDetailPage.aspx?AllDataNo=59268

e http://srdata.nist.gov/xps/XPSDetailPage.aspx?AllDataNo=26849

f http://srdata.nist.gov/xps/XPSDetailPage.aspx?AllDataNo=26630

g http://srdata.nist.gov/xps/XPSDetailPage.aspx?AllDataNo=26645

h http://srdata.nist.gov/xps/XPSDetailPage.aspx?AllDataNo=26616

i http://srdata.nist.gov/xps/XPSDetailPage.aspx?AllDataNo=26624

j http://srdata.nist.gov/xps/XPSDetailPage.aspx?AllDataNo=26633

k http://srdata.nist.gov/xps/XPSDetailPage.aspx?AllDataNo=26503

l http://srdata.nist.gov/xps/XPSDetailPage.aspx?AllDataNo=26524

m http://srdata.nist.gov/xps/XPSDetailPage.aspx?AllDataNo=26522

n http://srdata.nist.gov/xps/XPSDetailPage.aspx?AllDataNo=27255

o http://srdata.nist.gov/xps/XPSDetailPage.aspx?AllDataNo=26515

5.3 PBG Effects to PL Property

PBG packing is a special structure, which consists of ordered submicron particles. Intuitively, the phosphor materials with submicron size packing as a PBG structure could perform better properties, such as the enhancement of PL emission [81, 82, 83].

In order to investigate the effect of PBG structure to PL property, an experiment was conducted to compare the phosphor particles with the same process, formula, heat treatment, except packing conditions. One was a set showing random packing, and the other one was constructed as PBG structure in Fig. 5- 14. Both of the samples were reacted with precursors diluted to 5 times and annealed at 1000^{o}C for 2 hr. The effect to the PL property is shown in Fig. 5- 15, which illustrates the phosphor with PBG structure and perform a stronger PL property (up to about 170%) compared with non-PBG one. This phenomenon was also discovered in recent researches. It is believed that if the emitting wavelength located near toe of the stop band of PBG crystal, the PL intensity would be enhanced [84]. For the case in this study, the average particle size of ZSpVI series is about 240 nm, and the assembled crystal produces PL emission at 520 nm (about twice greater than the particle size) visible green light. Therefore, the emission peak was enhanced. Li *et al.* [85] suggested that this enhancement effect was contributed from the ***band edge effect*** of the stop band, i.e. the electromagnetic wave near the edge of the stop band exists a lower group velocity of light along with higher electric field density. Therefore, the PL property is improved if the emission band located at the edge of stop band, while PL property was reduced as the emission band located in the stop band.

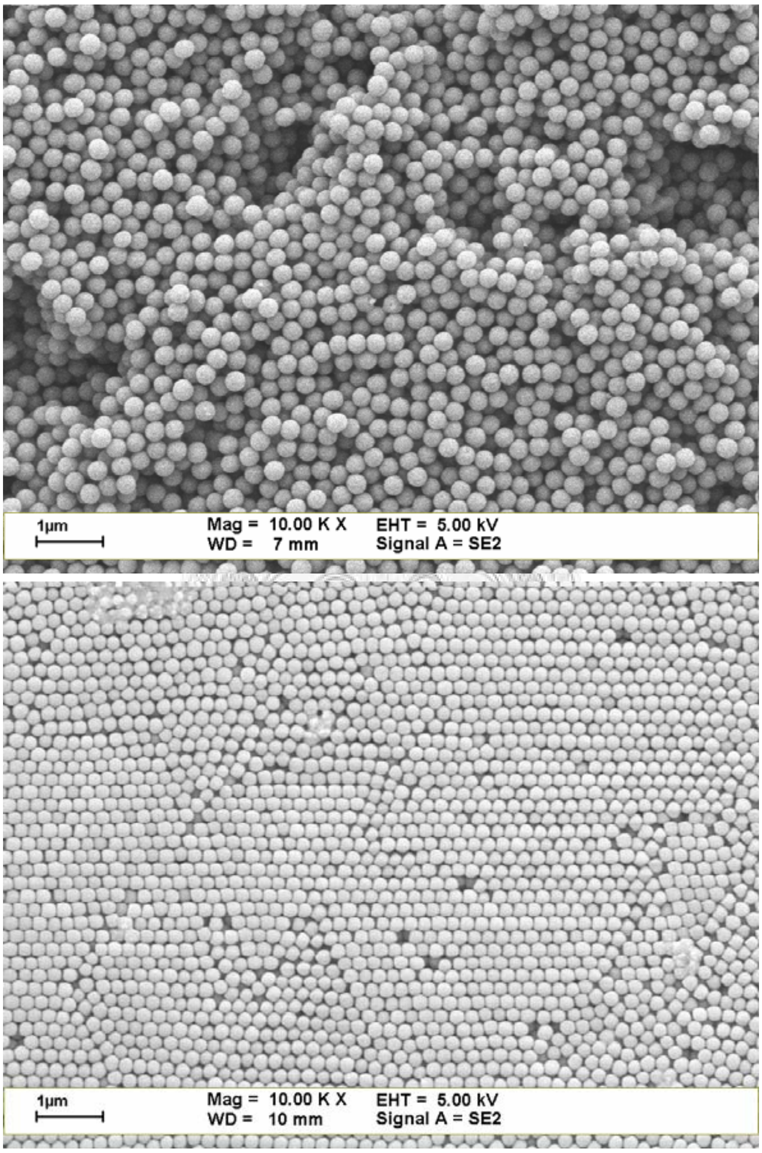

Fig. 5- 14 SEM images of ZSpVI samples in random (top) and ordered (bottom) packing, respectively. Both of the samples were annealed at 1000°C for 2 hr.

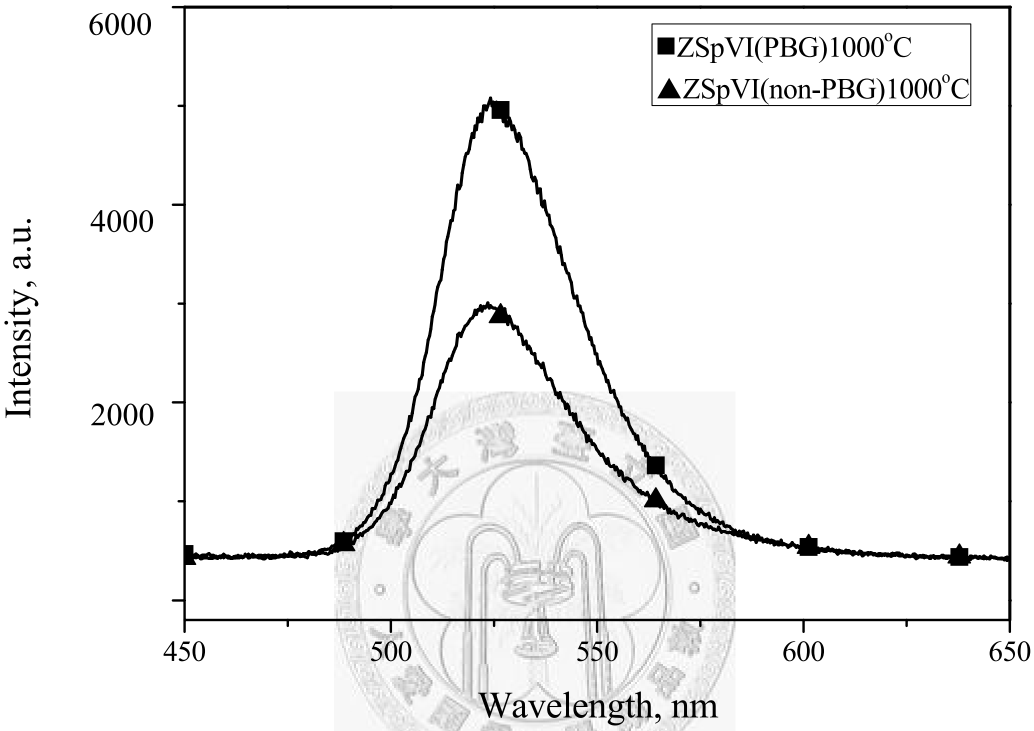

Fig. 5- 15 PL spectra of ZSpVI samples with and without PBG structure. The sample that was ordered packing performed a stronger PL intensity (about 70%) greater than the other one.

Chapter 6 Conclusions

We have developed two methods that are able to synthesized SiO_2 core-Zn_2SiO_4:Mn shell phosphor successfully either in powder or assembled PBG structure. XRD result shows that Zn_2SiO_4 is formed as the annealing temperature higher than 800^{o}C. 1100^{o}C heat treatment is the best annealing temperature, which performs strongest PL property. 5 mol% of Mn doping corresponding to concentration quenching effect shows the best PL properties.

The precipitation behaviors of Zn and Mn under the variation of pH value are also concerned for ZSpII (powder coating case). Co-precipitation of Zn/Mn on SiO_2 shows a better chemical uniformity than that of solid state reaction, therefore, performs a stronger PL intensity.

For the original experimental design, ZnO (with IEP ~ 9) is expected to be attracted by SiO_2 (with IEP ~ 3) surface as the pH value of system controlled at 8.5. However, according to the calculation of solubility for Zn^{2+} (and also Mn^{2+}), Zn^{2+} and Mn^{2+} does not co-precipitate at the setting pH value (8.5) and therefore there's always a difference existing between the design value (i.e. 0.16/5 mol%) for Zn/Mn and the prepared one (i.e. 0.14/4.5 mol%).

The thickness of the coated layer outside silica core was observed by EM. Alcohol added results in a lower PL intensity, while the diluting step in ZSpVI (PBG coating case) case is necessary to maintain a good coating condition. For the performance of PL property, 5 mol% Mn doping, 1000^{o}C heat treatment for 2 hr and also dilute to 3 times by alcohol lead to a best PL emission.

In addition, these Zn_2SiO_4:Mn phosphor is able to operated by applied voltage (at the threshold voltage of 175 V) as a luminescence device and thus performs visible light as a CL emission.

In this study, the submicron size SiO_2 core-Zn_2SiO_4:Mn shell spherical particles are synthesized successfully which perform a green light (520 nm) PL emission. Via ZSpVI method, the Zn_2SiO_4:Mn is able to be coated on assembled silica template and thus become a phosphor PBG crystal.

Reference

1. Website, http://ab-initio.mit.edu/photons/tutorial/
2. Website, http://en.wikipedia.org/wiki/
3. Y. H. Yun, K. W. Park, S. C. Choi, “Photoluminescence and surface morphologies of ZnGa2O4 thin film phosphors deposited by a chemical solution method,” J. Ceram. Pross. Res., **6** [4] 305-08 (2005)
4. 楊素華, *螢光粉在發光上的應用*, 科學發展, 358, 66-71 (2002)
5. Website, http://www.lostseaopals.com.au/opals/index.asp
6. Website, http://nano.nchc.org.tw/photonic/ch1.php
7. Website, http://en.wikipedia.org/wiki/
8. P. Russell, “Photonic crystal fibers,” *Science*, **299**, 358-62 (2003)
9. S. Noda, K. Tomoda, N. Yamamoto, and A. Chutinan, “Full three-dimensional photonic band-gap crystals at near-infrared wavelengths,” *Science*, **298**, 604-06 (2000)
10. S. Y. Lin, E. Chow, V. Hietala, P. R. Villeneuve, and J. D. Joannopoulos, “Experimental demonstration of guiding and bending of electromagnetic waves in a photonic crystal,” *Science*, **282**, 274-76 (1998)
11. 陳啟昌, 張正揚, 張利銘, T. Pertsch, 侯佳宏, M. P. Bernal, 羅仕守, 邱華恭, 蕭輔力, A. Khelif, 欒丕綱, 丁于真, 詹益仁, 綦振瀛, 李建階, “光子晶體的過去, 現在與未來,” *台灣奈米會刊*, **5**, 24-35 (2006)
12. N. A. M. Verhaegh and A. V. Blaaderen, “Dispersions of Rhodamine-Labeled Silica Spheres: Synthesis, Characterization, and Fluorescence Confocal Scanning Laser Microscopy,” Langmuir, **10**, 1427-38 (1994)
13. D. J. Norris, E. G. Arlinghaus, L. Meng, R. Heiny, and L. E. Scriven, “Opaline photonic crystals: How does self-assembly work?,” *Adv. Mater.*, **16** [16] 1393-99 (2004)
14. J. Cesarano III and I. A. Aksay, “Stability of aqueous α-Al_2O_3 suspensions with poly (methacrylic acid) polyelectrolyte,” *J. Am. Ceram. Soc.*, **71** [4] 250-54 (1998)
15. B. V. Velamakanni and F. F. Lange, “Effect of interparticle potentials and sedimentation on particle packing density of bimodal particle distributions during pressure filtration,” *J. Am. Ceram, Soc.*, **74** [1] 166-72 (1991)
16. J. S. Reed, *Principle of ceramics processing*, 2nd edition, John Wiley and Sons., New York, 1995
17. R. G. Horn, “Surface forces and their action in ceramic materials,” *J. Am. Ceram. Soc.*, **73** [4] 1117-1135 (1990)

18. A. W. Adamson, 陶雨台譯, *表面物理化學*, 千華出版社, 1998
19. S. H. Im, Y. T. Lim, D. S. Suh, and O. O. Park, “Three-dimentaionl self-assembly of colloids at a water –air interface: A novel technique for the fabrication of photonic band-gap crystals,“ *Adv. Mater.*, **14** [19] 1367-69 (2002)
20. S. H. Park, D. Qin, and Y. Xia, “Crystallization of meso-scale particles over large areas,” 10, No. 13, *Adv. Mater.*, **10** [13] 1028-32 (1998)
21. H. Cong and W. Cao, “Colloidal crystallization induced by capillary force,” *Langmuir*, **19**, 8177-81 (2003)
22. D. Xia, A. Biswas, D. Li, and S. R. J. Brueck, “Directed self-assembly of silica nanoparticles into nanometer-scale patterned surface using spin-coating,“ *Adv. Mater.*, **16** [16] 1427-32 (2004)
23. A. V. Blaaderen, R. Ruel, and P. Wiltzius, “Templated-directed colloidal crystallization,“ *Nature*, **385** [23] 321-24 (1997)
24. 鄭子樵, 李紅英, *稀土功能材料*, 化學工業出版社, 北京, 2003
25. A. Safari, B. Kulwicki, *IEEE, Piscataway, NJ*, 127 (1997)
26. R. C. Ropp, *Luminescence and the Solid state*, Elsevier, Boston, 2004
27. P. D. Rack, P. H. Holloway, “The structure, device physics, and material properties of thin film electroluminescent displays,” *Mat. Sci. and Eng.*, **R21**, 171-219 (1998)
28. K. Liu, Z. Ji, C. Wang, Z. He, L. Sun, and Z. Ye, “Emission from a planar structured electroluminescent device on silicon wafer,” *Mater Sci. & Eng.* ,**B 121**, 145-47 (2005)
29. Website, http://en.wikipedia.org/wiki/Electroluminescence
30. D. B. Williams, and C. B. Carter, *Transmission electron microscope*, PLNUM, New York and London, 1996
31. A. H. Kitai, “Oxide phosphor and dielectric thin films for electroluminescence devices,” *Thin Solid Films*, **445**, 367-376 (2003)
32. W. D. Callister, Jr., *Materials science and engineering an introduction*, 5th edition, John Wiley and Sons., New York, 1995
33. N. Kawahashi and H. Shiho, “Copper and copper compounds as coatings on polystyrene particles and as hollow spheres,” *J. Mater. Chem.*, **10**, 2294-2297 (2000)
34. A. Imhof, “Preparation and characterization of titania -coated polystyrene spheres and hollow titania shells,” *Langmuir*, **17**, 3579-85 (2001)
35. X. C. Guo and P. Dong, “Multistep coating of thick titania layers on mono-disperse silica nano-spheres,” *Langmuir*, **15**, 5535-40 (1999)
36. H. Shiho, and N. Kawahashi, “Titanium compounds as coatings on polystyrene latices and as hollow spheres,” *Colloid Polym. Sci.*, **278**, 270-74 (2000)
37. H. Shiho, and N. Kawahashi, “Iron Compounds as Coatings on Polystyrene Latex

and as Hollow Spheres," *J. Colloid and Int. Sci*., **226**, 91-97 (2000)

38. S. F. Wang, Y. F. Hsu, T. C. K. Yang, C. M. Chang, Y. Chen, C. Y. Huang, and F. S. Yen, "Silica coating on ultrafine α-alumina particles," *Mater. Sci. Eng. A*, **395**, 148-52 (2005)
39. J. H. Park, Y. G. Kim, C. Oh, S. I. Shin, Y. C. Kim, S. G. Oh, and S. H. Kong, "Fabrication of hollow silver spheres by MPTMS-functionalized hollow silica spheres as templates," *Mat. Res. Bull*., **40**, 271-80 (2005)
40. R. I. Walton, R. I. Smith, F. Millange, I. J. Clark, D. C. Sinclair, and D. O'Hare, "An in situ time-resolved neutron diffraction study of the hydrothermal crystallization of barium titanate," *Chem. Commun*., 1267-68 (2000)
41. F. Caruso, R. A. Caruso, and H. Mohwald, "Production of hollow microspheres from nano-structured composite particles," *Chem. Mater*., **11**, 3309-14 (1999)
42. K. Zhang, X. Zhang, H. Chen, X. Chen, L. Zheng, J. Zhang, and B. Yang, "Hollow titania spheres with movable silica spheres inside,“ *Langmuir*, **20**, 11312-14 (2004)
43. M. Okubo, K. Ichikawa, and M. Fujimura, "Production of multi-hollow polymer microspheres by stepwise alkali/acid method II. Alkali treatment process," *Colloid Polym. Sci*., **269**, 1257-62 (1991)
44. C. P. Li, J. S. Chang, and W. F. Su, "Synthesis of monodispersed silica particles," J. *Mater. Sci. Eng*., **35** [4] 245-249 (2003)
45. J. W. Kim, Y. G. Joe, and K. D. Suh, "Poly(methyl methacrylate) hollow particles by water-in-oil-in-water emulsion polymerization," *Colloid Polym. Sci*., **277**, 252-56 (1999)
46. Website, http://www.chemat.com/html/solgel.html
47. Website, http://ruby.colorado.edu/~smyth/min/willemite.html
48. Website, http://www.minweb.co.uk/
49. K. Liu, Z. Ji, C. Wang, Z. He, L. Sun, and Z. Ye, "Emission from a planar structure electroluminescent devise on silicon wafer," *Mater. Sci. Eng.* B, **121**, 145-47 (2005)
50. T. S. Ahmadi, M. Haase, and H. Weller, "Low-temperature synthesis of pure and Mn-doped willemite phosphor (Zn_2SiO_4:Mn) in aqueous medium," *Mat. Res. Bull*., **35**, 1869-79 (2000)
51. T. S. Copeland, B. I. Lee, J. Qi, and A. K. Elrod, "Synthesis and luminescent properties of Mn^{2+}-doped zinc silicate phosphors by sol-gel methods," *J. lumin*., **97**, 168-73 (2002)
52. Z. Ji, L. Kun, S. Yongliang, and Y. Zhizhen, "Fabrication and characterization of Mn-doped zinc silicate films on silicon wafer," *J. cryst. growth*, **255**, 353-56 (2003)
53. Website, http://webmineral.com/

54. H. Chang, H. D. Park, K. S. Sohn, and D. Lee, “Electronic structure of Zn2SiO4 and Zn2SiO4:Mn,” *J. Korean phy. Soc.*, **34** [6] 545-48 (1999)
55. Y. M. Chiang, D. Birnie III, and W. D. Kingery, “*Physical Ceramics*”, John Wiley and Sons., New York, 1995
56. E. N. Bunting, *J. Am. Ceram. Soc.*, **13** [1] 8 (1930)
57. T. Taghavinia, G. Lerondel, H. Makino, A. Parisini, A. Yamamoto, T. Yao, Y. Kawazoe, and T. Goto, “Activation of porous silicon layers using Zn_2SiO_4:Mn^{2+} phosphor particles,” *J. lumen*, **96**, 171-75 (2002)
58. A. Morell, and N. E. Kiati, “Green phosphors for large plasma TV screens,” *J. Electrochem. Soc.*, **140** [7] 2019-2022 (1993)
59. Y. H. Yun, K. W. Park, and S. C. Choi, ”Photoluminescence and surface morphologies of $ZnGa_2O_4$ thin film phosphors deposited by a chemical solution method,” *J. Ceram. Process. Res.*, **6** [4] 305-08 (2005)
60. T. Minami, “Oxide thin-film electroluminescent devices and materials,” *Solid-States Electronics*, **47**, 2237-43 (2003)
61. G. H. Lee, N. Iwata, S. J. Kim, and M. S. Kim, “Photoluminescence of ZnO fine powders synthesized by sol-gel process,” *J. Ceram. Soc. Jp.*, **113** [1] 64-66 (2005)
62. 陳右儒 (Y. R. Chen), *固態氧化物燃料電池之氣相法薄膜合成與鉍系封裝玻璃/氧化鋯之介面接合反應*, 國立台灣大學材料科學與工程所碩士論文,(2007)
63. C. C. T. Yang, H. J. Cho, and W. J. Wei, “Quantitative characterization of various tetragonal zirconia polycrystals (TZPs),” *J. Eur. Ceram. Soc.*, **22**, 199-207 (2002)
64. Website: http://www.hic.ch.ntu.edu.tw/
65. Y. C. Kang and S. B. Park, “Zn_2SiO_4:Mn Phosphor particles prepared by spray pyrolysis using a filter expansion aerosol generator,” *Materials Research Bulletin*, **35**, 1143-51 (2000)
66. T. H. Cho and H. J Chang, “Preparation and characterizations of Zn_2SiO_4:Mn green phosphors,” *Ceram. Int.*, **29**, 611-18 (2003)
67. 國立台灣師範大學科學教育中心, *高中化學*, 國立編譯館, 台北市, 1990
68. Website, http://www.ktf-split.hr/periodni/en/abc/kpt.html
69. 汪健民, *陶瓷技術手冊*,中華民國粉末冶金學會, 新竹縣, 1999
70. 巫柏奇, 呂宗昕, *Modification and Characterization of Strontium Orthosilicate and Yttrium Oxide Phosphors*, 國立台灣大學碩士論文, 2005
71. Website, http://140.134.32.129/nowsci/img/dspapp-0/dspapp-1.htm
72. C. Lara, M. J. Pascual, M. O. Prado, and A. Duran, “Sintering of glasses in the system RO-Al_2O_3-BaO-SiO_2 (R = Mg, Ca, Zn) studied by hot staged microscopy,” *Solid State Ionics*, **170**, 201-08 (2004)
73. T. S. Ahmadi, M. Haase, and H. Weller, “Low-temperature synthesis of pure and Mn-doped willemite phosphor (Zn_2SiO_4:Mn) in aqueous medium,” *Mat. Res. Bull.*,

35, 1869-79 (2000)

74. A. Beiser, *Concepts of Modern Physics 6th*, McGraw-Hill, Boston, 2003
75. F. J. Blatt, *Modern Physics*, McGraw-Hill, New York, 1992
76. M. W. Barsoum, *Fundamentals of ceramics*, Taylor & Francis, New York, 2003
77. J. E. Huheey, E. A. Keiter, and R. L. Keiter, *Inorganic chemistry : principles of structure and reactivity 4th*, Harper Collins College Publishers, New York, 1993
78. R. P. S. Chakradhar, B. M. Nagabhushana, G. T. Chandrappa, K. P. Ramesh, and J. L. Rao, “Solution combustion derived nanocrystalline Zn_2SiO_4:Mn phosphors: A spectroscopic,” *J. Chem. Phys.*, **121** [20] 10250-59 (2004)
79. H. Chang, H. D. Park, K. S. Sohn, and J. D. Lee, “Electronic structure of Zn_2iO_4 and Zn_2SiO_4:Mn,” *J. Korean Phys. Soc.*, **34** [6] 545-48 (1999)
80. Website, http://srdata.nist.gov/xps/
81. M. Zelsmann, E. Picard, T. Charvolin, E. Hadji, M. Heitzmann, B. Dal’zotto, M. E. Nier, C. Seassal, P.Rojo-Romeo, and X. Letartre, “Seventy-fold enhancement of light extraction from a defectless photonic crystal mad on silicon-on-insulator,” *Appl. Phys. Lett.*, **83** [13] 2542-44 (2003)
82. L. I. Halaoui, N. M. Abrams, and T. E. Mallouk, “Increasing the conversion efficiency of dye-sensitized TiO_2 photoelectrochemical cells by coupling to photonic crystals,” *J. Phys. Chem., B*, **109**, 6334-42 (2005)
83. Y. A. Vlasov, K. Luterova, I. Pelant, and B. Hönerlage, “Enhancement of optical gain of semiconductors embedded in three-dimensional photonic crystals,” *Appl. Phys. Lett.*, **71** [12] 1616-18 (1997)
84. C. M. Chuang, W. B. Lu, W. F. Su, C. M. Lin, and Y. F. Chen, “Manipulation of luminescence from CdSe nanoparticles by three-dimensional photonic crystal,” *J. Appl. Phys.*, **97**, (2005)
85. Y. Li, T. Kunitake, S. Fujikawa, and K. Ozasa, “Photoluminescence modification in 2D-ordered films of fluorescent microspheres,” *Langmuir*, **23** [17] 9109-13 (2007)